Aalto-yliopisto
Insinööritieteiden
korkeakoulu

Wudi Hao

A study on pre-combustion conditions in the Cooperative Fuel Research (CFR) Engine

Thesis submitted for examination for the degree of Master of Science in Technology
Gothenburg 10.09.2020

Supervisor: Prof. Martti Larmi
Advisor: D.Sc (Tech.) Ossi Kaario

Aalto-yliopisto
Insinööritieteiden
korkeakoulu

Aalto-yliopisto, P L 11000, 00076 AALTO
www.aalto.fi

Diplomityön tiivistelmä

Author Wudi Hao	
Title of thesis A study on pre-combustion conditions based on the CFR engine	
Master programme Innovative sustainable energy engineering	**Code** ENG215
Thesis supervisor Prof. Martti Larmi	
Thesis advisor(s) D.Sc (Tech.) Ossi Kaario	
Date 10.09.2020 **Number of pages** 7 + 80	**Language** English

Abstract

Knocking can produce adverse effect on engine performance. When knocking combustion occurs inside the cylinder, fuel combustion efficiency decreases, fuels do not combust fully, resulting in the improvement of exhaust gas emissions. In addition, knocking causes irreversible damage to the cylinder. Therefore, it is important to understand the physical phenomena in different parts of the engine during a combustion process under different engine operation conditions. It is also important to understand fuels' physical properties' effects on the physical phenomena inside an engine under various operation conditions.

In this study, cooperative fuels research (CFR) engine modellings under research octane number testing conditions and motor octane number testing conditions are built by using Gt-Power software. Those two modelling are employed in order to observe the pre-combustion conditions of spark ignition (SI) engine. The temperature, pressure and gaseous mass fraction variations in the intake system are simulated with the surrogate of gasoline, indolene. Variations on temperature, pressure and burnt mass fraction in the engine cylinder are simulated based on 19 kinds of fuels with different octane numbers. Density and heat of evaporation (HoV) are main parameters. Density and evaporative heat are mainly parameters for investigating the impact of fuels physical properties on the physical phenomena.

The simulation results show the variation trend of pressure, temperature and gaseous mass fraction in the intake system. Besides, it is revealed by simulations that in-cylinder pre-combustion conditions are more severe with higher pressure and higher temperature when the octane number of fuels increase. Density of fuel has no significant effect on the in-cylinder pre-combustion conditions, while heat of vaporization (HoV) of a fuel can manipulate in-cylinder temperature to some extent based on simulation results.

Keywords octane numbers, octane number rating, knocking, CFR engine, pre-combustion conditions, gasoline surrogates

Preface

This master's thesis was conducted in the Energy Conversion Research Group, School of Engineering, Aalto University. The funding of this master's thesis came jointly from Aalto University and Neste Corporation. I would like to express my great appreciation to all the supports I receiced during the period to accomplish my research.

I would like show my special and sincere appreciation to my supervisor, Professor Martti Larmi and my advisor, Dsc (Tech.) Ossi Kaario. They offerred me not only the sufficient knowledge, but also the methodology of conducting a research. From those two excellent sophisicated researchers, I realized the importance of shifting myself from a student to an independent researcher, which I am still working on that.

I also want to express many thanks to my colleagues, Yuri Kroyan and Michal Wojcieszyk, who inpsired me a lot when I was in a dilemma. Besides, I would like to show great appreciations to Dsc (Tech.) Qiang Cheng, Dsc (Tech.) Zeeshan Ahmad and Otto Blomstedt for their inspirations on engines and engine models building. In addition, my co-supervisor from Chalmers University of Technology D.Sc (Tech.) Carl Johan Linderholm offered me many helps related to this thesis work.

At last, I want to especially thank my parents. They spur me on when I am too proud, and encourage me when I am down. They put their selfless love on me, letting me pursuit my dream freely.

Gothenburg, Sweden

10.10.2019

Wudi / Wudi Ha

Contents

Symbols

T	temperature
p	pressure
V_{max}	the maximum in-cylinder volume
V_{min}	the minimum in-cylinder volume
E	net energy of a system
E_{in}	energy entering to a system
E_{out}	energy leaving from a system
η	efficiency of an Otto cycle
c_v	specific heat under constant temperature
c_p	specific heat under constant pressure
γ	specific heat ratio
h_c	heat transfer rate
B	cylinder bore
ω	average gas velocity in the cylinder

Abbreviations

OECD	Organization for Economic Co-operation and Development
FSU	Former Soviet Union
SI engine	Spark-ignited engine
CFR	Cooperative fuel research
HCCI	Homogeneous charge compression ignition
PRF	Primary reference fuels
TRF	Toluene reference fuels
LPG	liquefied petroleum gas
WWII	World war II
TEL	Tetraethyllead
ASTM	American society for testing and materials
DI	Driveability index
ICE	Internal combustion engines
CI engine	Compression ignition engine
BDC	Bottom dead center
TDC	Top dead center
CR	Compression ratio
HRR	Heat release rate
KI	Knocking index
RON	Research octane number
MON	Motor octane number
RTT	Reynolds transport theorem
CV	Control volume
CR	Control surface
VFF	Vaporized fluid fraction
BTDC	Before top dead center
CHDIR	Cylinder height dial indicator readin

1 Introduction

From 2010 to 2017, the energy consumption for end-use passenger transport increased by 38% [1]. In 2017, the end-use passenger transport energy accounted for 19% of the total energy consumption globally [1].

Back to 2012, the worldwide oil demand was 88.9 million of barrels per day (mb/d). It was predicted that the global oil demand would increase to 93.5 mb/d in 2017. And it was projected to increase to 94.4 mb/d in 2018 [2].

Table 1 Worldwide oil demand predictions made in 2012 (mb/d) [2]

	2012	2013	2014	2015	2016	2017	2018
OECD	46.0	45.6	45.4	45.2	45.0	44.8	44.6
Developing countries	37.8	38.9	40.1	41.1	42.2	43.3	44.4
India	3.7	3.8	3.9	4.0	4.2	4.4	4.6
China	9.7	10.1	10.4	10.8	11.1	11.5	11.9
Eurasia	5.0	5.1	5.2	5.3	5.3	5.4	5.4
World	88.9	89.5	90.7	91.6	92.5	93.5	94.4

However, the actual worldwide oil demand was 97.32 mb/d in 2017 and 98.73 mb/d in 2018, both data turned out to be higher that predictions made in 2012. Moreover, the global oil demand was predicted to increase to 104.7 mb/d in 2023 [3]. The oil demand in Asia and Pacific will grow with the fastest rate (by 4.2 mb/d totally). In America and Africa, it will rise with a moderate rate. The European oil demand is projected to decline with the rate of 0.2 mb/d from 2017 to 2023 [3].

Table 2 Worldwide oil demand growth in 2017 and 2018 (mb/d) [3]

	2017	1Q18	2Q18	3Q18	4Q18	2018	Growth	%
Americas	25.06	25.20	25.40	25.78	25.74	25.53	0.48	1.90
US	20.27	20.57	20.64	20.93	20.78	20.73	0.46	2.26
Europe	14.33	13.98	14.23	14.71	14.34	14.32	-0.01	-0.10
Asia Pacific	8.06	8.54	7.65	7.70	8.08	7.99	-0.07	-0.89
Total OECD	**47.45**	**47.72**	**47.28**	**48.19**	**48.16**	**47.84**	**0.39**	**0.82**
Other Asia	13.22	13.52	13.84	13.35	13.84	13.64	0.42	3.14
India	4.53	4.83	4.74	4.40	4.96	4.73	0.20	4.43
Latin America	6.51	6.35	6.48	6.81	6.47	6.53	0.02	0.31
Middle East	8.20	8.22	7.98	8.43	7.85	8.12	-0.08	-0.98
Africa	4.20	4.35	4.32	4.27	4.40	4.33	0.13	3.13
Total DCs	**32.13**	**32.43**	**32.62**	**32.86**	**32.56**	**32.62**	**0.49**	**1.52**
FSU	4.70	4.66	4.65	4.94	5.01	4.82	0.12	2.45
Other Europe	0.72	0.73	0.69	0.73	0.82	0.74	0.03	3.48
China	12.32	12.28	12.84	12.65	13.07	12.71	0.39	3.18
Total "others"	**17.74**	**17.68**	**18.18**	**18.32**	**18.90**	**18.27**	**0.53**	**2.99**
Total world	**97.32**	**97.83**	**98.08**	**99.38**	**99.62**	**98.73**	**1.41**	**1.45**
Previous Estimates	97.32	97.83	98.05	99.38	99.63	98.73	1.41	1.45
Revision	0.01	0.00	0.04	0.0	-0.02	0.00	0.00	0.00

In Organization for Economic Co-operation and Development (OECD) countries, the oil demand decreased by around 4300 kb/d from 2005 to 2014, after that, it jumped by

685 kb/d, 460 kb/d and 375 kb/d in 2015, 2016 and 2017 respectively with the recovery of oil price [3]. The demand for gasoline showed similar trend. From 2005 to 2014, it kept falling in OECD countries, and from 2015 to 2017, it increased by 145 kb/d [3]. Due to more intensive industry activity and robust trade, the gasoline demand has been strong in recent years [3].

In OECD European countries, the gasoline demand expressed a downward trend in long period. It showed an annual decline of 80 kb/d due to the increasing share of diesel vehicles and advanced in fuel economy. As a matter of fact, Europe has very stringent standards for fuels and its economy. Back to 2008, Europe set an emission target for passenger fleet in 2015, which was 130 grams carbon dioxide (CO2) emission per kilometer. When it came to 2015, the passenger vehicle average CO2 emission in Europe reduced to 120 g/km [3]. New target for 2021 is even stricter. The required new CO2 emission for passenger vehicle target will be less than 95 g/km in 2021, which is around 70% of the target achieved in 2015. New CO2 emission target in 2021 means an average gasoline consumption of 4.1 l/km.

Table 3 Oil demand by product in OECD European countries (mb/d) [3]

	2017	2018	2019	2020	2021	2022	2023	2017-2023 growth rate
LPG & ethane	1.189	1.223	1.230	1.238	1.245	1.250	1254	0.9%
Naphtha	1.211	1.229	1.236	1.244	1.253	1.257	1.260	0.7%
Motor gasoline	1.916	1.912	1.892	1.868	1.840	1.810	1.782	-1.2%
Jet fuel & kerosene	1.436	1.447	1.449	1.450	1.448	1.444	1.440	0.0%
Gasoline/diesel	6.495	6.499	6.454	6.566	6.432	6.288	6.198	-0.7%
Residual fuel oil	0.888	0.888	0.900	0.708	0.790	0.877	0.916	0.5%
Other products	1.227	1.211	1.217	1.224	1.229	1.234	1.238	0.1%
Total products	**14.33**	**14.408**	**14.379**	**14.298**	**14.237**	**14.160**	**14.089**	**-0.3%**

In the face of increasingly stringent carbon dioxide emission standards and limited fossil fuels, improving engine performance is of great importance. For spark ignition engines (SI engines) or gasoline engines, knocking is negative to the engine performance. Knocking means the self-ignition of in-cylinder end gas.

Many researchers have done experimental research on SI engines knocking phenomenon of various fuels. Some fuels completely replaced gasoline combusting in the engine, while others are mixed with gasoline in the combustion chamber before combustion. Mørch et al. implemented experimental tests based on a cooperative fuel research (CFR) engine in order to explore the combustion conditions when ammonia and hydrogen are mixed in the intake air [4]. Cheng et al. conducted an experimental study on the knocking tendency of three isomers of pentane with the presence of a CFR engine [5]. Kolodziej et al. operated the CFR engine with PRF98Alk, PRF71E30 and PRF98E30 respectively and compared the engine performance from operation with PRF98, in order to understand the combustion reaction mechanism in octane number rating processes better [6]. Szwaja et al. did a research on gasoline combustion with or without the presence of hydrogen based on a CFR engine. And they compared the combustion mechanism in the cylinder of two cases [7]. Juan et al. chose 4 kinds of fuels: biogas, natural gas, propane and hydrogen, and operated the CFR engine with different equivalent ratio. The purpose was to investigate the influence of equivalent ratio on knocking tendency [8]. A series of combustion experiments of synthesis gas with different carbon monoxide/hydrogen ratio on the CFR engine were performed by Bika et al., so that they could find the knocking ratio limit of synthesis gas [9]. Zhongyuan et al. mixed nitric oxide in the intake air for the purpose of the relevance between nitric oxide and the knocking tendency. In order to optimize the homogeneous charge compression ignition (HCCI) combustion performance [10]. Truedsson et al. tested with 40 kinds of fuel with the CFR engine [11]. A research related to combustion characteristics of primary reference fuels (PRF), toluene reference fuels (TRF) and ethanol was done by Hoth et al. [12]. Apart from those mentioned fuels above, liquefied petroleum gas (LPG) attracts many researchers' attention as well. For example, Morganti et al. took a research on the autoignition of hydrocarbons with 3 or 4 carbon atoms in a CFR engine, which are main components of LPG [13]. However, LPG is not a liquid fuel, it is a challenge to apply conventional octane rating on LPG directly. Morganti et al. created a mode, defining the CFR engine so that conventional octane rating can be conducted on LPG as well [14] .

In addition to experimental research, many researchers carried out numerical simulation studies on knocking by building single or multi-dimensional modellings. Choi et al. built a single-dimensional CFR engine modelling using GT-Power. The simulation results were further validated with three pressure analysis [15]. Salih et al. built 1-D CFR engine modelling with GT-Power, with a modified laminar flame model in the cylinder [16]. Pal et al. made a 3-D modellings about the CFR engine to investigate the exact knocking mechanism [17] [18]. Westbrook et al. predicted several kinds of fuels' octane number with a chemical kinetic reaction modelling [19]. Morganti et al. developed a modelling to acquire fundamental understanding of LPG combustion mechanism and knocking mechanism in a CFR engine [20].

These studies focus on the specific chemical reactions that occur after ignition in the combustion chamber. To some extent, these studies explain the fuel chemistry that influences the detonation. However, the research on the relevance between knocking tendency and fuels' physical properties is relatively rare. Moreover, these studies concentrate on the in-cylinder post-ignition combustion stage, that is, the combustion stage in which the knocking is likely to occur. In this work, pre-combustion conditions in the intake system and cylinder on different timings are focused on.

In this work, parameters about intake system, cylinder and exhaust system of the Waukesha F1/F2 CFR engine were collected from several academic sources. Those parameters were further verified with one reference. Based on the collected data, two one-dimensional CFR modellings was built with GT-Power V2019. Those two 1-D modellings strictly cope with the American Society for Testing and Materials (ASTM) standards testing conditions of D2699 (for research octane number) and D2700 (for motor research number). After that, those two modellings ran with primary reference fuels, the modelling results were validated with experimental measurement results from references. After that, representative in-cylinder curves are revealed by simulations, together with the condition variations in the intake system. Then, to get the relationship between the combustion conditions and the octane number of the fuel, the two modellings ran 19 different types of fuel. Finally, effects physical properties of the fuel (density and heat of vaporization) on in-cylinder conditions are analyzed based on simulation results based on indolene.

2 Background

2.1 Gasoline

Gasoline is the product of fractionation, cracking, or cracking of petroleum. It is a mixture of hydrocarbons in the form of liquid, and it can be utilized as fuel. Gasoline is a colorless liquid, but in order to distinguish between the gasoline with different octane numbers, color additives are added to gasoline. Gasoline has a special smell. It is easy to volatilize and can be ignited easily.

2.1.1 Brief History of Gasoline

The history about gasoline always relates to two topics: how to improve the engine performance and how to make gasoline more environmental-friendly.

Back to the late 19th century, two kinds of oil widely drove automobile. One is the oil distillated from the coal tar. The other one was lighter fraction products from the crude oil distillation process. Joshua Merrill is believed as the first person who successfully separates gasoline, and it was utilized for lighting at that time [21]. Gasoline was used also in Nicolaus Otto's first 4-stroke cycle engine in 1876 [22].

By the late 19th century, refiners produced gasoline by distillation from crude oil. However, there were no standard testing methods, specifications or quality indicators for gasoline until early 20th century. In the 1920s, initial testing methods on gasoline were introduced. At the same time, automotive engine performance enhanced dramatically, requiring gasoline with higher quality. To meet more requirements, refiners and engineers developed new testing techniques, specifications and distillation processes. Those developments resulted in higher-quality gasoline and higher content of octane in gasoline. After that, several processes were developed to improve gasoline specifications in terms of octane, volatility and cleanliness.

During the 1930s, fixed bed cracking process significantly increased octane content. According to the octane test conditions of that time, gasoline with higher content of octane was considered as advanced gasoline. During World War II (WWII), some upgrades enabled gasoline with better alkyl lead response and lower sulfur content. Besides, the term of "performance number" occurred. "Performance number" means the increased percent power obtained above the baseline of isooctane.

From 1920s to 1950s, alkyl lead (tetraethyllead or methyllead, short for TEL) was always a popular additive to gasoline in order to boost the octane rating. Almost all gasoline in North America was with alkyl lead back to WWII period. At the period around 1960, deterioration of attracted people's attention. An area with denser population tended to be with worse air quality. Researchers identified NOx, CO, unburnt hydrocarbons and their products after sunlight photochemical reactions as contaminants. Besides, the concentration of those pollutants related to driving cycles, sunlight intensity, local geography and wind patterns. [22] In 1966, automobile emission standards were firstly put in place in California. After that, the American Federal passed national automobile emission standards in 1968. [22] Those regulations were targeted on the reduction on unburnt hydrocarbons and carbon monoxide emissions. In 1985, regulations targeting on alkyl lead (mainly TEL) were introduced. From that

time, lead gradually faded away from gasoline. The last regular gasoline with lead was sold in 1990 in North America. [22]

2.1.2 Gasoline Components

Hydrocarbons

Gasoline consists of more than five hundred hydrocarbons. The number of carbon atoms in these hydrocarbon molecules is between four and fourteen. Hydrocarbons with molecular carbon number less than or equal to three have strong volatility. Hydrocarbons with more than 14 carbon atoms are heavy and less volatile. Besides, these large-molecules hydrocarbons tend not to combustion completely in the combustion chamber, resulting in high emission of unburnt hydrocarbon and soot issues [22].

Saturated hydrocarbons

The chemical properties of saturated hydrocarbons are very stable. Cycloalkanes, alkanes or paraffins are saturated hydrocarbons. Hydrogen atoms cannot be added to the carbon chain of saturated hydrocarbons, but they can be displaced at extreme conditions like high temperatures and pressures. Saturated hydrocarbons are less soluble in water and produce carbon dioxide and water after completely combustion.

The chemical structure formula of alkanes can be summarized as C_nH_{2n+2}, thus, the chemical equation of complete combustion can be expressed as:

$$C_nH_{2n+2} + \frac{3n+1}{2}O_2 = nCO_2 + (n+1)H_2O \tag{2.1}$$

Methane, ethane and propane only have one structure respectively. However, alkanes with four or more carbon atoms can have various structure, this fact is described as structure isomerism. For linear alkanes, carbons are arranged on one line. For branched alkanes, the carbon backbone extends to different directions. For example, isomers of pentane are normal pentane (n-pentane), isopentane and neopentane. The density of alkanes is always less than 1 kg per cube meter. Under atmospheric conditions, alkanes with less than 5 carbon atoms are gaseous, alkanes with carbon atom number from 5 to 16 are liquid. And those alkanes with more than 16 carbon atoms are solid. The melting point and boiling point of alkanes increase with the increase of molecular weight. Besides, for alkanes with the same carbon atoms, the more branches a alkane molecular has, the lower the boiling point will be. [23]

Unsaturated hydrocarbons

Unsaturated hydrocarbons are hydrocarbons containing unsaturated chemical bonds such as double covalent bonds or triple covalent bonds between two carbon atoms. Alkenes, alkynes and the aromatics are unsaturated hydrocarbons. Hydrogen atoms can be added on those unsaturated chemical bonds, so that unsaturated hydrocarbons will be “saturated”. In an aromatic molecular, the covalent bond between adjacent carbon atoms is a special covalent bond between a single and a double bond, and hydrogen atoms can still be added on the carbon ring. Similar to saturated hydrocarbons, unsaturated hydrocarbons can have isomers as well. [23] Alkenes, alkynes can be expressed as C_nH_{2n} and C_nH_{2n-2} respectively. They produce CO_2 and H_2O after complete combustion. The chemical equations of complete combustion are:

$$C_nH_{2n} + \frac{3n}{2}O_2 = nCO_2 + nH_2O \quad (2.2)$$

$$C_nH_{2n-2} + \frac{3n-1}{2}O_2 = nCO_2 + (n-1)H_2O \quad (2.3)$$

Aromatic hydrocarbons

Aromatic hydrocarbons have benzene ring structure in the molecule. Aromatic hydrocarbons are insoluble in water, but soluble in organic solvents. Generally, aromatic hydrocarbons are lighter than water. The boiling point increases with the relative molecular weight. The melting point is related not only to the relative molecular weight, but also to the structure.

2.1.3 Additives for Gasolines

There are several kinds of additives to gasoline. Those additives could improve the performances of gasoline in terms of preservation, transportation and combustion.

Table 4 Gasoline additives and purposes [24]

Additives	Chemicals	Purposes
Antioxidants	Aromatic amines, hindred phenols	To prevent reaction between alkanes and oxygen in air
Corrosion inhibitors	Carbonxylic acids and carbonxylates	To decrease the tendency of transportation pipes corrosion from free water in gasoline
Demulsifiers	Polyglycol	To stop the formation of emulsions
Anti-icing	Surfactants, alcohols and glycols	To stop the formation of ice in the carburetor and fuel system
Dyes and markers	Solids or liquids which are soluble in gasoline	To make various kinds of gasoline distinguishable visually
Drag reducers	Polymers with high molecular weight	To enhance the fluid flow characteristic of petroleum products with low viscosity

2.1.4 Physical Properties of Gasoline

EN228 gasoline properties standard in a nutshell

The European Union (EU) implemented a series of improvements on fuel quality in the past decades. Those improvements enabled achievements of less exhaust emission and more stringent emission standards. With those strict emission standards, the sulfur content, for example, has declined a lot. [28]

The standard of gasoline quality was firstly introduced in EU back to 1993. However, at that time, this standard was not mandatory. After that, in 1998, compulsive fuel regulations were firstly set. Further revision of fuels properties regulations were made gradually after the initial version was set. And in 2009, it's worth noting that there was a low-carbon fuel regulation added to the original regulations. From that time, the EN228 gasoline properties standard in EU aims at not only the reduction of exhaust emissions, but also the decrease of CO2 emission. The following table express the detailed limits data of each single parameter of gasoline in 2008. [28]

Table 5 EEN228 Gasoline properties standard in 2008 [29]

Parameter	Unit	The minimum limit	The maximum limit
Research octane number		95	
Motor octane number		85	
Vapor pressure in summer	kPa	-	60
Distillation		46.0	
percentage evaporated at 100 degrees	volumetric percentage	75.0	
percentage evaporated at 150 degrees	volumetric percentage	-	18
Density at 15 degrees	kg/m^3	720	775
Hydrocarbon analysis			1
Olefins	volumetric percentage	-	18
Aromatics	volumetric percentage	-	35
Benzene	volumetric percentage	-	1
Oxygen content	%m/m		3.7
Oxygenates			
Methanol	volumetric percentage		10
Ethanol	volumetric percentage		12
Iso-propyl alcohol	volumetric percentage	-	15
Tert-butyl alcohol	volumetric percentage	-	15
Iso-butyl alcohol	volumetric percentage	-	22
Ethers containing five or more carbon atoms per molecular	volumetric percentage	-	15
Other oxygenates	volumetric percentage	-	15
Sulphur content	mg/kg	-	10
Lead content	g/L	-	0.005

Auto-ignition temperature

Auto-ignition temperature is the lowest temperature at which the process of heat-generation from combustion is faster than the process of heat-loss to air.[7] It is impossible for fuel-air mixture to combust continuously below the ignition temperature unless extra heat is offered. [27]

Flammability limits

Fuels can combustion self-sustainably when the air-to-fuel ratio ranges between the upper flammability limit (UFL) and the lower flammability limit (LFL) at standard temperature and pressure conditions. Alternations of temperature and pressure cause alternations of those two flammability limits.

With the increase of the air-fuel mixture temperature, the UFL increases and the LFL decreases. Or in a word, higher mixture temperature widens the flammability limits range. As the pressure of the air-fuel mixture declines, the flammability limits range narrows with the upper limit declining and the lower limit rising. When the pressure goes higher than the atmospheric pressure, the flammability limits range widens with the lower limit remaining relatively stable. [27]

The ignition temperature and flammability limits measure the ignition property of fuel.

Heating Value

Heating value is as called as caloric value or heat of combustion as well. It represents the thermal energy released during the combustion process of certain amount of a combustible substance. There are two types of heating value. One is higher heating value (HHV), the other one is lower heating value (LHV). Higher heating value consists of the thermal energy released during a complete combustion during with all products from this complete combustion process are brought to initial pre-combustion temperature, and the thermal energy from condensation of produced vapor. As for lower heating value, the thermal energy from condensation of produced vapor is not included. This treats any formed water as vapor. Thus, the relation between HHV and LHV can be concluded as:

$$HHV = LHV + lantent\ heat\ of\ water\ vapor \tag{2.4}$$

Density

The density of gasoline is the ratio of its mass to its volume at a given temperature. Generally, the density of gasoline is lower than water's density. According to EEN228 standards, at 15C, the density of the gasoline ranges between 720 and 775 kg/m3. The density of the gasoline is strongly related to the energy content. Higher density means more combustible substances at the same volume of a fuel.

Volatility related properties

Vapor pressure, distillation temperatures, driveability index and vapor-liquid ratio are gasoline's properties related to volatility. The vapor pressure of a substance, also called as the saturated vapor pressure, is the pressure at which the equilibrium between the gaseous phase and the non-gaseous phase is achieved [25]. Temperature can indicate the volatility of a substance. For example, temperatures at which respectively 10 volumetric percent (v%), 50 volumetric percent and 90 volumetric percent of gasoline evaporates are utilized to measure the gasoline volatility. Those temperatures can be expressed as $T10$, $T50$ and $T90$, defining another one index indicating the gasoline volatility: driveability index (DI). Driveability index was created by the ASTM Driveability Task Force. [25] Driveability index is expressed as [25]:

$$DI = 1.5 \times T10 + 3 \times T50 + T90 \tag{2.5}$$

At certain temperatures, the vapor-liquid ratio in critical parts of the fuel system can express gasoline vaporization tendency as well. [25]

Higher vapor pressure and low $T10$ are beneficial to ease of cold starting. They could contribute to vapor sealing and vapor formation in the fuel system under high temperature operation. Thus, adjustments to vapor pressure and $T10$ of gasoline according to temporal conditions in a year are necessary in order to keep satisfying engine performance.

When fuel changes its state from liquid to gas in the fuel delivery system, it can decrease the feed pressure to carburetor or fuel injection system. Due to the loss of feed pressure, temporal power loss or even stalling may occur. This kind of problem is defined as vapor locking. Under the locking conditions, vapor pressure alone is not a good index indicating gasoline volatility tendency. The temperature at which vapor-liquid ratio is 20 under atmospheric pressure condition, is a better index of gasoline vapor locking performance. With lower temperature at which vapor-liquid ratio is 20, vapor locking related issues tend to occur. [25] For fuel-injected vehicles, vapor locking is less problematic since extra pressure is imposed on the fuel system. Instead, if the gasoline is too volatile, vehicles can be difficult to start. Idling related problems will happen as well. In an extreme case, the vehicle would not start.

$T10$, $T50$ and $T90$, those three temperatures indicate the warm-up performance under cold operation conditions. Among those three special temperatures, $T10$ is related to the cold-start of a car. If the $T10$ is relatively low, it is easier to cold start an engine. However, if the $T10$ is too low, fuels in pipes may evaporate due to the thermal energy from high-temperature components of the engine, producing unnecessary vapor. The unnecessary vapor may stop fuels entering into combustion chamber, causing ignition issues, affecting engine performance in a bad way.

The $T50$ is related to engine warming-up time, acceleration as well as the working stability. The $T50$ marks the average evaporation property. Gasoline with a reasonably lower $T50$ tend to be more volatile, which means larger amount of fuel evaporate, mixing with the air. As a consequence, engine warming-up time shortens. Moreover, the required air-fuel mixture can be supplied in time when the engine working load transmits from lower to higher.

$T90$, together with the boiling point, are indicators to the amount of substances with a high boiling point and a high molecular weight. When $T90$ is relatively low, the fuel contains fewer heavy components. Fuels entering the cylinder can completely volatilize, which is beneficial to the fuel process. However, if this temperature is too high, the fuel contains more heavy components, which are not easy to volatilize and further adhere on the cylinder wall. Carbon deposition might occur after combustion, those deposits flow along the cylinder wall into the oil sump, diluting the oil and damaging the lubrication system consequently. In addition, incomplete combustion of heavy components result in higher hydrocarbons emissions.

The DI is obtained by $T10$, $T50$ and $T90$, thus, it can well-roundedly express distillation performance of gasoline. Gasoline with lower DI values is with better volatility. During the wintertime, greater volatility enables a car with a easier starting. If the driveability index is higher, which means the volatility of the gasoline is worse, car cold-start and warm-up driveability can be worse. [25]

Latent heat and heat of evaporation

Latent heat of a substance means the heat released or absorbed when the phase changes under a constant temperature condition. [26] The process from liquid phase to gaseous phase is endothermic, so is the process from solid phase to liquid phase. While the process from gaseous to liquid phase is exothermic, as well as the process from liquid phase to solid phase.

The heat evaporation of gasoline indicates specifically the thermal energy absorbed when the phase switches from liquid to gaseous. With higher heat of evaporation, more energy is required to produce the same amount of fuel-air mixture vapor. Thus, the formation of air-mixture decreases, affecting the cold-start of cars and the acceleration process.

Viscosity

The viscosity measures a liquid's resistance to deformation. Informally, the viscosity can be considered as the concept of "thickness". High-viscosity liquids are less likely to flow. Liquids with low viscosity tend to flow. For example, pouring water from high place can cause water-spraying, however, when the oil is poured from high position, it drops slower compared with water, and it barely sprays.

Compared with viscous lubricates, the viscosity does not influence gasoline's quality that much. [22] The gasoline has a typical viscosity of around 0.5 centistokes (cSt) under atmospheric conditions. As for the viscosity of water, it is around 0.9 cSt at ambient temperature. Therefore, the gasoline is even less viscous than water. Besides, viscosity of the gasoline is not sensitive to temperature, it does not alter dramatically with the change of temperature.

Lead content

Concerning the grievous pollution issues related to the lead, lead-gasoline gradually fade away. The vanishing of lead-gasoline is mainly reflected in road vehicles. In terms of agricultural equipment, gasoline with lead still works. [25] According to EN228 standards, the maximum lead content limit is 0.005 grams per liter.

Sulfur content

Similar to lead, sulfur can cause serious pollution to environment as well. After combustion, sulfur could form sulfur oxides, such as sulfur dioxide and sulfur trioxide. Sulfur dioxide in the atmosphere is further oxidized by oxygen, producing sulfur trioxide. Sulfur trioxide is one of the main sources of acid rain formation. The acid rain damages the acid-base balance of soil, and causes irreversible harm to the environment consequently.

Gum

Gum is formed by the oxidation reaction between gasoline and air. During long-term storage or transportation, gum tend to form due to long-term presence of gasoline and air. There are other kinds of products after the oxidation reactions, gum is the only insoluble in gasoline. Those insoluble residues could build in the fuel system, and even block the fuel system. [25]

2.2 Internal Combustion Engines

2.2.1 Engines and Internal Combustion Engines

An engine is a machine that converts one form of energy into mechanical energy. An engine can be called as a motor. There are several types of engines: heat engines, non-thermal chemically powered engines, electric engines, physically powered engines, etc. The energy source (input) and the motion created (output) are two main criteria for engine categorization. The detailed categorization of engines is represented in the following graph.

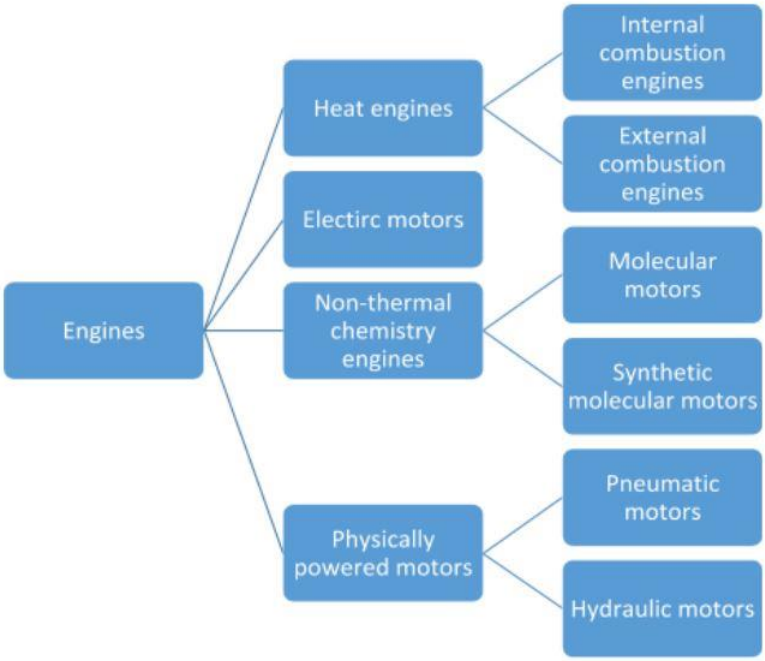

Figure 1 Engine categorization

Heat engines, driven by thermal energy together with chemical energy, output mechanical energy to do mechanical work. This process is achieved by the descending temperature alteration of a working substance. In order to bring the working substance to high temperature state, a thermal energy source is employed.

Heat engines can be categorized further: internal combustion engines and external combustion engines. Internal combustion engines (ICE), as the name implies, consume fuels inside the engine. As for the external combustion engine, for example the steam turbine, produces mechanical work by the expansion process of steam. Even though the expansion process of steam happens inside the steam turbine, the steam is formed in a boiler, the combustion process occurs “externally”, but not in the steam turbine.

2.2.2 Piston Engines, Reciprocating Piston Engines and SI Engines

Combustion engines are piston engines. In piston engines, energy is transferred between a fluid and a moving displacer (for example, a piston). Energy can pass from a

fluid to a piston, and vice verse. In a piston engine, piston moves periodically, resulting in continuous energy transformation processes. Pistons can be classified as reciprocating displacer engines and rotary displacer engines. in terms of the movement of the displacer. [30]

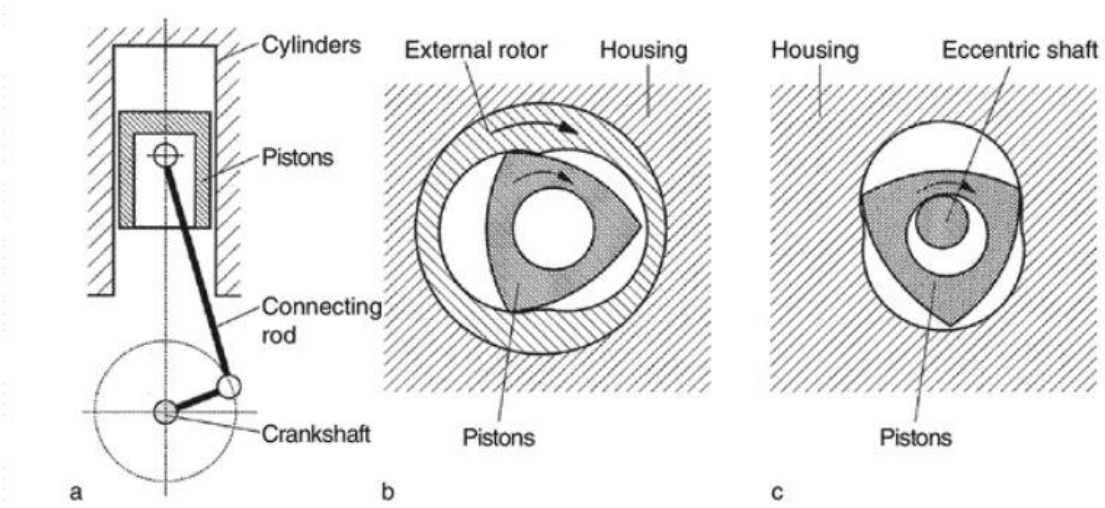

Figure 2 Working principals for piston engines [30].

a. reciprocating displacer engine. b and c. rotary displacer engines

In a reciprocating displacer engine, the piston in cylinders moves upward and downward, accepting energy from fuels combustion process in the cylinder and passing energy to the crankshaft through the connecting rod. The detailed working principle of a reciprocating displacer engine will be illustrated later in this thesis.

For rotary displacer engines, they can be sub-classified into rotary engines and planetary engines. [30] The rotary engine consists of external rotor, pistons and housing. The internal and external rotors both rotate with a fixed point. The planetary rotary engine has the following components: a fixed eccentric shaft, a piston and the housing. It is noticing that in a planetary rotary engine, the piston is the only part which moves. Those two kinds of rotary displacer engines have the similar internal structure.

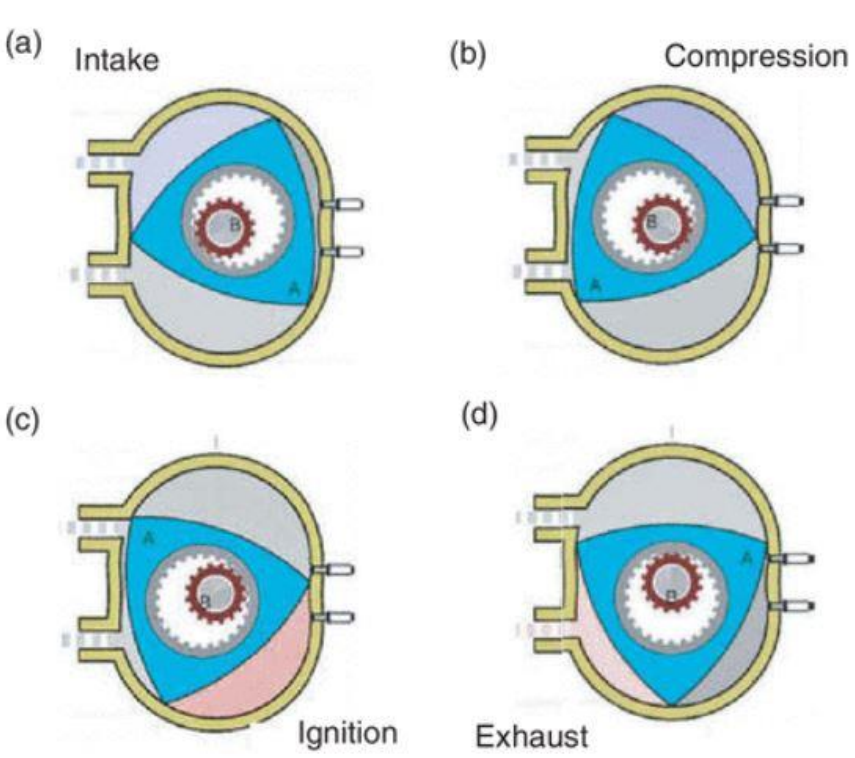

Figure 3 Wankel engine: a planetary rotary engine's working process [31]

Figure 3 shows the working principle of a Wankel engine, which is a planetary rotary engine.

Intake phase:

The intake phase or one working cycle starts when one of the tips of the rotator passes the intake port. With the further movement of the rotator, the volume of chamber increases, intaking the air-mixture into the chamber. When the next tip of the rotator passes the intake port, the chamber is hermetic, the intake phase ends and the next stage starts.

Compression phase:

At this stage, the air-fuel mixture is compressed since the volume of chamber decreases. When the chamber volume reaches to its minimum, the face of the rotator faces towards spark plugs. At the same time, the fuel-air mixture is exposed to spark plugs. This stage ends.

Combustion phase:

The combustion process occurs in this stage. After ignition, the flame inside the chamber propagates, creating heat energy and gaseous products. The gaseous mixture in the chamber expands a lot due to both the released energy and the newly-produced products. Thus, the rotator is forced to continue moving, and heat energy is transformed into rotary energy (or mechanical energy) by the rotator and the eccentric shaft. Under most of the cases, a rotary engine is equipped with dual spark plugs. [31] The reason is the combustion chamber of a rotary engine is narrow and long, weakly making the flame propaganda. Two spark plugs enable the flame spreading faster. This stage ends at the point when the tip passes the exhaust port.

Exhaust phase:

This phase starts when the tip passes the exhaust port. Since the gaseous mixture in the combustion chamber is with very high pressure, they will flow naturally out of the combustion chamber. Besides, the chamber shrinks with the motion of the rotator, the residual exhaust gas would be pushed out of the chamber. When the chamber reached its minimum volume, one working cycle ends.

2.2.3 Working Principles of SI Engines

Nowadays, reciprocating displacer engines are dominating internal combustion engines, and many vehicles are running with reciprocating displacer engines. [32] In terms of the ignition method, reciprocating displacer engines are be classified as spark-ignited engines (SI engines) and self-ignited or compression ignited (DI engine). Reciprocating displacer engines can be categorized into 2-stroke cycle engines and 4-stroke cycle engines further. [30]

Otto cycle is the principle of a 4-stroke SI engine operation. (The SI engine refers to the 4-stroke SI engine in this thesis). It is an ideal thermodynamic cycle that illustrates the gas conditions changes in SI engine cylinder. Picture shows how the in-cylinder pressure and temperature of gas change within an Otto cycle.

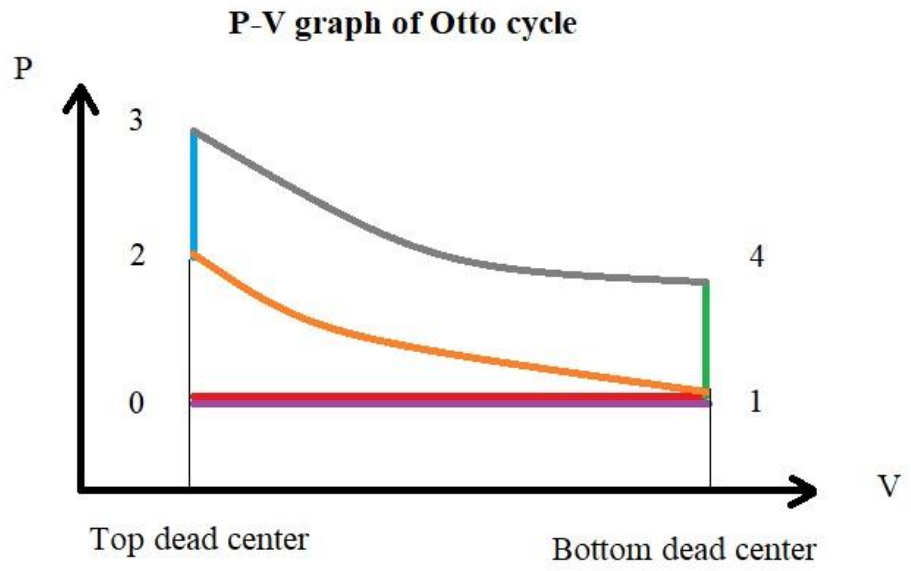

Figure 4 p-V graph of an ideal OTTO cycle

Phase 0-1 describes the intake process of working gas, also called as intake stroke. At the point 0, the intake valve opens, gas with atmospheric pressure is drawn into the cylinder, where the in-cylinder pressure is constant. After that, when it comes to point 1, the intake valve closes, the gas-intake process ends. [33]

Phase 1-2 is the compression phase, or compression stroke. After the intake valve closes, the piston moves from the bottom dead center (BDC) position, where the in-cylinder volume is maximum, V_{max}, to the top dead center (TDC) position, where the in-cylinder volume reaches to its minimum, V_{min}. During this isentropic phase, the

gas is compressed by the piston, and the mechanical energy is transformed to the gas. This isentropic stroke is assumed without the friction between cylinder walls and piston. Therefore, all mechanical energy goes to gas. Besides, there is no heat energy exchange involved with gas. The ratio maximum in-cylinder volume to the minimum in-cylinder volume is defined as the compression ratio (CR), this term is associated with knocking tendency. [30] At the end of this stroke, the in-cylinder gas is ready to be ignited.

Phase 2-3 illustrates the ignition instant. Within this short time, the piston position is a bit front of the TDC position. The gas is ignited by the spark plug, with a certain amount of energy acquired from the spark plug. Then the in-cylinder pressure increases substantially in an instant while the gas stays stable in terms of volume.

From state point 3 to state point 4, the in-cylinder gas goes through the expansion process, this process is called as power stroke. During this stroke, high pressure combustion gas drives the motion of piston from TDC position to BDC position, with heat energy from combustion transforming to mechanical energy through motions of piston and crankcase. This stroke is also assumed to be adiabatic, the friction between the cylinder wall and the piston is not considered, and energy is transferred only in the form of combustion heat and mechanical energy. At the end of this stroke, the in-cylinder volume reaches to its maximum Vmax again during an OTTO cycle,

Phase 4-1 is an instant phase, called ideal heat rejection phase, when the piston position is around the BDC. In this phase, the in-cylinder gas remains volumetrically constant, with a certain amount energy removed to an external sink ideally.

Phase 1-0 is the last phase of an Otto cycle, this phase is called as exhaust stroke. At the state point 1, the exhaust valve opens, gas is emitted to the atmosphere. The in-cylinder pressure is constant. After that, when it comes to state point 0, the exhaust valve closes, the stroke ends, and another one Otto cycle will start.

After one ideal Otto cycle, the in-cylinder conditions are the same as the initial state, and there is no net energy change in this system:

$$E = E_{in} - E_{out} = 0 \tag{2.6}$$

where E_{in} indicates the energy introduced to this system during compression stroke and ignition, E_{out} represent the energy rejected from the system during power stroke and heat rejection phase. Those two terms can be illustrated further:

$$E = E_{in} - E_{out} = 0 \tag{2.7}$$

$$E_{in} = W_{1-2} + Q_{2-3} \tag{2.8}$$

$$E_{out} = W_{3-4} + Q_{4-1} \tag{2.9}$$

where W_{1-2} means the energy passed to this system from piston, Q_{2-3} means the heat energy from combustion process, W_{3-4} is the energy consumed on the piston motion from gas expansion, and Q_{4-1}means the thermal energy rejected from this system.

The thermal efficiency of the Otto cycle is defined by the ratio of work done by this system to the input thermal energy. The thermal efficiency can be expressed as:

$$\eta = \frac{Work\ output}{Heat\ input} = \frac{Q_{2-3} + Q_{4-1}}{Q_{2-3}} = 1 + \frac{Q_{4-1}}{Q_{2-3}} \tag{2.10}$$

$$Q_{2-3} = \int_{T_2}^{T_3} C_v dT = C_v(T_3 - T_2) \tag{2.11}$$

$$Q_{4-1} = \int_{T_4}^{T_1} C_p dT = C_p(T_4 - T_1) \tag{2.12}$$

Thus, the thermal efficiency of OTTO cycle also can be expressed as:

$$\eta = 1 - \frac{T_4 - T_1}{T_3 - T_2} \tag{2.13}$$

As it was mentioned before, the compression stroke (phase 1-2) and the power stroke (phase 3-4) are both isentropic. Thus, pressures and temperatures related to those two strokes fulfill the following equations:

$$\frac{T_4}{T_3} = \left(\frac{p_4}{p_3}\right)^{\frac{\gamma-1}{\gamma}} \tag{2.14}$$

$$\frac{T_4}{T_3} = \left(\frac{V_3}{V_4}\right)^{\gamma-1} \tag{2.15}$$

$$V_2 = V_3 \tag{2.16}$$

$$V_1 = V_4 \tag{2.17}$$

$$\frac{T_4 - T_1}{T_3 - T_2} = \left(\frac{V_2}{V_1}\right)^{\gamma-1} \tag{2.18}$$

$$\gamma = \frac{c_p}{c_v} \tag{2.19}$$

where γ is the specific heat ratio, c_p is the specific heat under constant pressure, and c_v is the specific heat under constant temperature. V_2 and V_1 indicate the minimum and the maximum in-cylinder volume, V_{min} and V_{max} respectively, the ratio of V_{max} and V_{min} is define as compression ratio, r. Thus, the thermal efficiency of the otto cycle can be deduced as:

$$\eta = 1 - \left(\frac{1}{r}\right)^{\gamma-1} \tag{2.20}$$

$$r = \frac{V_{max}}{V_{min}} \tag{2.21}$$

The thermal efficiency of Otto cycle is relative to the compression ratio of an engine.

2.2.4 Actual Otto Cycle

Under real operation conditions, the working cycle of a SI engine do not follow the ideal Otto cycle. Figure x illustrates the relation between the in-cylinder pressure and the in-cylinder temperature of an actual Otto cycle. [34]

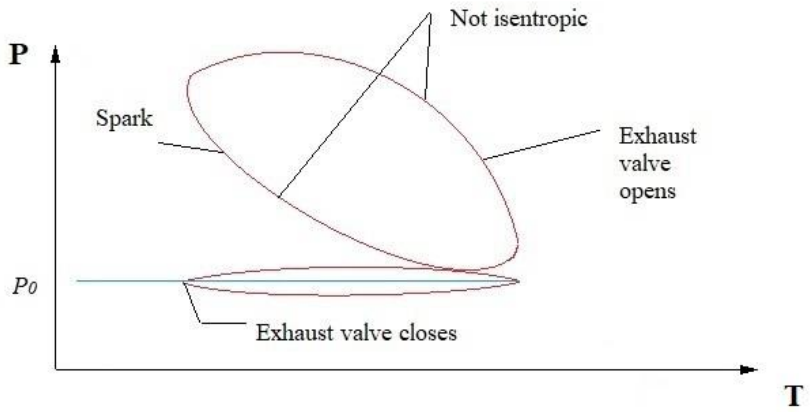

Figure 5 p-V graph of an actual Otto cycle

Under real operation conditions, the compression stroke is not isentropic. Part of the mechanical energy from piston results from the friction between cylinder walls and the piston. Thus, the lubricant is hired to reduce the friction in real engine operation. Besides, the sparking can happen before the timing of spark. In addition, in-cylinder flame propaganda takes time. Thus, the combustion process overlaps with the compression stroke and the power stroke.

For the power stroke, it is not isentropic neither. Partial thermal energy from the combustion process is lost to the lubricant and atmosphere through the cylinder wall. The exhaust valves can open earlier before the piston reaches to the position of BTC.

During the intake stroke, the in-cylinder pressure is lower than the atmospheric pressure, while during the exhaust, the in-cylinder pressure is higher that the atmospheric pressure.

2.3 Octane Number Rating

2.3.1 Knocking and Super-knocking

Knocking is related to the noise resulted from abnormal combustion process in cylinder. There are several terms describing the knocking phenomenon in other literature, in this thesis, ‘knocking’ is employed to describe this abnormal combustion phenomenon.

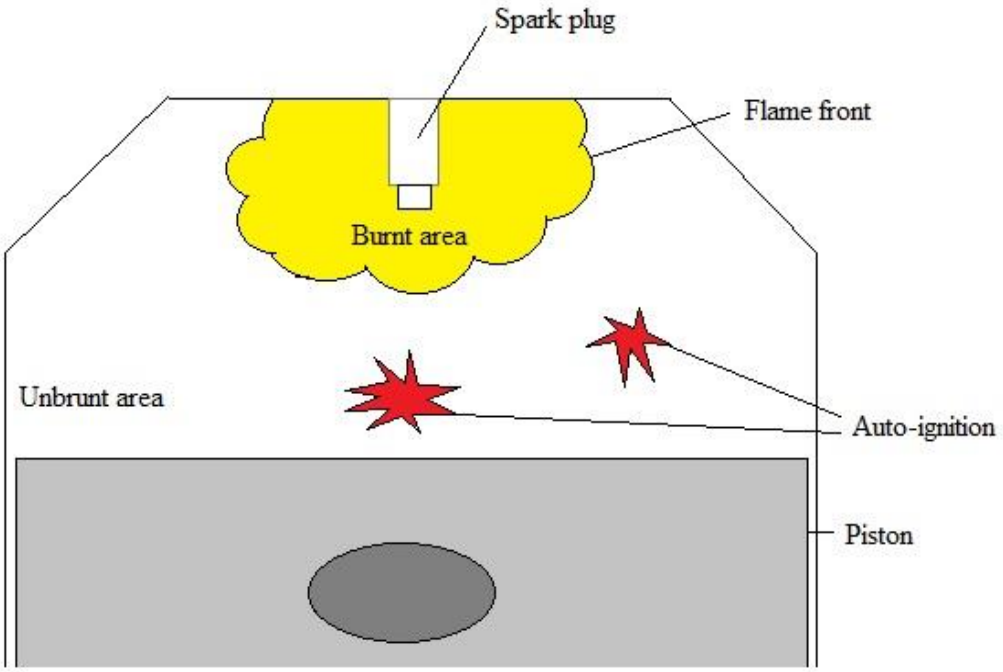

Figure 6 Knocking combustion in SI engines

The picture illustrates the formation of knocking phenomenon. After the sparking resulted from spark plug, the combustion process of air-fuel mixture starts, and the flame starts propagating inside the cylinder. With the expansion of burnt area, the flame front moves towards cylinder wall, passing heat energy from the burnt zone to the unburnt zone. This stage is called as flame propagation. After this stage comes the end-gas auto-ignition phase. When the temperature in the unburnt zone reaches to the auto-ignition point, auto-ignition occurs, causing pressure oscillation in the combustion chamber and detectable noise in the combustion chamber further. In conclusion, knocking phenomenon results from the auto-ignition of the unburnt zone in a combustion chamber. [35]

More information on knocking phenomenon is presented in **Figure 6**. And in this Figure, a few parameters related to knocking need to be illustrated. CA_{ko} is the onset of pressure oscillation, it indicates the crank angle where pressure in the cylinder start oscillating. p_{ko} is the pressure when pressure oscillation is firstly detected. p_{max} is the highest pressure detected in a cycle, and Δp is the difference p_{max} and p_{ko}. In addition, heat release rate (HRR), the temperature of unburnt gas ($T_{unburnt}$), maximum pressure rise (Δp) and knocking intensity (KI) are four important parameters. They can characterize the knocking. [35].

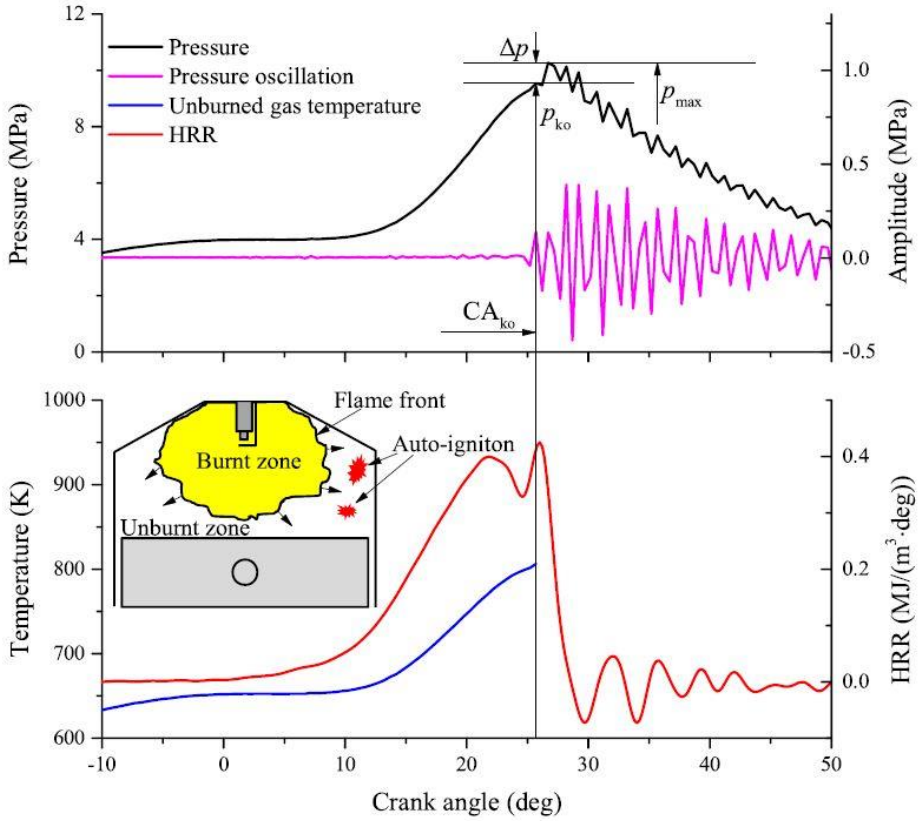

Figure 7 Pressure oscillations and heat release rate when knocking happens

The picture shows pressure oscillations and how knocking-related parameters change when knocking occurs. From the crank angle of ignition to the crank angle of CA_{ko}, which is also called as the flame propagation phase, the pressure, the HRR and the unburnt gas temperature in cylinder generally increase. It is noticing that the HRR experiences a small drop before reaching to the CA_{ko}. The dropping of the HRR before the CA_{ko} results from the downward movement of the piston. [35]

The phase after the CA_{ko} is called as end-gas auto-ignition phase. In this phase, the knocking starts, and the pressure in cylinder reaches to the higher-pressure peak of p_{max} within a very short period. After that the pressure shows a general declining trend with oscillation. Besides, the amplitude of pressure oscillation also decreases gradually. It can be seen that after the knocking, the pressure fluctuation becomes less and less severe. It can be deduced that once the end-gas is auto-ignited, the pressure wave from auto-ignition will reflect back to the pressure wave from burnt area, resulting in pressure oscillation in the cylinder. Then, those two pressure waves from different sources continue interacting with each other, and they neutralize each other gradually, easing the pressure oscillation eventually. The HRR in this phase shows first a dramatic decrease then a fluctuation trend. The HRR receives great effects from the knocking. [35]

2.3.2 RON, MON and Testing Conditions

As it is mentioned above, knocking phenomenon is considered as disadvantageous to engine performance. It can affect the engine efficiency, improve the fuel consumption and cause severe damages to combustion chamber. Consequently, a fuel's resistance to knocking is of great importance. A fuel's octane number is the index which quantifies its anti-knocking property. [17]

There are two kinds of octane number: research octane number (RON) and motor octane number (MON). The process of testing a fuel's octane number is called as octane number rating, or knocking rating.[36] The RON is tested under mild driving conditions, while the MON is tested from more severe engine operation conditions. Those two octane numbers, RON and MON, are tested under the D2699 and D2700 standard testing conditions respectively. Compared with the RON test conditions, there are three features about the MON test conditions:

The engine speed is increased from 600 rpm to 900 rpm. The air entering into the cylinder is preheated to 149 degrees. And the spark timings are generally ahead of 13 degrees before the TDC. The detailed testing conditions are listed in **Table 6**. [37][38]

Table 6 Standard octane numbers test conditions [37][38]

	RON	MON
Engine speed [RPM]	600	900
Intake air temperature [℃]	51.7	38
Intake mixture temperature [℃]	Not specified	149
Intake pressure	Atmospheric	Atmospheric
Spark timing [°]	-13 before the top dead center	Various, related to the compression ratio

The engine speed is only 600 RPM under RON test conditions, and the intake air temperature under RON test conditions is required to be 51.7℃, which is higher than that under MON test conditions. Those differences indicate that the RON is acquired under milder test or engine operation conditions.

There are other parameters which can measure a fuel's resistance to knocking, for example, octane index and octane sensitivity.

2.3.3 The CFR Engine

The CFR engine, also called as octane rating engine, is utilized to measure a fuel's octane number and to detect a fuel's knocking tendency. It is a single cylinder SI engine equipped with a series of sensors. In this thesis, engine modelling and simulations were implemented based on F1/F2 CFR engine from Waukesha. The F1/F2 CFR engine from Waukesha has the following features: a cylinder with an adjustable cylinder head, a four-bowl falling level carburetor, a powerful crankcase and the exhaust tank systems.[39] Among those features, the adjustable cylinder head in the cylinder makes the CFR engine distinguishing from other conventional SI engines.

The cylinder of F1/F2 CFR engine is equipped with a height-adjustable cylinder head, enabling the engine can be operated with various compression ratio. During an octane rating test, the compression of cylinder is related to the reference fuel's octane number. With higher octane number of the reference fuel, the compression ratio needs to higher. This height-adjustable cylinder head makes it possible to run octane rating tests under different conditions.

The crankcase of a CFR engine is with a heavy-duty design. [39] A CFR engine will go through octane number rating tests many times, and during those tests, the knocking phenomenon happens in the cylinder, resulting in pressure oscillations and unstable crank motions. Those unconventional combustion processes cause bad effects on conventional SI engines. However, for the CFR engines, unconventional combustion processes are 'conventional', thus, a strengthful and rigid crankcase is required for the CFR engine. Besides, side doors of the CFR engine crankcase can be removed, making it convenient to inspect, maintain and repair the internal part. [39]

2.3.4 Octane Number Rating Process

In order to test a fuel's octane number on a CFR engine, the reference fuels are employed. The reference fuels refer mainly to iso-octane and n-heptane. The chemical structures of iso-octane and n-heptane are shown in **Figure 8**.

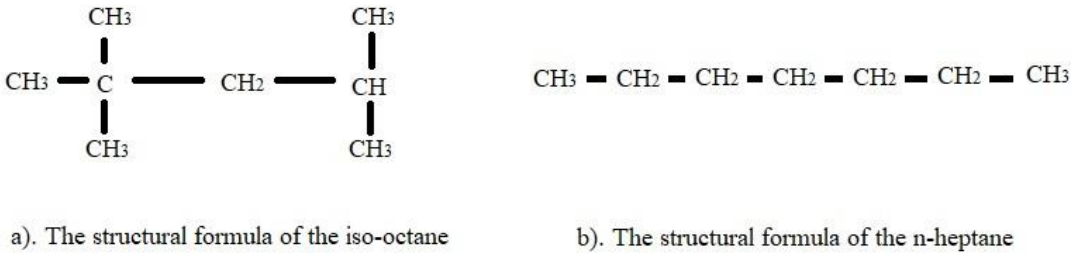

Figure 8 Structual formulas of iso-octane (a) and n-heptane (b)

In 1926, Graham Edgar tested gasoline's anti-knocking property by mixing gasoline with various volumetric percentage of iso-octane and n-heptane. He noticed that when the iso-octane is blended into gasoline, the knocking does not happen. This work revealed the importance of iso-octane in terms of knocking prevention and initialized the octane rating. [22] If a CFR engine runs with iso-octane only under certain conditions, producing a certain level of engine performance, this performance is defined as octane number 100. When the n-heptane is the only fuel for engine test under the same conditions, the engine performance produced is regarded as octane 0.

Detailed processes of the octane number rating assisted with a CFR is expressed in pic. The CFR engine firstly run with the fuel whose octane number is unknown. By adjusting the cylinder head, the compression ratio of the CFR engine changes. Under various compression ratio, engine performances with the same fuel are different. Under a certain compression ratio, a certain intensity of the knocking phenomenon will be detected by the knocking sensor equipped on the CFR engine.

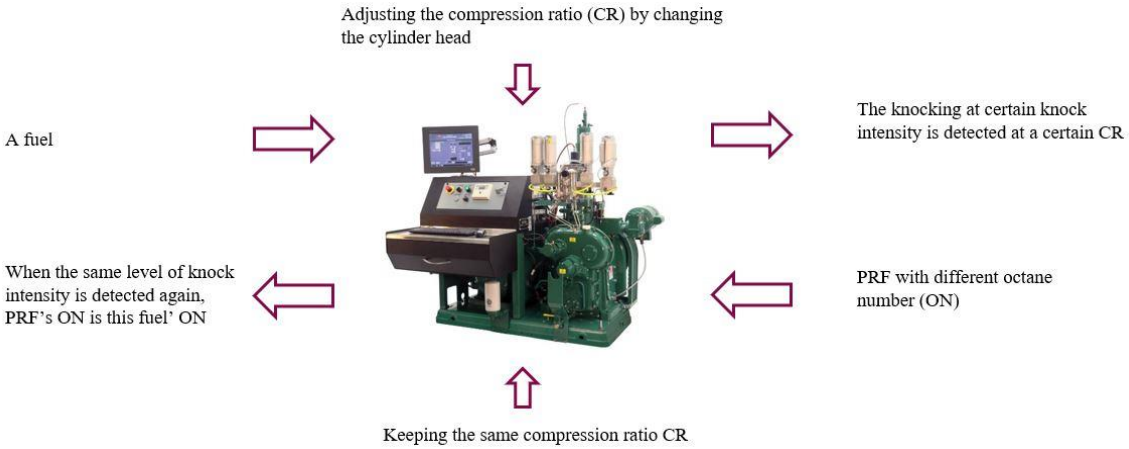

Figure 9 The process of octane number rating

Then, the CFR engine starts running again but with primary reference fuels of different octane numbers under the same compression ratio condition. When the same level of knocking intensity is detected again, the octane number of the primary reference fuel is the octane number of the unknown fuel.

2.4 Gasoline Surrogates

Surrogates of gasoline are certain blends of hydrocarbons utilized to replace the gasoline in experimental or numerical studies. As it is mentioned above, gasoline is a complex chemical mixture containing many kinds of components. During the combustion process, oxidation reactions of those components interact with each other, resulting in the emerging of many new components. These factors contribute to the complicatedness of the specific chemical reaction combustion mechanism of gasoline. Besides, the gasoline is with many physical and chemical properties, among which only few are focused on a research project. For example, laminar flame speed is essential in a knocking related research since the laminar flame speed is an indicator of the flame front speed. Thus, it is not necessary to investigate on all the properties of gasoline. Consequently, various gasoline surrogates are employed to emulate gasoline's properties. [40] So that researchers and engineers can only focus on a few of physical or combustion related properties of fuels by certain pattern of surrogates formation. The ASTM standard test methods are designed for measuring fuels' parameters in standard ways. [41] summarized some ASTM methods the corresponding fuels' properties.

2.4.1 Primary Reference Fuels

PRF refers to primary reference fuels, consisting of isooctane and n-heptane. PRF are employed for the ASTM D2699 and D2700 test methods for measuring a fuel's RON and MON respectively. With the help of PRFs, a unknown fuel's octane numbers can be tested on a CFR engine. The result scale varies from 0 to 100. The name of PRF fuels can represent its research octane number. For example, PRF50 means its research octane number is 50. It contains 50% volumetric percentage of iso-octane, and 50% volumetric percentage of n-heptane. [42] Likewise, PRF95 has a research octane number of 95. It consists of 95% volumetric percent of iso-octane and 5% volumetric

percentage of n-heptane. The motor research octane number of PRF is defined as the same as its research octane number.

2.4.2 Toluene Reference Fuels

TRF refers to toluene reference fuels. The main components of TRF fuels are isooctane, n-heptane and toluene. TRF can be summarized as blends of PRF and toluene.

Toluene, also called as Methylbenzene, consists of a benzene ring and a methyl group. The exact structural formula of toluene is shown in picture. Toluene is a colorless aromatic hydrocarbon with special fragrance. It is liquid and easily volatile under atmospheric conditions. [45] Toluene has similar chemical properties with beneze, but it is not toxic, therefore, under many occasions, toluene can replace the beneze.

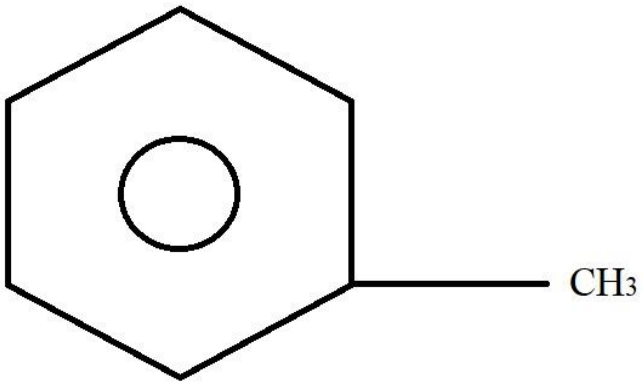

Figure 10 Structual formula of toluene

Many researchers have investigated octane numbers of toluene, **Table 7** lists toluene' octane numbers acquired from 3 references. From those measured data on toluene's octane numbers, it is obvious that toluene has very high octanes compared with conventional gasoline. Therefore, toluene is an ideal 'octane numbers booster' for gasoline, it can increase a fuel's octane numbers and thus it can improve engine performance by weakening the knocking tendency. TRF91-30 means this kind of fuel's RON is 91, but it is with 30%v of toluene content.

Table 7 Octane numbers of toluene from different references

RON	MON	References
121	107	[46]
120.1	103.5	[47]
124	112	[48]

2.4.3 Indolene

Indolene is produced from the petroleum refinery stream. It consists of several kinds of hydrocarbons. Thus, the indolene is not a chemical substance, but a mixture. It can be represented as $C_7H_{13.02}$ considering the ratio of carbon to hydrogen. [44] The production process of indolene is similar to that of commercial gasoline. Indolene was developed to reproduce emission qualities of gasoline in real engine tests. [49] Gasoline is one product from the petroleum refinery stream. The quality, properties of gasoline vary a lot with spatial and temporal factors. Due to this, indolene was formulated, and it was certified as a standard gasoline reference fuel to be implemented on engine tests by American Federal. [49]

Since the indolene is mixture produced from the petroleum refinery stream process, the complexity and instability of its components and properties also exist, just like gasoline. The fuel needs to go through several tests for physical, chemical and combustion properties. [49] And it is necessary that the reference gasoline for engine testing contains octane, so that it can represent commercially available fuels.[43] The test specifications applied on indolene include: distillation range, hydrocarbon composition, lead content, phosphorous content, total sulfur content and dry vapor pressure equivalent. [43]

In this thesis work, indolene is used to investigate how the physical properties affect the pre-combustion conditions. The octane number of indolene in this work is set as 91 to correspond to commercial gasoline.

Table 8 Several standard tests of gasoline properties from ASTM

ASTM Code	Description
D4814	Standard specification for automotive spark ignition engine fuel
D2699	Research octane number (RON)
D2700	Motor octane number (MON)
D4953, D5191	Vapor pressure
D86	Distillation
D4052	Density
D240	Heat of combustion and lower heating value (LHV)
D6730, D1319	Detailed hydrocarbon analysis (DHA)
D5291	Carbon and Hydrogen content (H/C)
D4815, D5599	Oxygenate content
D5580	Aromatic content
D6550	Olefin content

Table 8 presents some gasoline' properties various test method (an ASTM code indicated a certain test method). In order to acquire one property, certain surrogates are formulated in order to emulate this certain property. [41] When different target properties are taken in consideration, the formulation of surrogates will be complex. [41] Those selected surrogates need to be vertified and proven to be effective in terms of

combustion performance. [41] In this study, the effects of octane numbers and physical properties (density and heat of vaporization) on in-cylinder pre-combustion conditions are in the research scope, therefore, PRF, TRF, indolene are selected. Ethanol is also selected since it can affect fuels' octane numbers, and it is under widely commercial utilization.

2.5 The Intake System of the CFR Engine

Figure 11 shows the structure and the sectional view of the intake system of the CFR engine under RON testing conditions respectively.

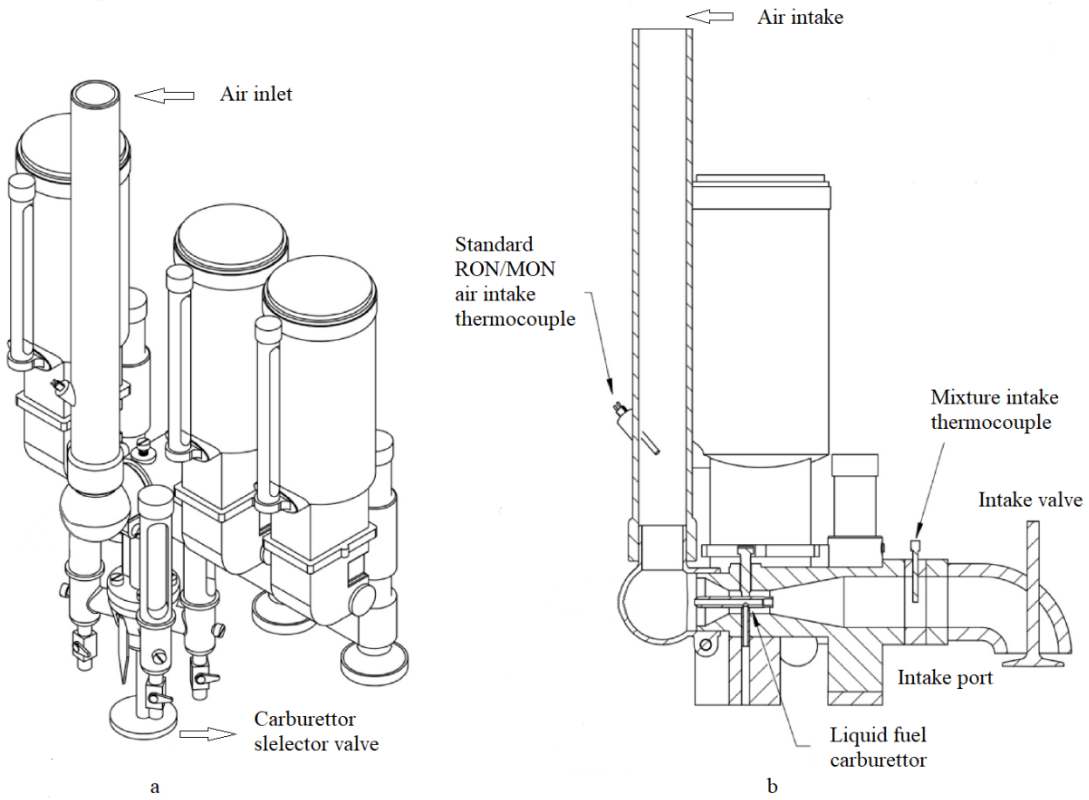

Figure 11 Schemtic (a) and sectional (b) diagrams of the CFR engine intake system under RON testing system, modified based on [13]

The CFR engine intake system comprises following parts: the intake manifold, the carburettor, injector for injecting liquid fuels, the intake port and the intake valve.

For the intake system with a carburettor, the intake air from is delivered from the atmosphere to the carburetor passing through an intake vertical pipe and an intake elbow. The carburettor works on the principle of a venturi pipe. The inhaled air is converged firstly, then the air flow flowing through the carburettor is accelerated through a narrow channel called a venturi pipe where the liquid fuel is injected. As the channel begins to diverge again, a vacuum will occur. It is this vacuum that draws fuel into the moving air column through the nozzle of the carburetor. The size of the injector is designed to allow a fairly precise amount of fuel to be drawn into the air stream, thereby creating a proper mixture of air and fuel. After that, air-fuel mixture passes intake port, intake port elbow and intake valve.

3 Methodology

In this section, a detailed methodology of the project is described. In order to complete this research project, the author has done a lot of theoretical reading and literature study. First, the author studied the basic structure of gasoline engine and the operating principle of combustion chamber. Then, the author makes a series of researches on conventional gasoline engine combustion and knock combustion. Then, the author collected data about CFR engine from different literatures, which were used to build the next model. Based on the data collected. Based on collected parameters, two CFR engine modellings under RON test conditions and MON test conditions respectively with GT-Power.

After the establishment of the models, three fuels are selected for simulation and compared the simulation results with the experimental data in the literature. After that, representative in-cylinder curves are revealed by simulations, together with the condition variations in the intake system. Then, to get the relationship between the combustion conditions and the octane number of the fuel, 4 groups, 19 kinds of fuels, are simulated. Finally, effects physical properties of the fuel (density and heat of vaporization) on in-cylinder conditions are analyzed based on simulation results based on simulations based on indolene.

3.1 Theoretical and Modelling Background

In this section, the basic theory on modelling work will be illustrated. Governing equation, discretization in terms of space and time, combustion model solver will be themes to further understanding.

Reynolds Transport Theorem

Reynolds transport theorem (RTT) is used to describe changes in fluid properties. Reynolds transport theorem is known as the transmission equation.

The transmission equation can be used to quantitatively describe the change of fluid properties in a flow field. For example, a control volume contains a certain fluid.

After a certain period of time, if the overall property B (also called as the extensive property) of the fluid in the control volume changes, the change must be caused by the following two reasons: (1) The overall property B may be affected by its own characteristics or external factors over a period of time. For example, the mass B can change over a certain period of time due to chemical reactions in the system. Under this circumstance, dB/dt is the rate of change in the mass of the substance. For another one example, B is the momentum of the fluid. Under the condition of external force, the momentum of the fluid will change. (2) Changes caused by fluid flow. The overall property alters depending on the inlet and outlet flow rate. When the overall property of the outflow control volume is greater than the inflow, the net outflow is positive, which will cause the overall property in the control volume to decrease. Conversely, if the inflow is greater than the outflow, the overall property will increase.

In order to understand the mathematic formulas of the Reynolds transport theorem, some terms will be introduced. The control volume (CV) is a fixed region in space where the system is considered as a certain amount of fluid. A piece of tube, a boiler or a heat exchanger can be analyzed as a control volume, and the fluid in the CV is

considered as a system. A boundary rounding the control volume is a control surface (CS). With those terms and their abbreviations, the Reynolds transport theorem can be expressed as:

$$\frac{\partial B_{sys}}{\partial t} = \frac{\partial \int_{sys} \rho b d\forall}{\partial t} \tag{3.1}$$

$$\frac{\partial B_{CV}}{\partial t} = \frac{\partial \int_{CV} \rho b d\forall}{\partial t} \tag{3.2}$$

$$\frac{DB_{sys}}{Dt} = \frac{\partial}{\partial t}\int_{CV} \rho b d\forall + \int_{CS} \rho b \boldsymbol{V} \cdot \hat{\boldsymbol{n}} d\forall \tag{3.3}$$

B in above equations indicates the extensive property, while b is the intensive property. The relation between B and b can be expressed as $B = mb$ where m is the mass of system. In formula, '$\frac{DB_{sys}}{Dt}$' means time rate of change of B in the system, '$\frac{\partial}{\partial t}\int_{CV} \rho b d\forall$' indicates the time rate of change of B in CV, and '$\int_{CS} \rho b \boldsymbol{V} \cdot \hat{\boldsymbol{n}} d\forall$' ($\hat{\boldsymbol{n}}$ is the unit vector in the n direction) is the net outflow rate of B. Here B can be mass, energy or momentum.

Governing equations

By rewriting RTT equations in terms of mass, energy and momentum, a set of equations can be deducted, which are Navier-Stokes equations. The Navier-Stokes equations are a set of descriptions of fluids like liquids and air. These equations establish the relationship between the rate of alteration of the particle momentum (force) of the fluid, the change of pressure acting inside the liquid, the dissipation of viscous force and gravity. These viscous forces arise from the interaction of molecules. It can also measure how viscous the liquid is. In this way, the Navier-Stokes equation can be expressed as the dynamic balance of forces applying on any given part of the liquid. These equations do not intend to establish the relationship between the variables being studied (like speed and pressure). But they intend to establish the relationship between the rate of change or flux of these quantities. Those equations are employed as governing equations for 1-D modelling in the GT-Power software. 1-D modelling is based on 1-D flows, which means the velocity at any location in the system depends on only the distance between this location and the centerline. [52]

In the CFR engine, the flow can be simplified as unsteady and compressible. Thus, the following Navier-Stokes equations will be written under the circumstance of unsteady compressible one-dimensional flow.

Mass Conservation [52]:

$$\int_{CV} \frac{\partial \rho}{\partial t} dV + \sum_{a} (\rho_a A_a \boldsymbol{V_a})_{out} - \sum_{b} (\rho_b A_b \boldsymbol{V_b})_{in} = 0 \tag{3.4}$$

The Momentum Equation [52]:

$$\sum F = \int_{CV} \frac{\partial}{\partial t} \rho \boldsymbol{V} dV + \sum_{a} (\dot{m}_a \boldsymbol{V_a})_{out} - \sum_{b} (\dot{m}_b \boldsymbol{V_b})_{in} \tag{3.5}$$

The Energy Equation [52]:

$$\dot{Q} - \dot{W}_s - \dot{W}_v = \frac{\partial}{\partial t}\left[\int_{CV}\left(\hat{h} + \frac{1}{2}\boldsymbol{V}^2 + \boldsymbol{g}z\right)\rho dV\right] + \int_{CS}\left(\hat{h} + \frac{1}{2}\boldsymbol{V}^2 + \boldsymbol{g}z\right)\rho V_b dA \qquad (3.6)$$

Where,

$$\int_{CS}(\hat{h} + \frac{1}{2}\boldsymbol{V}^2 + \boldsymbol{g}z)\rho V_b dA = \sum(\hat{h} + \frac{1}{2}\boldsymbol{V}^2 + \boldsymbol{g}z)_{out}\dot{m}_{out} - \sum(\hat{h} + \frac{1}{2}\boldsymbol{V}^2 + \boldsymbol{g}z)_{in}\dot{m}_{in}$$

Discretization

Discretization is the process of transferring continuous functions, models, variables, and equations to discrete equivalents. This process is usually the first step in making continuous functions, models, variables, and equations suitable for numerical computations and implementation on a digital computer. The discretization of a continuous can be both in time and in space. In a CFR engine, there are spaces in pipes, elbows and combustion chambers, those spaces can be discretized to several sub-volumes. This is discretization in space. Discretization in time occurs in each sub-volume. Computations on fluid propertied happen at each time step, which mean the whole process can be discretized in terms of time step.

For 1-D simulation or numerical computation in GT-Power, the natural continuous system is discretized into sub-volumes. The space of each object is divided into at least two sub-volumes. And all split flows are considered as a single volume at any time. At the boundary connecting adjacent sub-volumes, vector variables are calculated. Scalar variables are computed at the center of each sub-volumes. [52]

Mass flow rate, internal energy and density are the initial variables for the simulation process. Mass flow rate is defined by the input fuel delivery rate and air-to-fuel ratio. Internal energy and density of selected fuels and air are built-in from GT-Suite data library. The mass flow, internal energy, and density on each sub-volume side are fed into the mass conservation equation. So that the corresponding variable on the other side of each sub-volume can be calculated. [52]

The explicit methods calculate the state of a system at a later time from the state of the system at the current time. The momentum equation is computed on the border of every sub-volume considering the time step.

At each time step, the temperature and pressure of a sub-volume can be acquired. Based on Reynolds transport theorem equation and the energy balance equation, the mass and energy can be calculated. Those two variables yield the density then. The density and energy of a system are a function of the temperature and pressure of the system. The temperature and pressure of the system can be calculated from the density and energy given the state of the material components of the system. [52]

3.2 CFR engine Parameters and Modellings Under Two Conditions

In order to simulate a CFR engine on GT-Power, some data related to different parts of the CFR engine must be obtained. For the fuel systems, the length, diameter of straight

pipes and radius of the bending pipe are necessary. For the carburetor, it is divided to three pipes, one converging pipe, one venturi pipe and one diverging pipe, and each one of them requires detailed length and diameter. . For inlet valve outlet valves, the valve height changes with the angle of the cycle in the cylinder. For the cylinder, geometric data is also required. The main sources of these data were two pieces of reference and the D2699 and D2700 standard test instructions.[37][38] The geometric data of cylinder is listed in **Table 9**.

Table 9 Geometric parameters of the cylinder of the CFR engine [37][38]

Parameters	Value
Bore [mm]	82.5
Stroke [mm]	114.3
Connecting rod length	254
Compression ratio (CR)	Varies with fuels
TDC clearance height	114.3/(CR-1)
Head/bore area ratio	1
Piston/bore area ratio	1
Wrist pin crank offset	0
Stroke convention	True stroke
TDC angle convention	Piston position
Parameters	Value

The bore is the diameter of the cylinder. The stroke is the length of piston motion during a stroke, it is the difference the highest piston position and the lowest piston position. Connecting rod length is the length between the centers of the rod and piston-pin bearings [50]. TDC clearance height is the difference of height between the cylinder head and the highest piston position. Since compression ratio is the ratio of the maximum in-cylinder volume to the minimum in-cylinder volume, it can be expressed as the ratio of the highest piston position to the lowest piston position, which is:

$$R = \frac{Stroke + TDC\ clearance\ height}{TDC\ clearance\ height} \tag{3.7}$$

Therefore, the TDC clearance height can be calculated as 114.3/(CR-1). The cut-way view of a SI engine is shown as Figure 11, where those parameters above are intuitionstically showed.

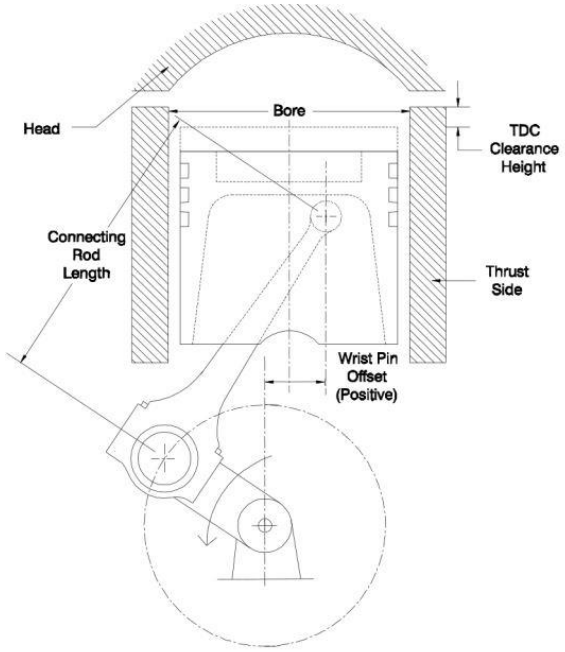

Figure 12 The cut-way view of a engine [50]

3.3 In-cylinder Heat Transfer Model

In this work, the selected heat transfer model of the cylinder is 'WoschniGT'. Under this heat transfer model, the in-cylinder heat transfer is calculated by a built-in formula. This build-in formula emulates the classical Woschni correlation without swirl.[33] The heat transfer speed is calculated by the following formula:

$$h_c\left(\frac{W}{m^2K}\right) = 3.26B^{-0.2}(m) \times p^{0.8}(kpa) \times T^{-0.55}(K) \times w^{0.8}\left(\frac{m}{s}\right) \tag{3.8}$$

where B is the bore of the cylinder, p is the in-cylinder pressure, T is the in-cylinder temperature. w is the average gas velocity in the cylinder. As is was mentioned before, the heat transfer rate under 'WoschniGT' model is calculated with the assumption of no swirl. Therefore, the mean gas velocity is defined by:

$$w = C_1 S_p + C_2 \frac{V_d T_r}{p_r V_r}(p - p_m) \tag{3.9}$$

where V_d is the displacement volume, p is the instant in-cylinder pressure, p_r, V_r, and T_r are the working fluid pressure, volume and temperature at reference state respectively [33]. C_1 and C_2 are two parameters, their values vary in different periods.

3.4 CFR Engine Modelling Schemes

The CFR engine modelling on GT-Power schemes are showed in. Those modellings were firstly built with GT-Power v2017, then modified with GT-Power v2019.

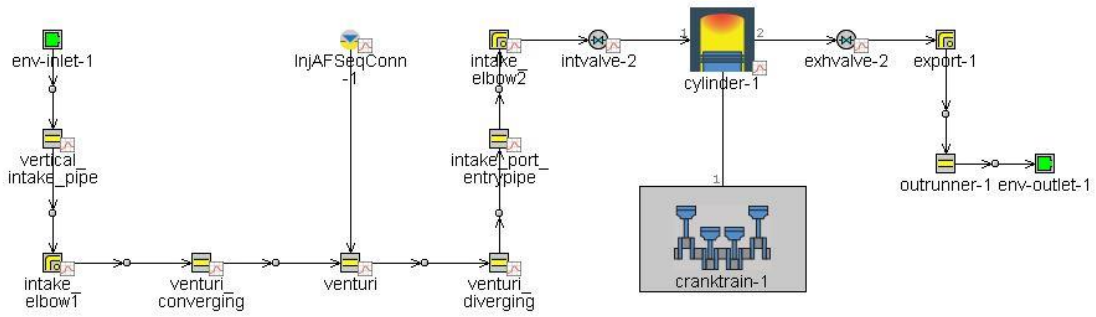

Figure 13 Modelling scheme of the CFR engine under RON test conditions

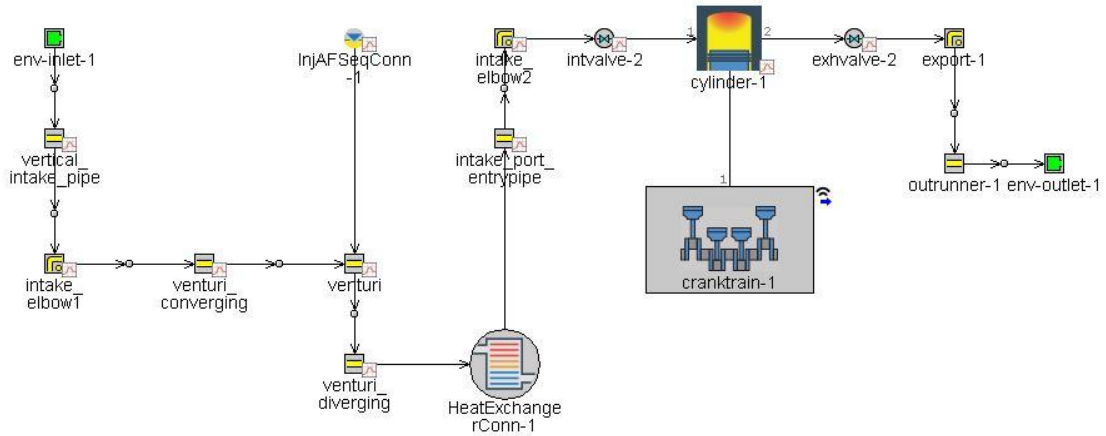

Figure 14 Modelling scheme of the CFR engine under MON test conditions

Figure 13 and **Figure 14** show that, the CFR engine model is divided into three main parts: the intake system, the exhaust system and the main engine. The intake system consists of straight and elbow pipes, a carburetor (a converging pipe, a venturi pipe and a diverging pipe), a direct injector, an intake port pipe, an intake port elbow and a preheat with is only hired under the MON testing conditions.

'env-inlet-1', this object in both model scheme indicates the pre-set conditions of intake air. The air composition is set as 76.7% of N_2 and 23.3% of O_2, with an absolute pressure of 1.01325 bar and a temperature of 325 K under RON conditions and 311.15 K under MON conditions.

'vertical_intake_pipe' and **'intake_elbow'** are set as the pipe where air flows through to the carburettor. 'vertical_intake_pipe' is set with a length of 90 mm and a diameter of 28mm. The discretization length is recommended to set approximately 0.4 times the cylinder bore diameter for the intake system and 0.55 times the bore for the exhaust system according to the built-in help instructions of GT-Power. The 28-mm-diameter 'intake_elbow' is 50-mm long, with a bend radius of 25 mm and a bend angle of 90 degrees [16].

'venturi_converging', **'venturi'** and **'venturi_diverging'** build what is a carburettor in reality in those two models. The diameter of 'venturi_converging' converges from 28 mm to 14.2875 mm on its 20-mm-length. The diameter of 'venturi' stays at 20 mm

with a length of 14.2875 mm. For the 'venturi_diverging', its diameter expands from 14.2875 mm to 30 mm on its 46-mm-length. [16]

All pipe related objects mentioned above are assumed with an imposed wall temperature of 325.15 K. Besides, they share the same initial air conditions as 'env-inlet-1.

'injAFSeqConn' mean the injector of the CFR engine. The fuel delivered stays at (engine speed)/600, which is 1 g/s under RON conditions and 1.5 under MON conditions in this work. Fuel Ratio specification (λ) is 0.88 in order to achieve the maximum power output and the least possibility of the occurrence of knocking in the cylinder. Injected Fluid Temperature is set as 298 K in this work, and the fuel is supposed to injected on the middle position of the 'venturi'. In this object, the injection timing angle indicates the crank angle relative to TDC firing of either the start of injection or the end of injection [50]. This term depends on a value called injection timing flag. In this work, the injection timing angle is set as 350, and the injection timing flag is set as 'injection-start'. It means that the fuel injection starts after 350 degrees of TDC. The vaporized fluid fraction (VFF) is the mass fraction of the injected liquid that will vaporize immediately upon injection [50]. This term can greatly manipulate simulation results on temperature and mass fraction graphs with respects to the crank angle in the intake system. The effects of this term will be illustrated later. In the part of simulating the combustion conditions inside the cylinder of this work, this term is set as 1, meaning that all fuels vaporize immediately upon injection.

'intake_port_entrypipe' and **'intake_elbows2'** simulate the pipes delivering to the engine cylinder via 'intvalve2' which indicates an intake valve of the CFR engine. 'intake_port_entrypipe' is 46 mm long, with a diameter of 30 mm. 'intake_elbows2' is 60 mm long, with a diameter of 30 mm, its radius of bend is 38.179 mm and its angel of bend is set as 90 degrees [16]. They share the same imposed wall temperature in this work, which is 400 K. **'HeatExchangerConn-1'** only exists in the model under MON test conditions, it is because the temperature of air-fuel mixture entering the cylinder is fixed at 149 ℃.

The exhaust gas leaving from the cylinder passes the exhaust valve, **'exhvalve-2'**, exhaust pipes, **'export-1'** and **'outrunner-1'**, to the atmosphere. The 31.75-mm- diameter 'export-1' is 60-inch long, with a bend radius of 38.2 mm and a bend angle of 90 degrees [16]. The 'outrunner-1' is 18.25-inch long with a diameter of 31.75 mm [16]. Both of them are assumed with an imposed wall temperature of 500 K in this work.

'intvalve-2' indicates the intake valve of the CFR engine. For the timing related attributes, a -4.32-degree cam timing angle is defined between cam timing anchor reference (TDC firing in this case) and the cam timing lift array reference (Theta = 0 in this case, indicating that cam timing angle above will be referenced to the 0.0 value in the angle array). Those three attributes determine the intake opens 4.32 degrees ahead of the TDC firing point, together with lift array, the intake valve lift curve could be ensured. The valve lash is 0.271 mm, and the angel multiplier is 1 in this work. The angle array will be scaled with respect to 0.0 in angle array by choosing 'Thera=0' for the attribute of 'Anchor for Angle Multiplier'.

Flow coefficients are several parameters measuring a valve's flow-passing ability. In GT-Power, the following attributes need to input in order to simulate the valve's flow-passing ability. The valve reference diameter (set as 34.18 mm in this work) is used to calculate the effective flow area from the discharge coefficients specified in this work.

The discharge coefficient reference area definition is for defining the method to calculate the reference area for forward discharge coefficients and reverse discharge coefficients array data. In this work, 'curtain' is chosen, meaning that discharge coefficients are calculated from the isentropic flow equations based on curtain reference:

$$discharge\ coefficient = \pi * valve\ reference\ diameter * lift\ position \quad (3.10)$$

The flow coefficient lift unit is mm in this case, indicating that the flow coefficients are input as a function of lift in unit of mm. The flow area multiplier has the function of scaling the reference area or discharge coefficients, in this work, this is set as 0.57. With above input attributed, forward discharge coefficients and reverse discharge coefficients can be calculated. The forward direction is the direction of the linking arrows through the valve connection. The discharge coefficients for valves must be calculated with respect to valve reference diameter using the isentropic flow equation. The reverse direction is the direction opposite of the linking arrows through the valve connection. The intake valve lifting data and fluid coefficients are acquired from [51].

'cylinder-1' is a key object in those models whose purpose is to simulate the in-cylinder combustion process conditions. Initial state object indicated the initial in-cylinder conditions. In this work, the in-cylinder conditions are: air, 1.013125 bar and 298 K Wall temperature defined by reference object defines the cylinder walls temperatures. In this work, head temperature, piston temperature, and cylinder temperature are 438.15 K, 438.15 K and 400 K respectively [16]. Heat transfer object has been illustrated above. The flow object specifies flow characteristics in this cylinder. In this case, all parameters are set as the default data. The combustion object is set to simulate the in-cylinder combustion model. Flame geometry object is (x.y.z = 0 mm, 40.5 mm, -10 mm). Spark timing or anchor angle depends on the test conditions. The initial spark timing is 5.5 mm. The flame laminar speed object is input according to **Table 10**. The data from table are mostly specified for isooctane, this group of data is chosen for the purpose of simplification.

Table 10 Flame laminar speed coefficients and exponents [16]

Parameters	Fuel	Value
Maximum laminar flame speed at the reference state (m/s)	Iso-oct	0.341
Laminar flame speed roll-off value (m/s)	Iso-oct	-1.132
Max flame speed equivalance ratio	Iso-oct	1.084
Temperature exponent	All	1.61
Pressure exponent	All	-0.273

Flame kernel growth multiplier, turbulent flame speed multiplier and Taylor length scale multiplier are set as 0.9, 1.15 and 1 respectively under standard flame speed mode.

'cranktrain-1' is employed to model crankcase chambers. The needed geometric data input has been mentioned above.

'exhvalve-2' indicates the exhaust valve of the CFR engine. Cam Timing Angle is chosen as 357.76 degrees. Cam timing anchor reference is set as 'TDC Firing'. Cam timing lift array reference is 'Theta=0'. Valve lash is 0.258 mm [16]. Valve reference

diameter is 34.45 mm [16]. Flow area multiplier is chosen as 1 in this work. The exhaust valve lifting data and fluid coefficients are acquired from [51]

3.5 Validations and Representative In-cylinder Curves

After the building of CFR engine under two testing conditions, PRF100, PRF91 and TRF91-30 are firstly simulated under RON test conditions in order to validate with experimental testing results. Simulated results (in-cylinder pressure curve) are validated with experimental measurement results from reference [51]. The validation results are shown as following figures.

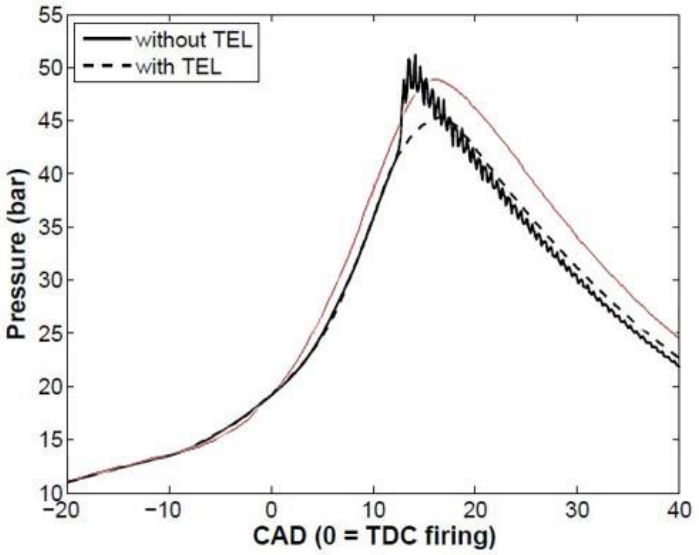

Figure 15 Modelling result (PRF100) compared with experimental results from [51]

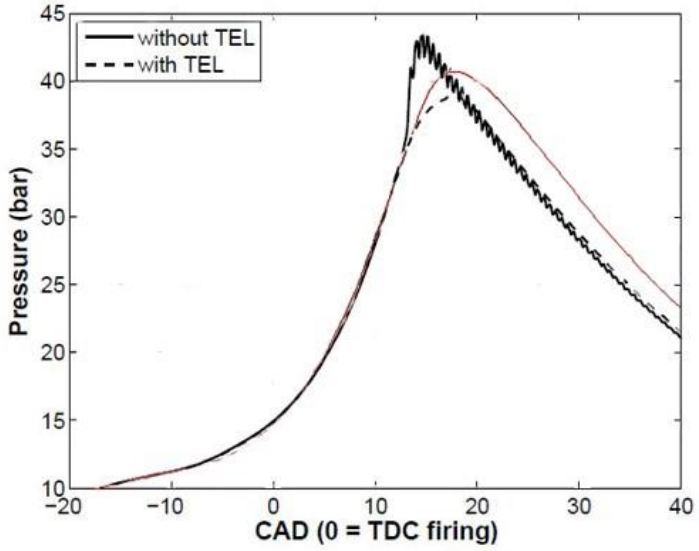

Figure 16 Modelling result (PRF91) compared with experimental results from [51]

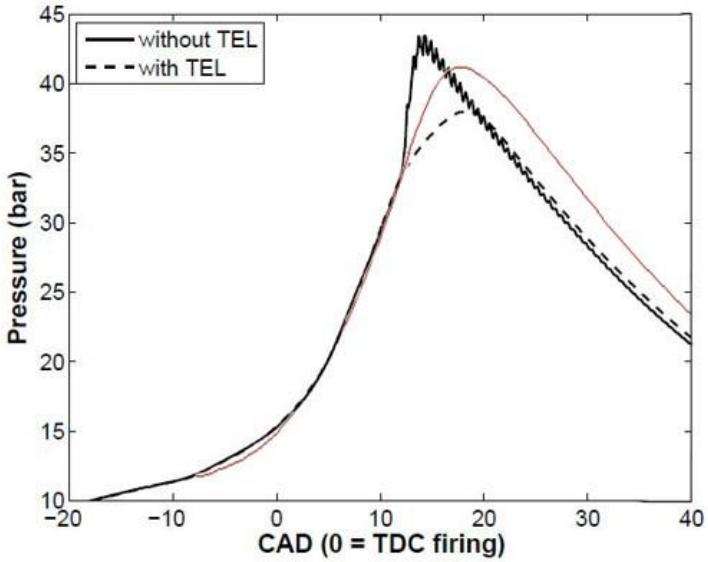

Figure 17 Modelling result (TRF91-30) compared with experimental results from [51]

From **Figure 15**, **Figure 16** and **Figure 17**, black lines indicate the experimental pressure curve when gasoline is operated without TEL (tetraethyllead, an anti-knocking additive to gasoline). Black dots lines mean the experimental pressure curve when gasoline is operated with TEL. Red lines show the simulated results of this work.

Validation results show that the simulated pressure curves match with the actual measured pressure curve well, especially before the timing of TDC.

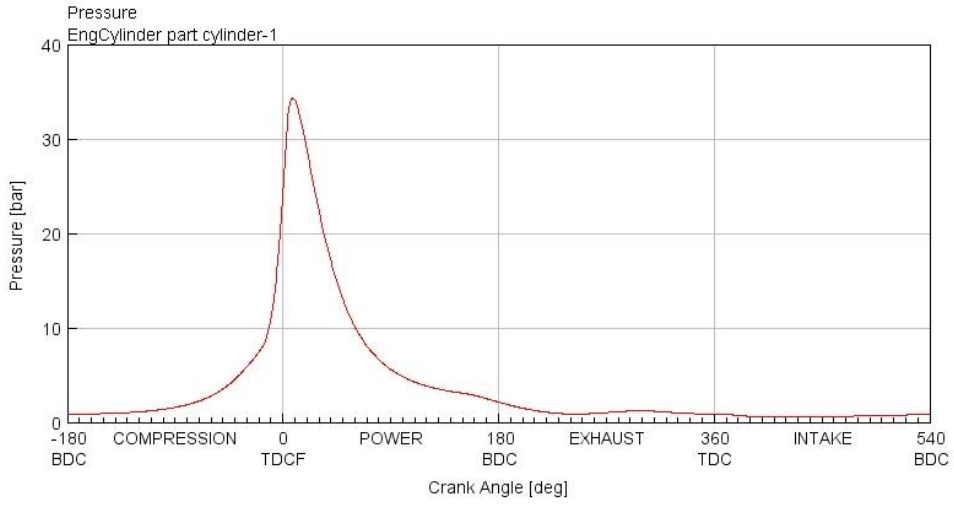

Figure 18 Representative in-cylinder pressure curve under RON conditions

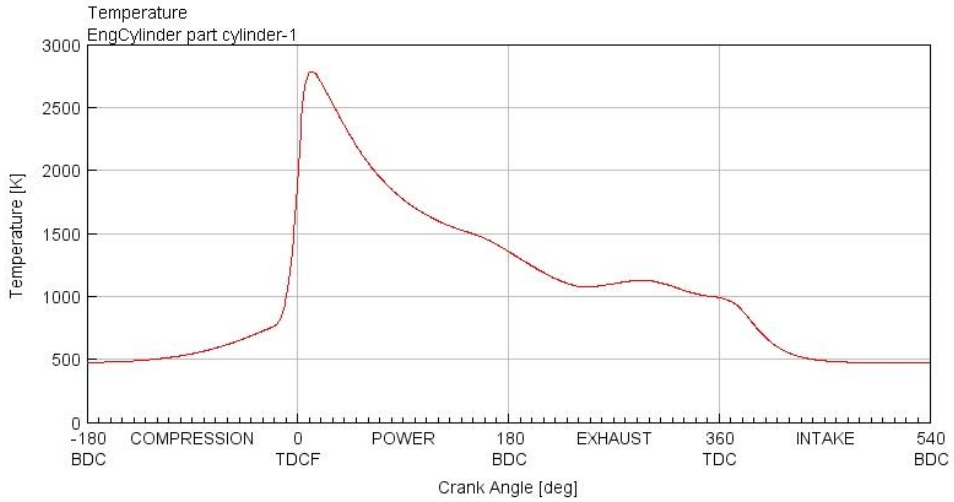

Figure 19 Representative in-cylinder temperature curve under RON conditions

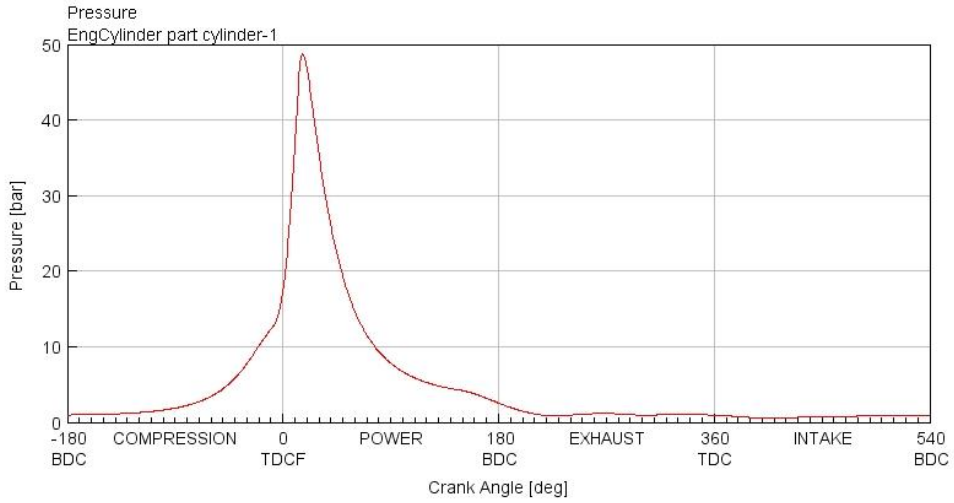

Figure 20 Representative in-cylinder pressure curve under MON conditions

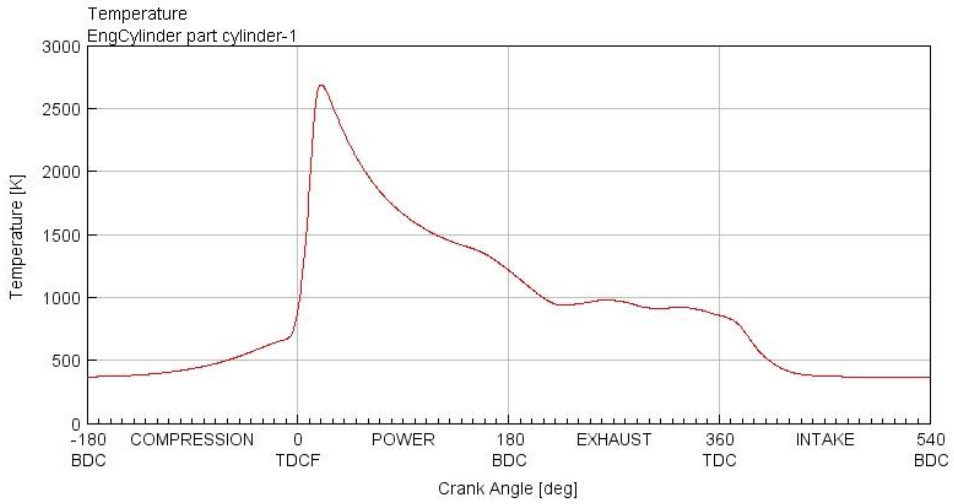

Figure 21 Representative in-cylinder temperature curve under MON conditions

Figure 18, **Figure 19**, **Figure 20**, **Figure 21** are representative in-cylinder pressure curve under RON conditions, in-cylinder temperature curve under RON conditions, in-cylinder pressure curve under MON conditions and in-cylinder temperature curve under MON conditions respectively. Those graphs are based on indolene simulation results, the octane number of indolene is assumed as 92 in this part of work. The pressure peak under RON conditions is lower than that under MON conditions, while temperature peaks under two conditions do not show much difference.

3.6 Selected Fuels

In the first part of this study, in order to study the relationship between octane numbers of a fuel and pre-combustion conditions, 4 groups of fuel are selected for simulation.

The first set of fuels is the PRF with various octane numbers. They are chosen because the PRF is the most basic surrogate fuel for gasoline, and they most intuitively reflect the relationship between the octane number of the fuel and the pre-combustion conditions.

The second group of fuels are the mixture of different PRF with the same percentage of alcohol by volume. Those fuels are selected to observe the effect of a fuel with the same volume fraction of alcohol on pre-combustion conditions. For this group of fuels, the MON data is missing.

The third group of fuels is PRF91-E. The purpose of this group of fuels is to observe the octane number change of fuels with different alcohol content and the change of pre-combustion conditions.

The last group is TRF91-30-Es. This group of fuels are selected for the same purpose as the third group, but toluene's effect on pre-combustion conditions was also taken into account.

Table 10 shows information on selected fuels, corresponding set compression ratio (CR in table) and spark timing. The RON and MON of selected fuels, together the corresponding compression ratio are acquired from reference[51]. Under RON test conditions, the set compression ratio of a simulation varies with octane numbers of a fuel. Generally, the higher research octane number is, the higher the compression ratio is. And the compression is fixed at 13° degrees before the TDC (BTDC). Under MON test conditions the set compression ratio increases with the increase of motor octane number. And the spark timing is not fixed. The spark timing under MON test conditions is related to Cylinder height Dial Indicator Reading (CHDIR), which is related to the CR. The spark timing under MON test conditions is calculated by [38]:

$$HDIR = \frac{114.3mm}{(CR-1) \times \frac{25.4mm}{inch}} \tag{3.10}$$

$$park\ timing = 19.4 \times CHDIR + 10.16 \tag{3.11}$$

For the equation of spark timing, it is deduced by the linear relation between cylinder height dial indicator reading and spark timing in reference [38]. When the calculated result of spark timing is higher than 26°, then it will be set as 26° since the spark timing range under MON test conditions is from 13° to 26° BTDC.

Table 11 Selected fuels and data input for simulations

Group	Fuels	RON	CR under RON	MON	CR under MON	Spark timing (°BTDC)
1	PRF100	100	7.82	100	8.03	22.46
1	PRF80	80	6.11	80	5.92	26
1	PRF60	60	5.55	60	5.14	26
1	PRF40	40	5.25	40	4.78	26
2	PRF91-E80	108.4	9.7	92.2	7.01	24.54
2	PRF91-E60	108.4	9.7	93.4	7.15	24.21
2	PRF91-E40	108	9.64	94.5	7.28	23.92
2	PRF91-E20	103.8	8.77	95.3	7.38	23.7
2	PRF91	91	6.72	91	6.87	24.88
3	PRF100-E20	109.4	9.89			
3	PRF80-E20	97	7.31			
3	PRF60-E20	83.5	6.26			
3	PRF40-E20	68.5	5.75			
3	PRF20-E20	53.3	5.43			
4	TRF91-30-E80	107.5	9.54	91.4	6.91	24.78
4	TRF91-30-E60	107.1	9.47	92	6.98	24.61
4	TRF91-30-E40	106	9.26	92.1	6.99	24.58
4	TRF91-30-E20	101.4	8.17	91.1	6.88	24.85
4	TRF91-30	91.3	6.75	86.1	6.38	26

4 Results

In this section, the simulation results on intake system and 19 kinds of fuels and indolene in the cylinder will be showed and illustrated.

4.1 Pressure, Temperature and Gaseous Mass Fraction Graphs in the Intake System

4.1.1 Under RON Conditions

Pressure curves

The pressure curves of the intake system do not vary greatly with the VFF. In all objects of the intake system, the pressure varies in certain range during the compression stroke, power stroke and exhaust stroke. The amplitude decreases as the crank angle approaches to intake stroke. With it comes the intake stroke, the internal pressure in all components of the intake system decreases with small fluctuations. Subsequently, the pressure gradually returned to the initial state of compression stroke. The closer to the part of cylinder, the greater the decrease of internal pressure is in the intake stroke.

Temperature curves

The temperature curve of each part of the intake system can be manipulated by the VFF to varying extensions. In the intake pipe and the intake elbow, the inside temperature shows a weak trend of decrease in compression stroke, power stroke and exhaust stroke. During the intake stroke, the inner temperature decreases and then returns to its original state in the intake stroke. VFF has a slightly greater effect on the temperature of the intake elbow.

In the carburettor, the effects of VFF can be clearly observed. In the converging pipe, the inside temperature remained stable in the compression stroke, power stroke and exhaust stroke. While in the intake stroke, the internal temperature decreases to a minimum within a short time, followed by a rapid rise to the state just entering the intake stroke, and then maintains until the end of the intake stroke. The higher the VFF is, the lower the minimum temperature of the intake stroke is. In the venturi pipe, the fuel is injected directly. It is here that the VFF has the greatest impact on the internal temperature, due to the fact that gasification of the fuel absorbs a lot of heat. Therefore, the higher the VFF is, the more heat is absorbed by the fuel, and the lower the overall temperature in the tube is. Here, the in-pipe temperature fluctuates during compression, power and exhaust strokes, but still remains stable as the initial temperature. During the intake stroke, the inner temperature drops sharply to the lowest point of the cycle, then rapidly increases to the state before the intake, and finally slowly decreases. It is worth noting that in this simulation, when VFF is set as 1, the lowest temperature in the venturi tube is down to about 180K, which is impractical. However, in subsequent researches on in-cylinder's internal combustion conditions, VFF is always set to 1. In the diverging pipe of the carburettor, the temperature curve is similar to that in the venturi tube, but the value of the lowest temperature is more realistic.

In the intake port entry pipe and the intake elbow, temperatures remain stable during the compression stroke, power stroke and exhaust stroke. However, in the intake stroke, inner temperatures experience a slow increase, a sharp decrease, a rapid increase, and a slow decrease to the initial state. Here, VFF has little influence on the temperature variation.

Gaseous mass fraction curves

With regard to the intake pipe and elbow, the composition of gaseous substances basically maintained at 100% in the whole engine cycle. This is because the fuel has not yet mixed with the gas. In the carburettor, due to the injection of fuel, the degree of vaporization of the fuel affects the gaseous mass fraction directly. The higher the VFF is, the higher the overall gaseous mass fraction in the carburettor is. During the intake stroke, gaseous mass fraction experiences a steep drop to the lowest point, as the fuel is directly injected. Then the value rises, indicating that the unvaporized fuel has vaporized further. Gaseous mass fractions in the intake port entry pipe and the intake port elbow undergo a similar process. It is worth noting that, despite the assumption that the VFF is only 0.1, the air-fuel mixture entering the engine cylinder is still with a 94% gaseous mass composition.

4.1.2 Under MON Conditions

Pressure curve

The overall pressure trend is similar with that under RON conditions. Generally speaking, pressure curves of different objects of the intake system do not vary greatly with the VFF. In all parts of the intake system, the pressure varies in certain range during the compression stroke, the power stroke and the exhaust stroke. The amplitude decreases as crank angle approaches to intake stroke. During the intake stroke, the internal pressure in all components of the intake system decreases with small fluctuations. Subsequently, the pressure gradually returns to the initial state of compression stroke.

Temperature curves

The temperature curve of each part of the intake system will also be influenced by the VFF to different degrees. In the intake pipe and the intake elbow, the in-pipe temperatures increase slightly during the compression stroke, the power stroke and the exhaust stroke. During the intake stroke, the inside temperature decreases first, then increases, and then decreases to the initial state. The impact of VFF is negligible.

In the carburettor, the effects of VFF can be clearly observed. In the converging pipe of the carburettor, temperatures during the compression stroke, the power stroke and the exhaust stroke keep increasing. While in the intake stroke, the internal temperature drops to a minimum within a short time, and then quickly rises back to the state at the very first stage in this stroke, and maintains consistently until the end of the intake stroke. The higher the VFF is, the lower the minimum temperature during the intake stroke is. In the venturi pipe, the internal temperature fluctuates with a slowly increasing trend during the compression stroke, the power stroke and the exhaust stroke. During intake stroke however, the inner temperature drops sharply to the lowest point of the engine cycle, then rapidly increases to the state before the intake stroke, and finally slowly decreases. It is worth noting that in this simulation, when VFF is 1, the lowest temperature in the venturi tube is down to about 180K, which is impractical. The trend of temperature change in the diverging pipe is similar to that in the converging tube.

In the intake port entry pipe and the intake port elbow, temperatures inside decrease slowly in the compression stroke, the power stroke and the exhaust stroke. While in the intake stroke, the temperature in the pipe decreases sharply and rises rapidly to the

initial state at the very first stage of this stroke. VFF has a little influence on temperatures here.

Gaseous mass fraction

The overall trend of gaseous mass fraction is similar to that under RON test conditions. With regard to the intake pipe and the intake elbow, gaseous mass fractions basically maintain at 100% during the overall engine cycle. This is because the fuel has not yet mixed with the gas. In the carebuttor, due to the injection of fuels, the degree of vaporization of the fuel affects the gaseous mass fraction directly. The higher the VFF is, the higher the overall gaseous mass fraction of the carebuttor will be. During the intake stroke, gaseous mass fraction experiences a steep drop in to the lowest point, as the fuel is directly injected. Then this value rises, indicating that the unvaporized fuels vaporize further. Gaseous mass fractions in the intake port entry pipe and the intake port elbow undergoes a similar process. It is worth noting that, despite the assumption that the VFF is only 0.1, the gas entering the engine chamber is still about 94% gas in composition.

4.2 Primary Reference Fuels with Different Octane Numbers (PRFs)

For primary reference fuels, the RON is the isooctane volumetric content, while the MON is defined as the same as the RON. Therefore, in this section, fuels' research octane number and motor octane number are represented by one grey line in all the following graphs.

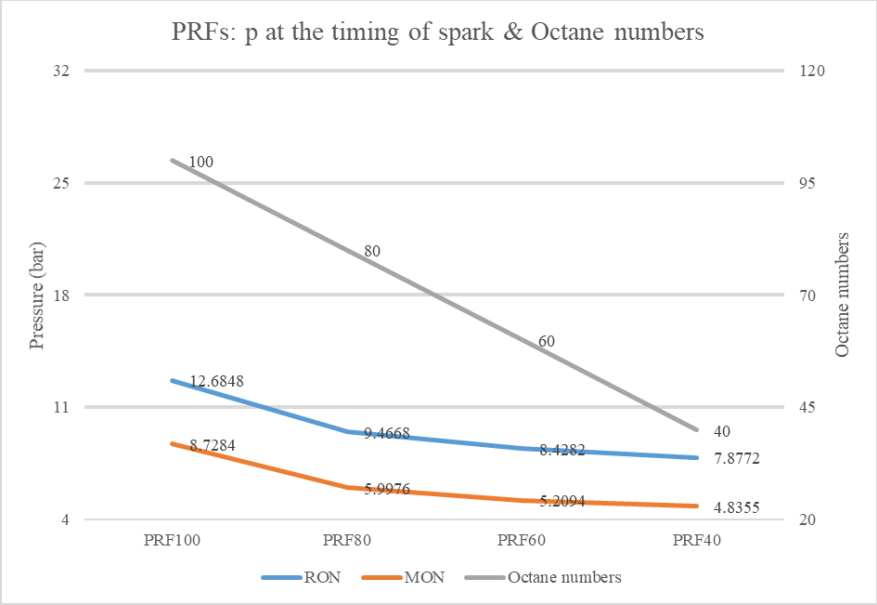

Figure 22 PRFs: in-cylinder pressures at the timing of spark

Figure 22 illustrates the in-cylinder pressure at the timing of spark of four primary reference fuels (PRF100, PRF80, PRF60 and PRF40 respectively) under two test conditions (for RON and for MON respectively). It is clear that with the increase of fuels' octane numbers, the in-cylinder pressure at the timing of spark under two test conditions increase as well. And the pressure under RON test conditions is always higher

than the pressure got from MON test conditions. Besides, when octane numbers jump from 80 to 100, the in-cylinder at the timing of spark shows a more dramatic increase.

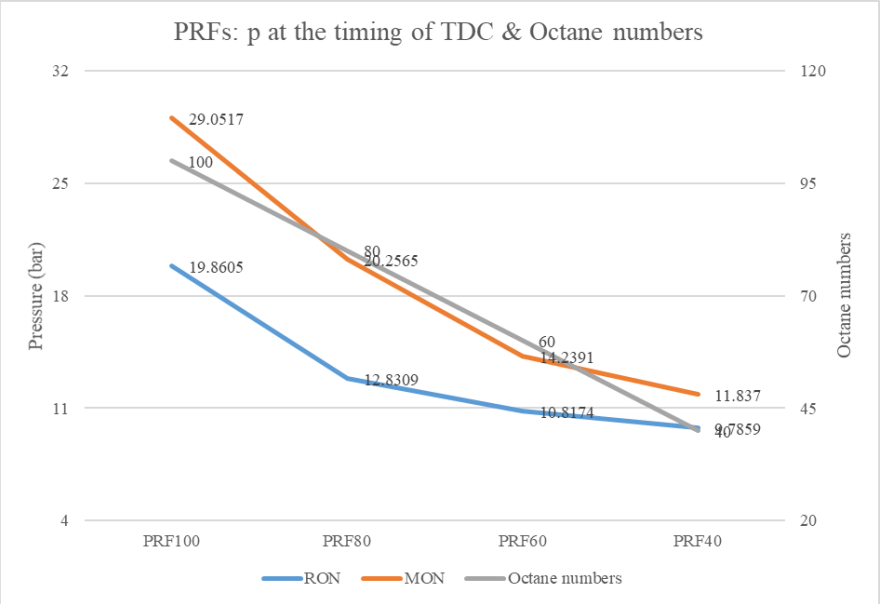

Figure 23 PRFs: in-cylinder pressures at the timing of TDC

Figure 23 shows the in-cylinder pressure at the timing of TDC of four primary reference fuels (PRF100, PRF80, PRF60 and PRF40 respectively) under two test conditions (for RON and for MON respectively). Similar as the pressure at the timing of spark, the TDC pressure rises with the rise of fuels' octane numbers. It is noticing that under MON test conditions, as the octane numbers increase, so does the rate of change in pressure.

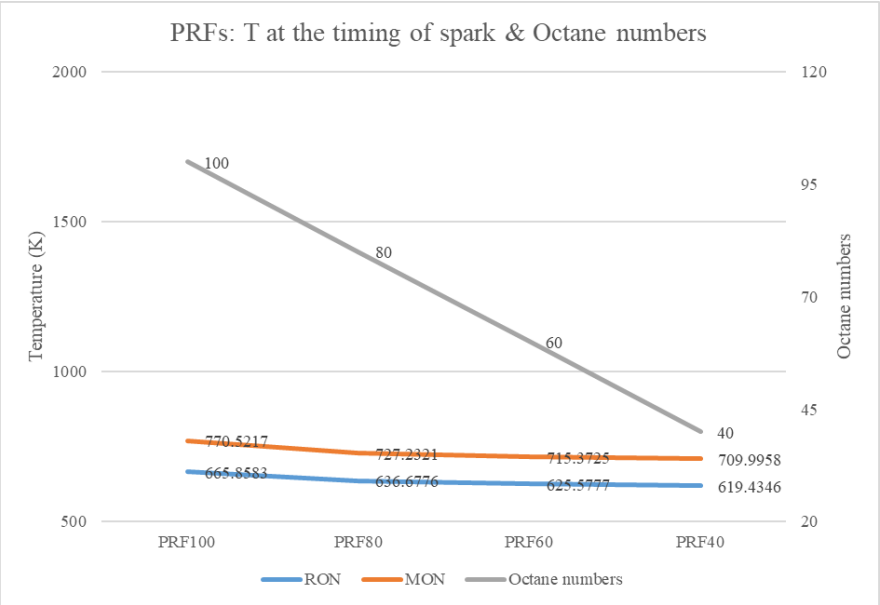

Figure 24 PRFs: in-cylinder temperatures at the timing of spark

Figure 24 explains the in-cylinder temperature at the timing of spark of four primary reference fuels (PRF100, PRF80, PRF60 and PRF40 respectively) under two test conditions (for RON and for MON respectively). As the octane numbers of the fuel increase, the in-cylinder temperatures at the timing of spark also rise. However, in this instantaneous condition, the change in temperature is slight. Besides, the spark temperature under RON test conditions is always lower than that under MON test conditions.

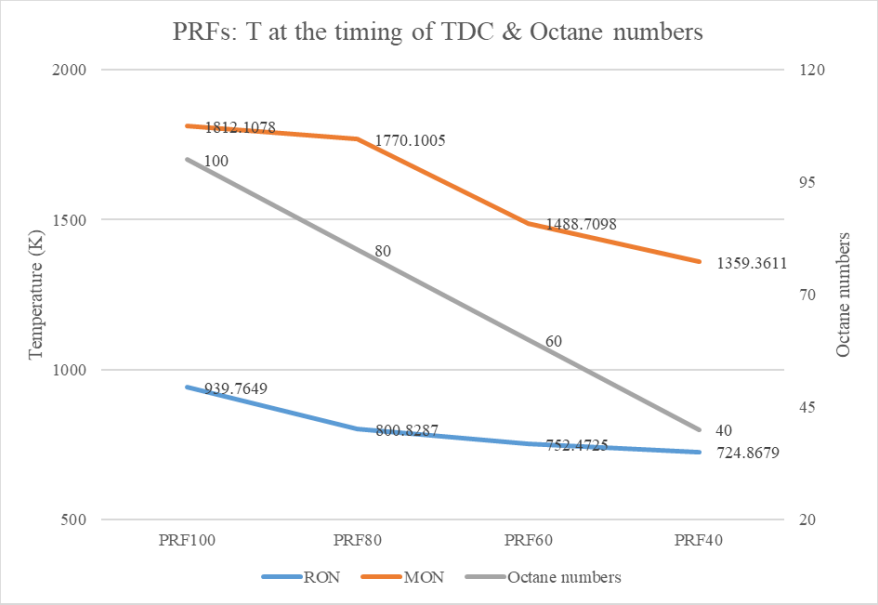

Figure 25 PRFs: in-cylinder temperatures at the timing of TDC

Figure 25 demonstrates the in-cylinder temperature at the timing of TDC of four primary reference fuels (PRF100, PRF80, PRF60 and PRF40 respectively) under two test conditions (for RON and for MON respectively). The temperature of TDC shows the same change trend as spark temperature, that is, the temperature at this moment increases with the increase of fuel octane number. Similarly, the temperature at the timing of TDC under RON test conditions is always lower than that under MON test conditions.

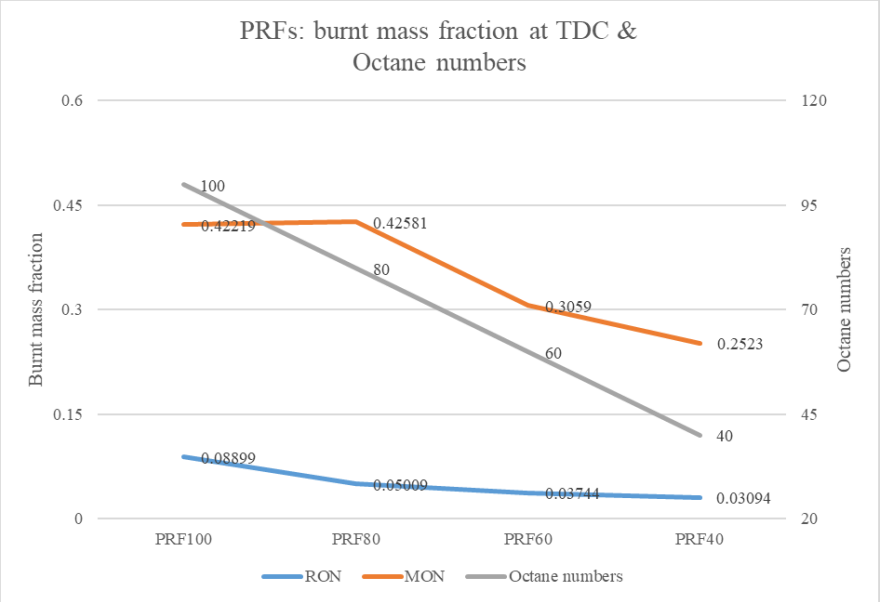

Figure 26 PRFs: in-cylinder burnt mass fractions at the timing of TDC

Figure 26 represents the burnt mass fraction only at the timing of TDC of four primary reference fuels (PRF100, PRF80, PRF60 and PRF40 respectively) under two test conditions (for RON and for MON respectively).As the octane number of primary reference fuels rise, the burnt mass fraction rise as well, just the like the trend which temperature and pressure show above. Under the RON test conditions, less than 10% of the fuel combusts. However, when it comes to MON test conditions, consumed fuel fraction can rise up to 43%.

4.3 Primary Reference Fuels with Fixed Ethanol Volumetric Content (E20-PRFs)

In this section, all simulations are implemented only under RON test conditions since MON data is missing.

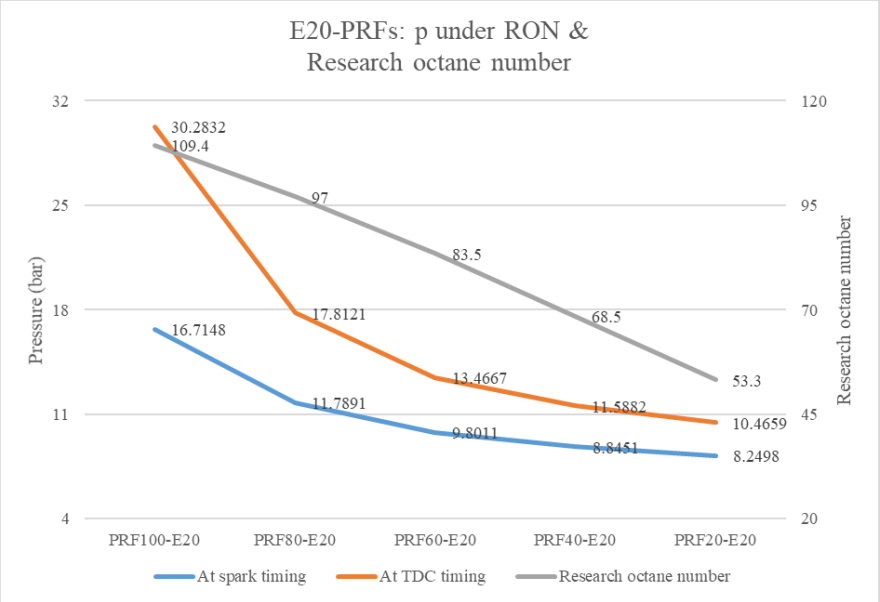

Figure 27 E20-PRFs: in-cylinder pressures under RON test conditions

Figure 27 shows the pressure simulation results for five fuels (PRF100-E20, PRF80-E20, PRF60-E20, PRF40-E20 and PRF20-E20 respectively) at two instantanetities (spark and TDC, respectively). The pressure of these five fuels decreases under two instantaneous conditions generally. From PRF100-E20 to PRF80-E20, the simulation results of two instantaneous pressures vary greatly. But from PRF80-E20 to PRF20-E20, two instantaneous pressures drop slight.

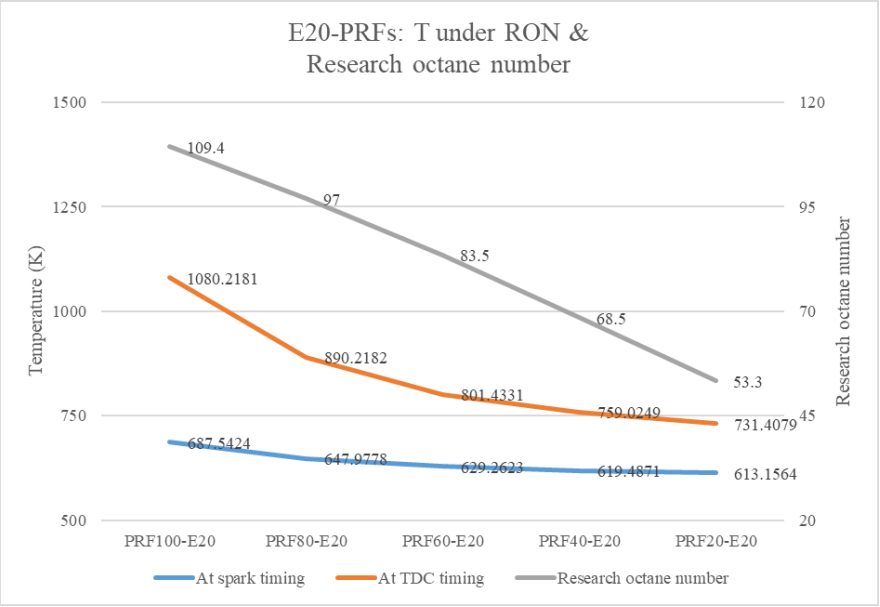

Figure 28 E20-PRFs: in-cylinder temperatures under RON test conditions

Figure 28 illustrates the temperature simulation results for five fuels (PRF100-E20, PRF80-E20, PRF60-E20, PRF40-E20 and PRF20-E20 respectively) at two instantanetities (spark and TDC, respectively). As with the pressure curves, the temperature decreases with the decline of research octane number of fuels. It is worth noting that

the change in pressure at TDC timing is more noticeable than the change at spark timing.

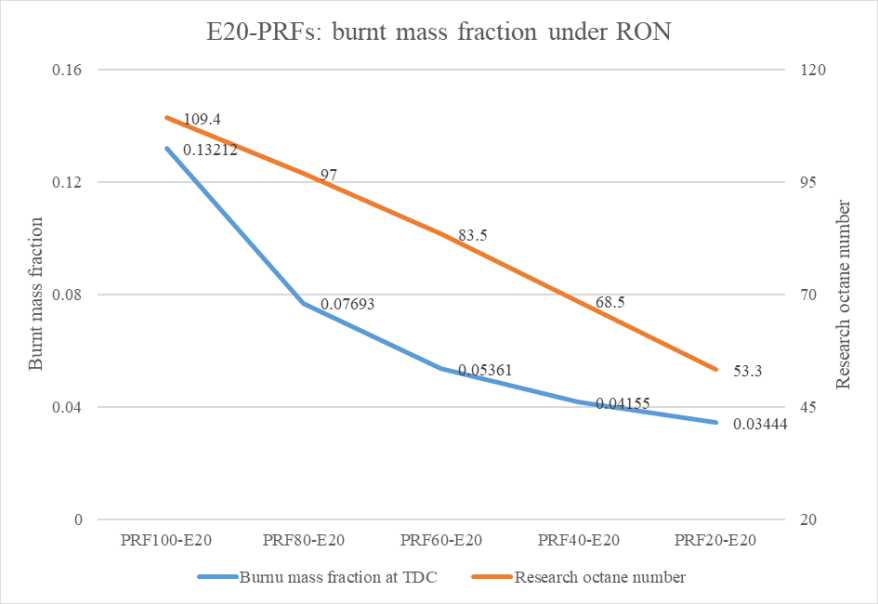

Figure 29 E20-PRFs: in-cylinder burnt mass fractions under RON test conditions

Figure 29 illustrates the burnt mass fraction simulation results for five fuels (PRF100-E20, PRF80-E20, PRF60-E20, PRF40-E20 and PRF20-E20 respectively) at the timing of TDC. Compared with two other parameters, pressures and temperatures shown in the first two images, the ratio of burned fuel has the same gradual relationship with the octane number of the fuel. In other words, the higher the research octane number of the fuel, the higher the proportion of fuel consumed at the timing of TDC.

4.4 PRF91 with Various Volumetric Content of Ethanol (PRF91-Es)

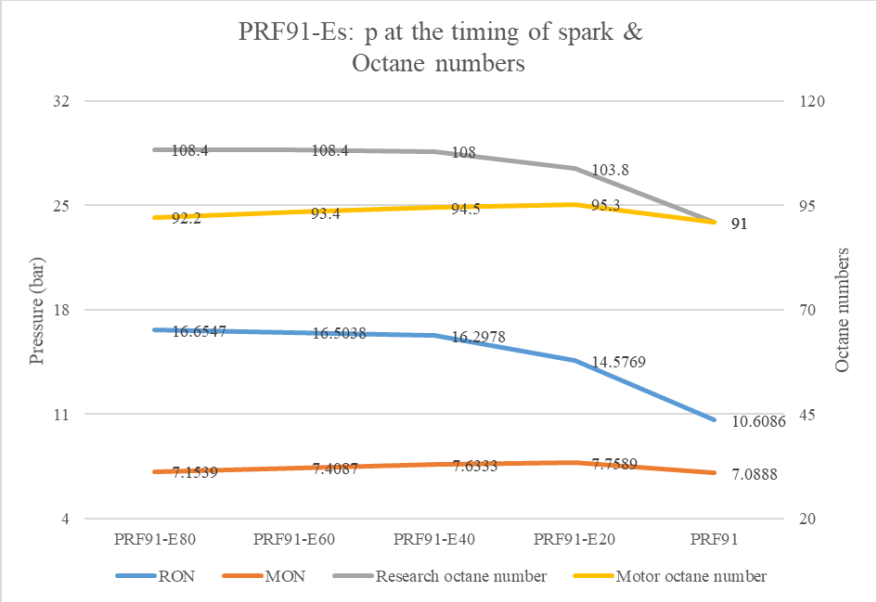

Figure 30 PRF91-Es: in-cylinder pressuress at the timing of spark

Figure 30 shows the in-cylinder pressure of five fuels (PRF91-E80, PRF91-E60, PRF91-E40, PRF91-E20 and PRF91 respectively) under two test conditions (for RON and for MON respectively). As the ethanol volumetric content in the fuel increased, the research octane number of fuels increases, and the motor octane number peaks when the ethanol content is 20%, after which it drops slowly. It is also worth noting that when the ethanol content is above 40 percent, the octane numbers of the blend flatten out. As for the pressure at the timing of spark, it peaks at 40 percent ethanol and then slowly declines as the ethanol percentage increases. Under RON test conditions, the pressure at the timing of spark is constantly higher than that under MON test conditions.

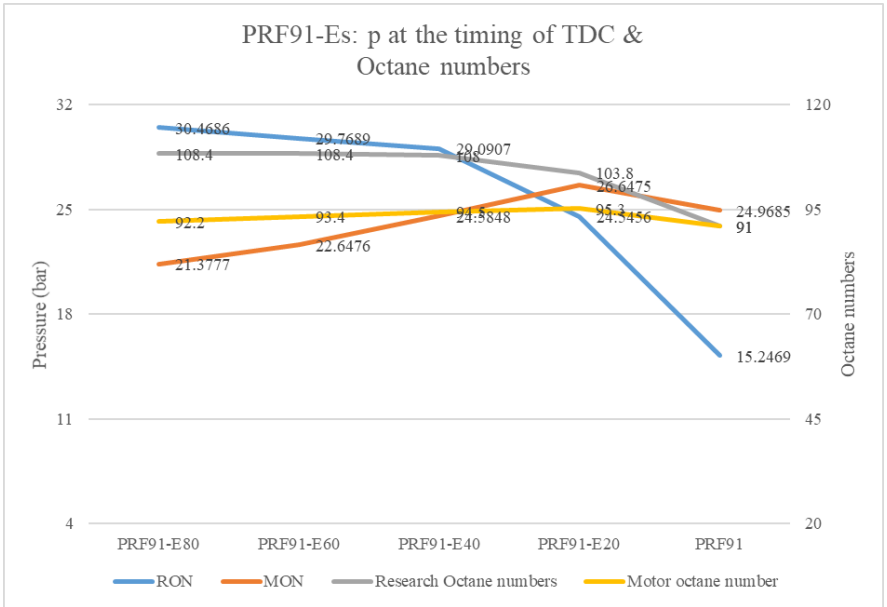

Figure 31 PRF91-Es: in-cylinder pressures at the timing of TDC

Figure 31 demonstrates the in-cylinder pressure of five fuels (PRF91-E80, PRF91-E60, PRF91-E40, PRF91-E20 and PRF91 respectively) under two test conditions (for RON and for MON respectively). Under RON test conditions, the pressure at the timing of TDC increase with the increase of ethanol content, however, when the ethanol content is higher than 40 percent, it rises slowly, which corresponds to the tendency of the RON. Under MON test conditions, the TDC pressure curve matches the MON curve to some extent since both of them reach to peak when the ethanol content is 40%.

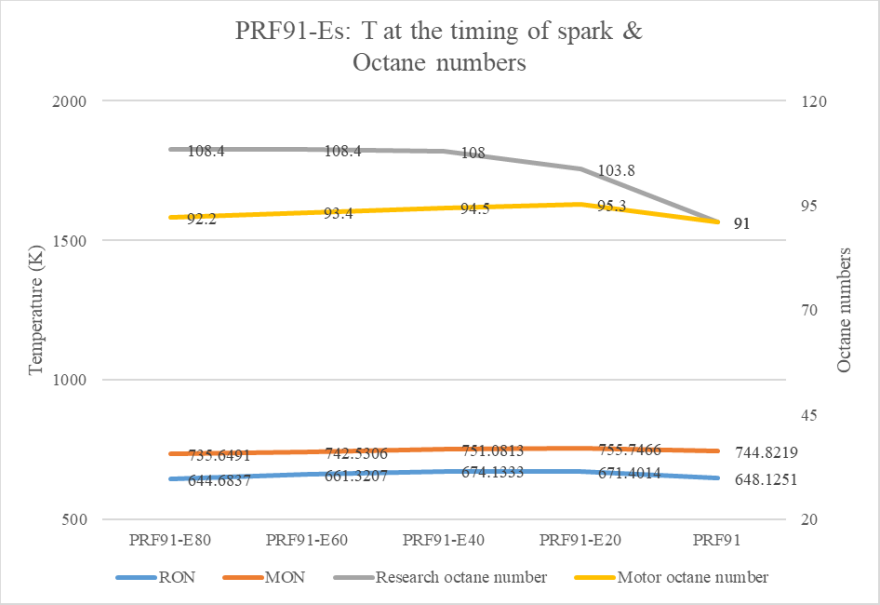

Figure 32 PRF91-Es: in-cylinder temperatures at the timing of spark

Figure 32 illustrates the in-cylinder temperature of five PRF91 related fuels (PRF91-E80, PRF91-E60, PRF91-E40, PRF91-E20 and PRF91 respectively) under two test conditions (for RON and for MON respectively) at the timing of spark. Under those two conditions, temperatures at the timing spark vary very mildly. The spark temperature under RON test conditions peaks at ethanol content of 40%, while that under MON test conditions shows a downward trend with the increase of ethanol content.

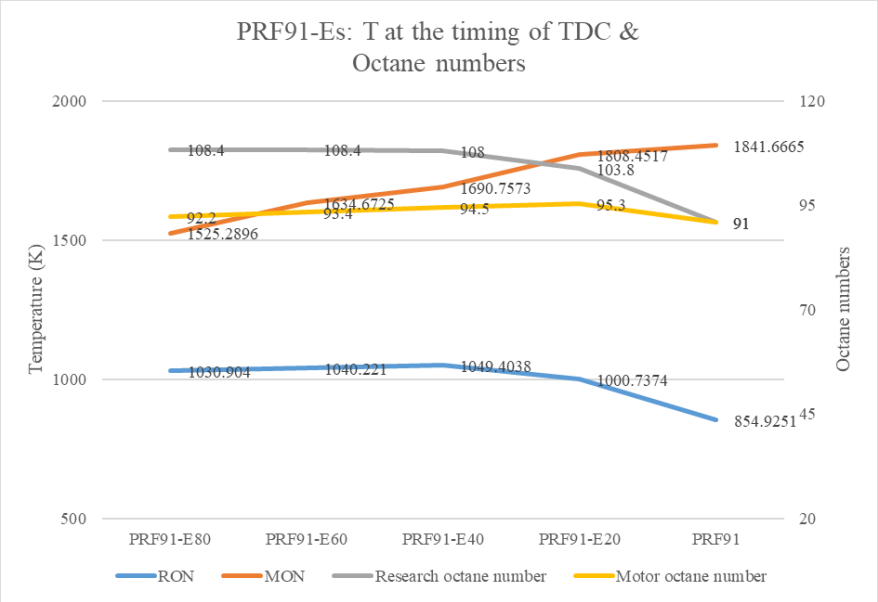

Figure 33 PRF91-Es: in-cylinder temperatures at the timing of TDC

Figure 33 represents the in-cylinder temperature at the timing of TDC of five PRF91 related fuels (PRF91-E80, PRF91-E60, PRF91-E40, PRF91-E20 and PRF91 respectively) under two test conditions (for RON and for MON respectively). Variation of temperature at the timing of TDC are more greatly compared with that of temperatures at the timing of spark. Similar as the spark temperature, the TDC temperature under RON test conditions reaches to the highest peak when the ethanol content is 40%, and under MON test conditions, the temperature at the timing of TDC shows a decreasing trend with the increase of ethanol content.

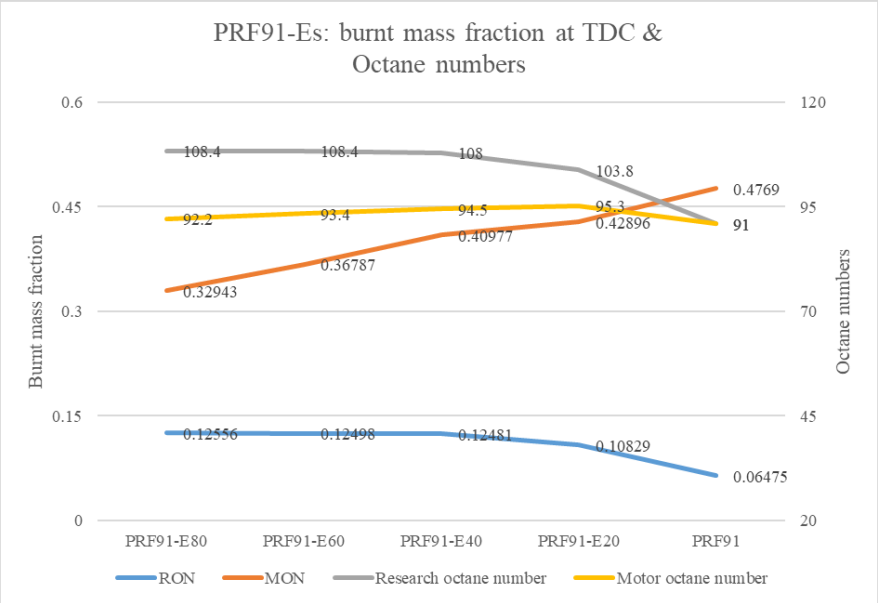

Figure 34 PRF91-Es: in-cylinder burnt mass fraction curves at the timing of TDC

Figure 34 shows the burnt mass fraction only at the timing of TDC of five fuels (PRF91-E80, PRF91-E60, PRF91-E40, PRF91-E20 and PRF91 respectively) under

two test conditions (for RON and for MON respectively). Under RON test conditions, this parameter increases with the increase of ethanol content, but when the ethanol content is higher than 40%, the change becomes milder. As for the burnt mass fraction under MON test conditions, it shows a descending trend when the ethanol percentage rises.

4.5 TRF91-30 with Various Volumetric Content of Ethanol (TRF91-30-Es)

TRF91-30, is this kind of fuel that the research octane number is 30 and the toluene volumetric percentage is 30%. When TRF91-30 blends with ethanol, with the increase of ethanol content, octane numbers of the mixture do not necessarily increase. For the research octane, it always rises if the ethanol content increases, but when the ethanol content is higher than 40%, it flattens. For the motor octane number, it reaches to its highest peak when the ethanol content is 40 percent.

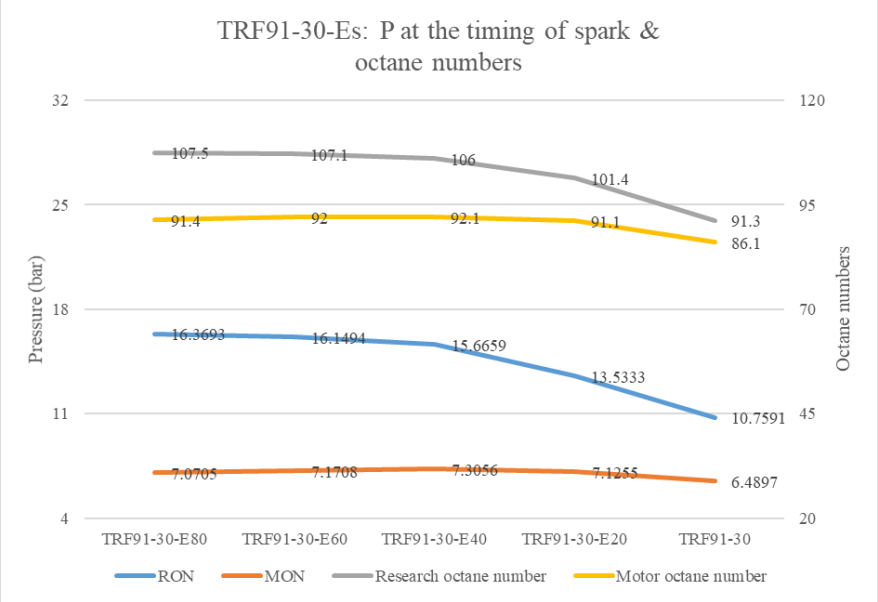

Figure 35 TRF91-30-Es: in-cylinder pressures at the timing of spark

Figure 35 demonstrates spark pressures of 5 fuels (TRF91-30-E80, TRF91-30-E60, TRF91-30-E40, TRF91-30-E20 and TRF91-30 respectively) simulation results under two test conditions (for RON and for MON respectively). Under the RON test conditions, the pressure at the timing of spark increase with the increase of ethanol content, however, when the ethanol content is higher than 40 percent, the pressure does not vary too much. As for the spark pressure under MON test conditions, it reaches to its highest peak when the ethanol content is 40 percent, which is similar to the tendency of the MON.

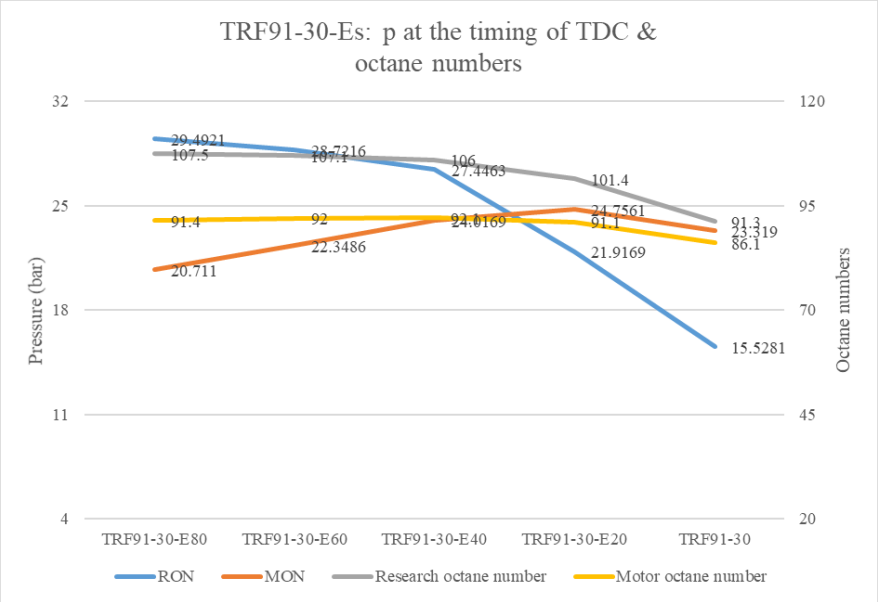

Figure 36 TRF91-30-Es: in-cylinder pressures at the timing of TDC

Figure 36 shows TDC pressures of 5 fuels (TRF91-30-E80, TRF91-30-E60, TRF91-30-E40, TRF91-30-E20 and TRF91-30 respectively) simulation results under two test conditions (for RON and for MON respectively). Similar as the spark pressures, the TDC pressure firstly increase until the ethanol content is 40 percent, then it flattens under RON test conditions. While under MON conditions, it reaches to its highest peak when the ethanol content is 40 percent.

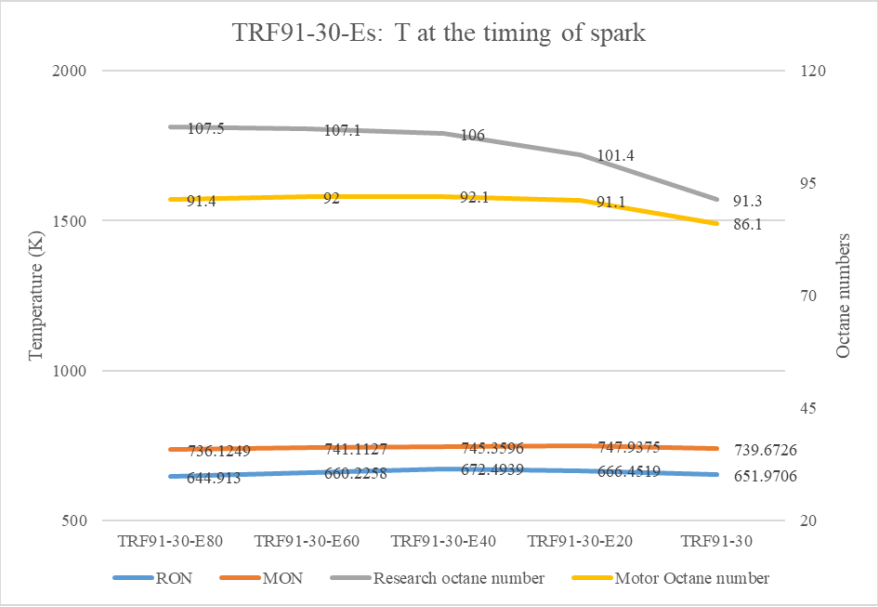

Figure 37 TRF91-30-Es: in-cylinder temperatures at the timing of spark

Figure 37 illustrates spark temperatures of 5 fuels (TRF91-30-E80, TRF91-30-E60, TRF91-30-E40, TRF91-30-E20 and TRF91-30 respectively) simulation results under two test conditions (for RON and for MON respectively). Under RON conditions, the spark temperature rises to the highest data when the ethanol content is 40%, then it

decreases. Under MON test conditions, however, the highest peak occurs when the ethanol content is 20%.

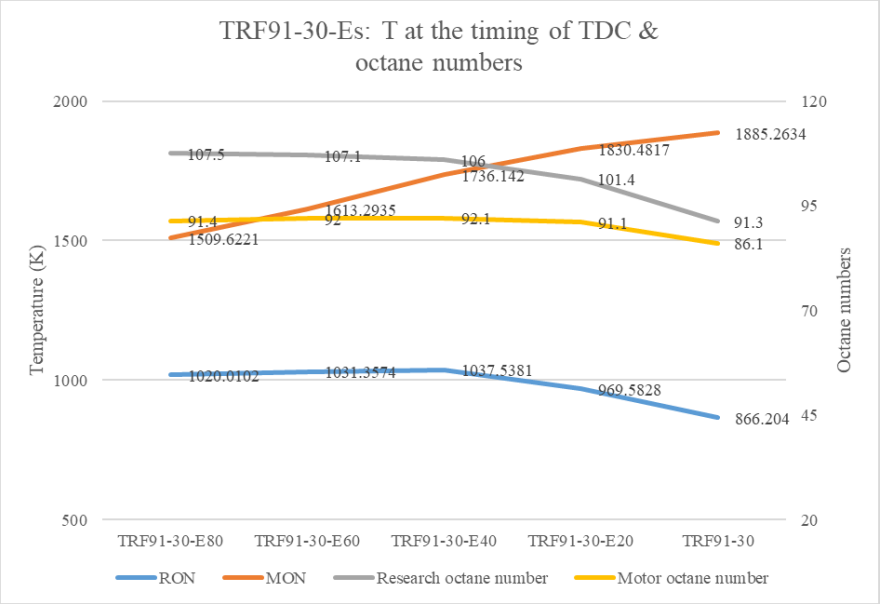

Figure 38 TRF91-30-Es: in-cylinder temperatures at the timing of TDC

Figure 38 provides information on TDC temperatures of 5 fuels (TRF91-30-E80, TRF91-30-E60, TRF91-30-E40, TRF91-30-E20 and TRF91-30 respectively) simulation results under two test conditions (for RON and for MON respectively). Under RON conditions, the TDC temperature rises to the highest data when the ethanol content is 40%. Under MON test conditions, the TDC temperature shows a reducing trend with the increase of the ethanol content.

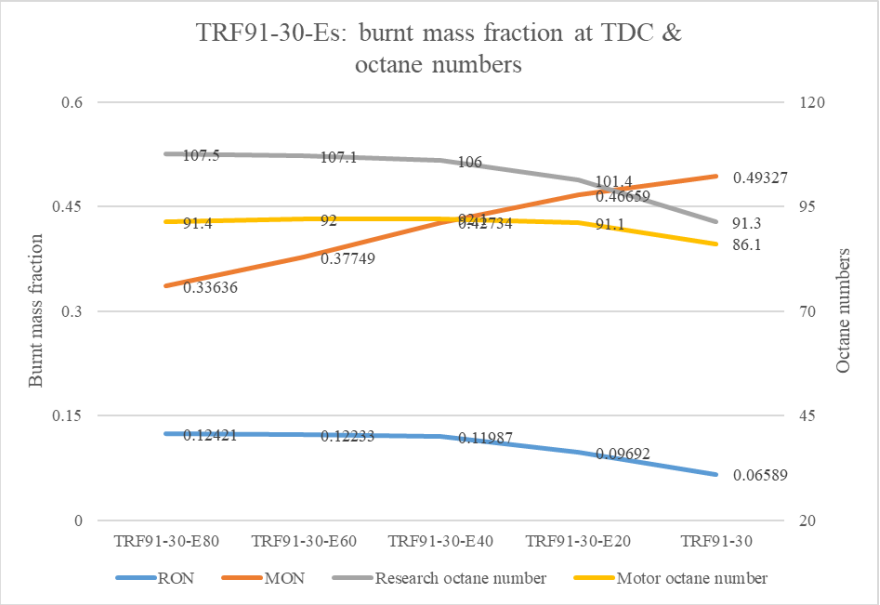

Figure 39 TRF91-30-Es: in-cylinder burnt mass fractions at the timing of TDC

Figure 39 illustrates TDC burnt mass fractions of 5 fuels (TRF91-30-E80, TRF91-30-E60, TRF91-30-E40, TRF91-30-E20 and TRF91-30 respectively) simulation results under two test conditions (for RON and for MON respectively). Under RON conditions, the burnt mass percentage peaks when the ethanol content is 40%. And under MON test conditions, less mass is consumed with the rise of ethanol content at the timing of TDC.

4.6 The Density of Indolene

The density of indolene is 750 kg/m3. In this section, the density of indolene is manually changed from 400 kg/m3 to 800 kg/m3 with a gap of 50 kg/m3.

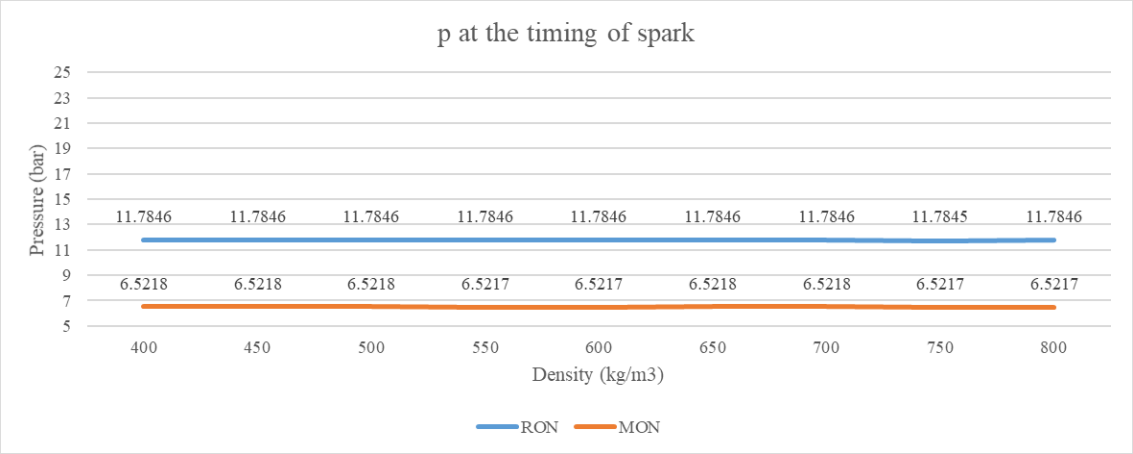

Figure 40 When the density of indolene changes: in-cylinder pressures at the timing of spark

Figure 40 shows pressures at the timing of spark of simulation results of indolene with various density under two test conditions (for RON and for MON respectively).

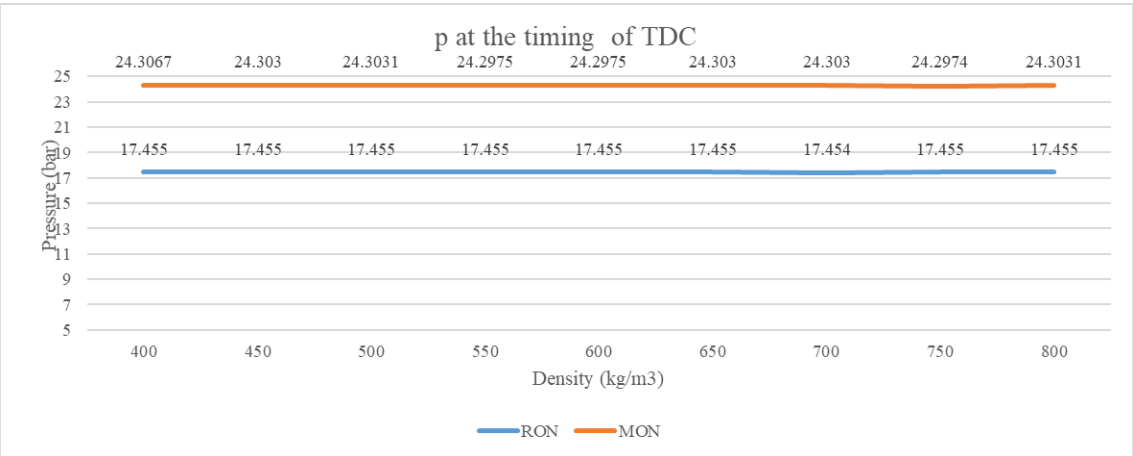

Figure 41 When the density of indolene changes: in-cylinder pressures at the timing of TDC

Figure 41 represents pressures at the timing of TDC of simulation results of indolene with various density under two test conditions (for RON and for MON respectively).

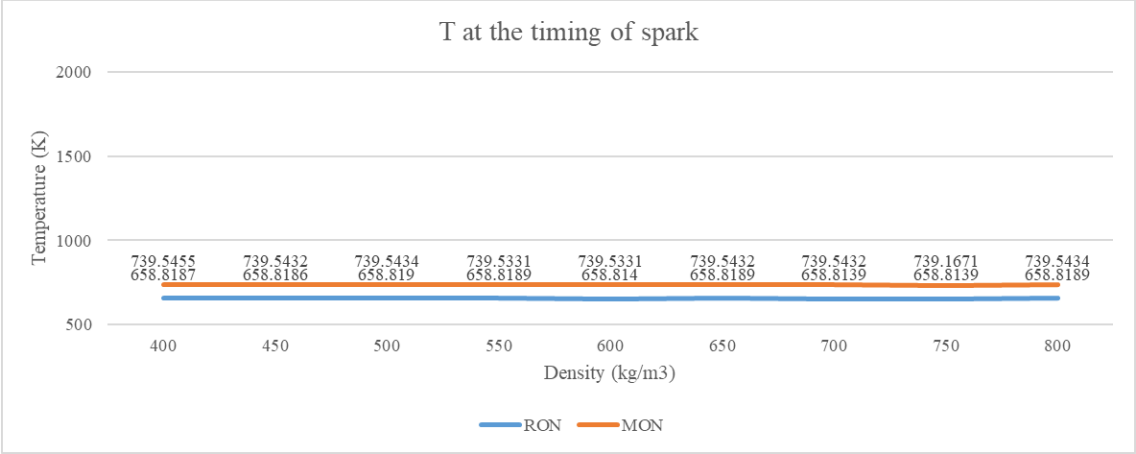

Figure 42 When the density of indolene changes: in-cylinder temperatures at the timing of spark

Figure 42 demonstrates temperatures at the timing of spark of simulation results of indolene with various density under two test conditions (for RON and for MON respectively).

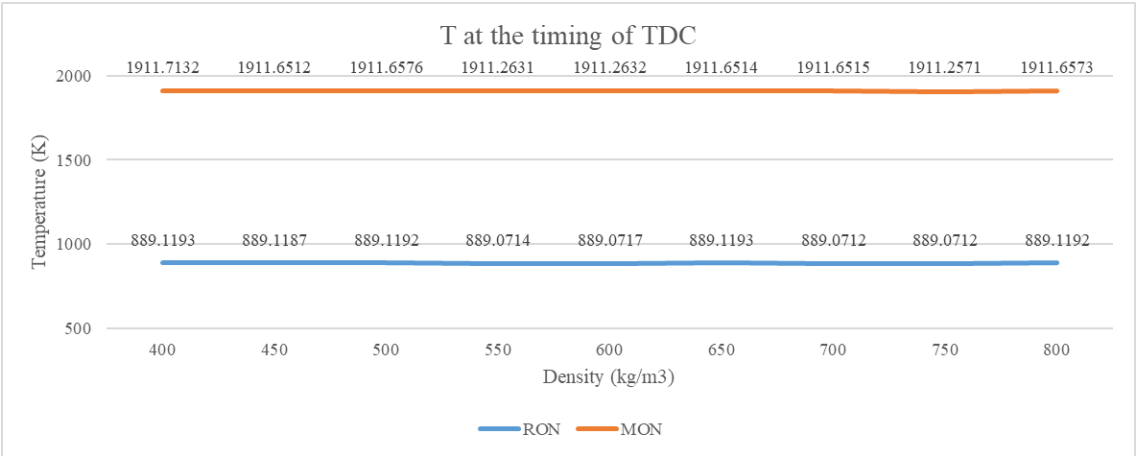

Figure 43 When the density of indolene changes: in-cylinder temperatures at the timing of TDC

Figure 43 illustrates temperatures at the timing of TDC of simulation results of indolene with various density under two test conditions (for RON and for MON respectively).

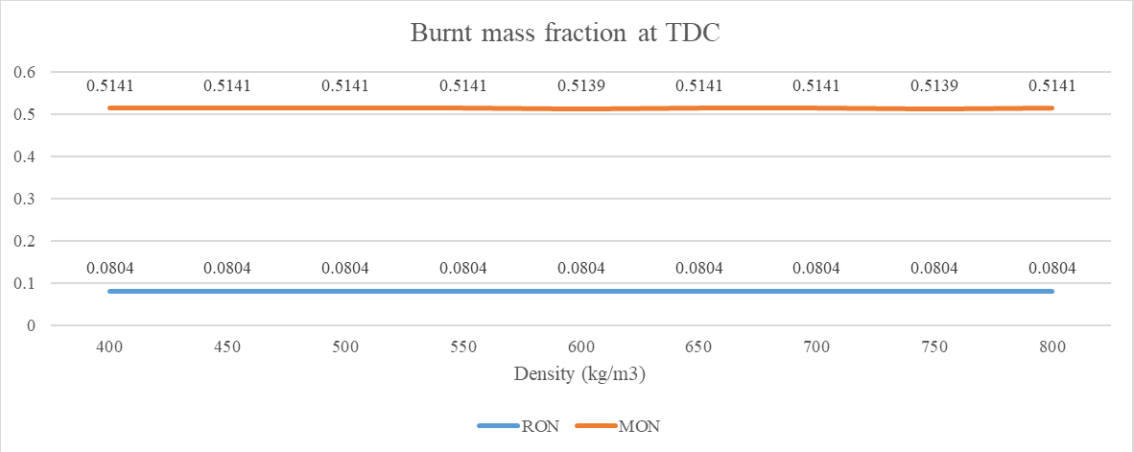

Figure 44 When the density of indolene changes: in-cylinder burnt mass fractions at the timing of TDC

Figure 44 shows the burnt mass fraction of simulation results of indolene with various density under two test conditions (for RON and for MON respectively).

The above five graphs show that both the pre-combustion conditions on instantaneous spark and the combustion conditions on instantaneous TDC remain stable when the density of indolene changes.

4.7 The Heat of Vaporization (HoV) of Indolene

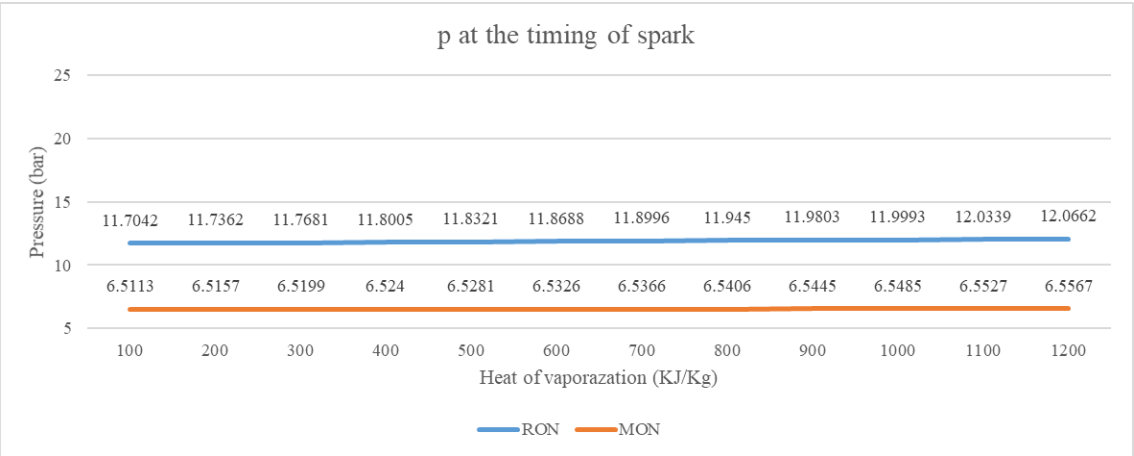

Figure 45 When the HoV of indolene changes: in-cylinder pressures at the timing of spark

Figure 45 shows pressures at the timing of spark of simulation results of indolene with various heat of vaporization under two test conditions (for RON and for MON respectively). Under RON test conditions, the pressure at the timing of spark increases very slightly as the HoV increases, so does the spark pressure under MON test conditions.

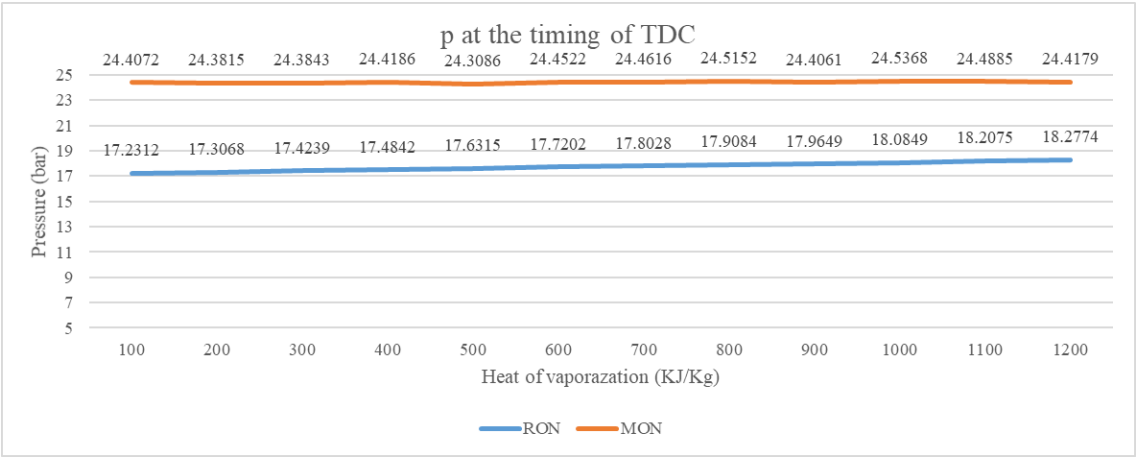

Figure 46 When the HoV of indolene changes: in-cylinder pressures at the timing of TDC

Figure 46 represents pressures at the timing of TDC of simulation results of indolene with different heat of vaporization under two test conditions (for RON and for MON respectively). Under RON test conditions, the pressure at the timing of spark increases noticeably as the HoV increases. However, under MON test conditions, the TDC pressure remains stable.

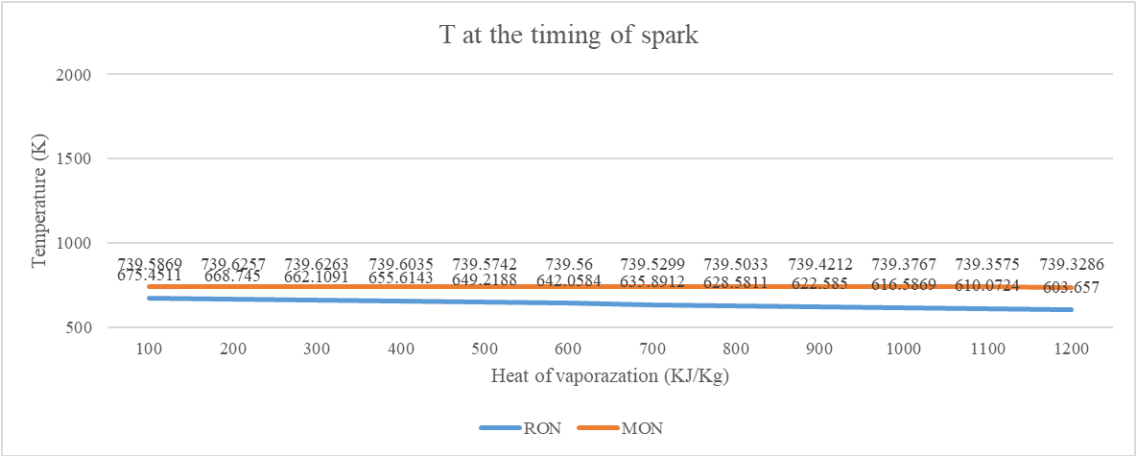

Figure 47 When the HoV of indolene changes: in-cylinder temperatures at the timing of spark

Figure 47 demonstrates temperatures at the timing of spark of simulation results of indolene with various HoV under two test conditions (for RON and for MON respectively). Under RON test conditions, the temperature at the timing of spark shows a reducing trend as the HoV increases. However, under MON test conditions, the spark temperature does not change when the HoV changes.

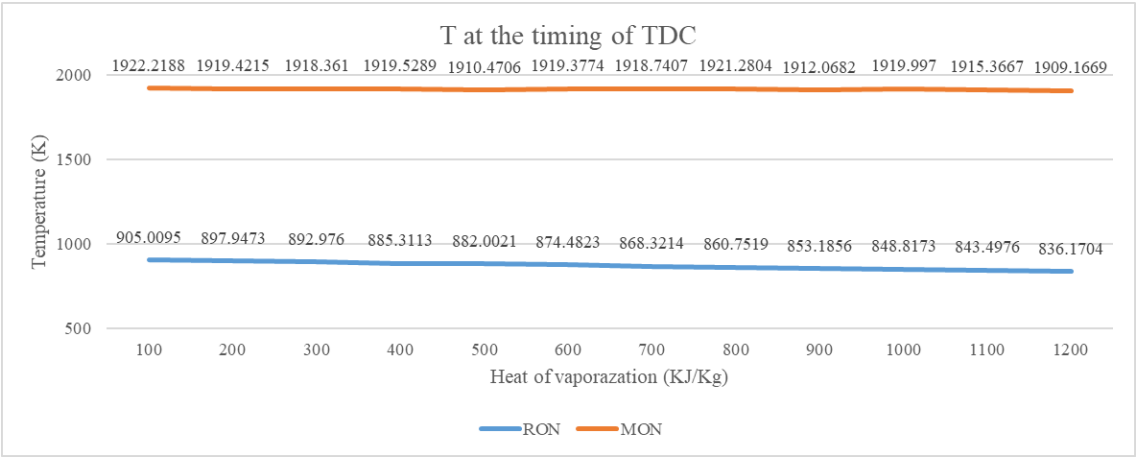

Figure 48 When the HoV of indolene changes: in-cylinder temperatures at the timing of TDC

Figure 48 illustrates temperatures at the timing of TDC of simulation results of indolene with various HoV under two test conditions (for RON and for MON respectively). Under RON test conditions, the temperature at the timing of TDC shows a reducing trend as the HoV increases. While the TDC temperature does not change when the HoV changes under MON test conditions.

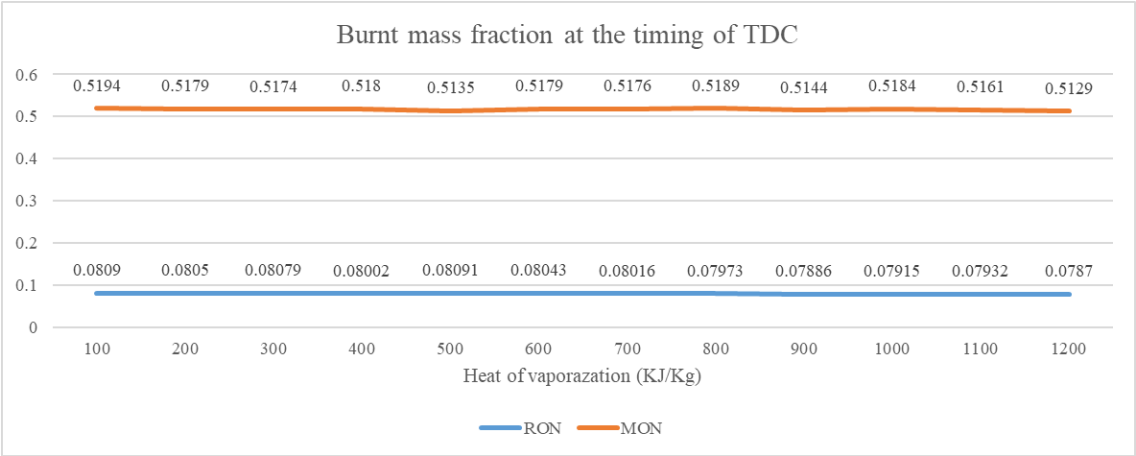

Figure 49 When the HoV of indolene changes: in-cylinder burnt mass fractions at the timing of TDC

Figure 49 shows the burnts mass fraction of simulation results of indolene with various HoV under two test conditions (for RON and for MON respectively). Under both of the test conditions, the burnt mass fraction does not react to the change on HoV very much.

5 Conclusions

In the intake system, the pressure maintains steady in the stroke of compression, power and exhaust, but experiences a downward fluctuation before slow returning to the initial state in the intake stroke regardless of operation conditions and vaporized fuels fraction upon the injection. The gaseous mass fraction undergoes a noticing drop in the carburettor and intake port during the intake stroke due to direct fuels injection to the carburettor. Regardless the vaporized fuels fraction upon the injection, the gaseous mass fraction of the air-fuel mixture entering to the cylinder can be kept at least around 94%. Temperature in the intake system can be manipulated by the vaporized fuels fraction upon the injection in the carburettor. In the venturi pipe where fuels are injected, the temperature experiences a dramatic drop due to fuels evaporation.

In generally, in-cylinder pre-combustion conditions become more severe with the increase of a fuel' octane number. In another way, the in-cylinder pressure and temperature become higher when a fuel' octane numbers are higher. For one group of selected fuels, if octane numbers vary a lot from case to case, the simulated in-cylinder pre-combustion conditions also vary much. In addition, with slight variation of octane numbers within one group of fuels, in-cylinder pre-combustion conditions do not show much variation as well.

The in-cylinder temperature under MON test conditions is always higher than that under RON test conditions, regardless the timing. As for the in-cylinder pressure, it is always lower under MON test conditions at the timing of spark. And at the timing of TDC, the in-cylinder pressure shows a complex tendency.

When a fuel is blended with ethanol, octane numbers of the mixed fuel increase with the increase of volumetric percentage of ethanol generally. However, the 40% of ethanol content point is special based on results. When PRF91 is mixed with ethanol, the RON of mixed fuels increases very slightly when volumetric content of ethanol is higher than 40%, the MON even starts decreasing when volumetric content of ethanol is 40%. Similar trend happens on blended fuels of TRF91-30 and ethanol, the RON of mixed fuels shows little increase when volumetric content of ethanol is higher than 40%, and the MON begins to drop when volumetric content of ethanol is 40%. In-cylinder pre-combustion conditions show the same tendency as octane numbers with the change of fuels' ethanol percentage.

The density of a fuel has very little influence on in-cylinder pre-combustion conditions. In-cylinder pre-combustion conditions barely change with the increase of density of selected surrogate fuel of gasoline.

The HoV of a fuel affect the in-cylinder pre-combustion conditions to some extent. Under RON test conditions, at the timing of spark, the in-cylinder pressure increases slightly with the increase of HoV, and the in-cylinder temperature drops noticeably when the HoV rises. At the timing of spark, in-cylinder pressure and temperature show the same trend. Under MON test conditions, in-cylinder pressure and temperature decrease gently at both of the timings.

6 Discussion and Future Work

In this master's thesis study, the author successfully established the CFR engine modellings based on RON and MON conditions, with the help of Gt-power. Three kinds of fuels are attempted to simulate on created modellings, and the simulated results are validated with experimental data from references [51] The validation results show that the simulation results match well with the experimental data from the references [51]. Therefore, to a large extent, the CFR engine modellings established in this research is credible. Simulation results based on these two models are also reliable. In addition, although the study does not involve knocking onset and detailed chemical reaction mechanism of in-cylinder combustion, simulated pre-combustion conditions can be referred as boundary conditions for further two-dimensional modeling work. At the same time, there are still many limitations in this study.

First, as mentioned in the introduction section of this thesis, studies on pre-combustion conditions of internal combustion engines are very rare. There is basically no data on pre-combustion conditions of engines that can be compared or validated. In the process of literature study, although a large number of studies on the knocking tendency of internal combustion engines are discovered or investigated, these literatures did not clearly indicate the pre-combustion conditions and detailed data on the pre-combustion conditions. After the engine model are established, even though the author validate the simulation results, within a limited time, the author only find three kinds of fuels that could be validated, and the experimental measurement data from the references [51] is only the pressure curve under the condition of RON. If more adequate experimental data are available, the validated results would be more convincing.

Second, in this study, in order to establish the engine model, the engine related are not from measurements, but "pieced together" from various literatures. The geometric parameters of engine cylinder are from D2600 [37] and D2700 [38] In the fuel system, geometric data for each component is obtained from [16]. These obtained data are compared with data from [51]. Moreover, the data about valve and xx are also from [51]. Therefore, the engine modellings established in this study deserve more correction and modification.

Third, the fuel system setting of CFR engine modellings has been greatly simplified. In this study, the heat transfer parameters of the tubes in the fuel system are all from the default settings in Gt-power. And those input parameters cannot be modified for actual situation since the absence of data sources. In the process of simulation, when the 'vaporized fuel fraction' in the injector (it indicates the proportion of vaporized fuel when the fuel is injected to the venturi) is set to less than 50%, the lowest temperature in the venturi tube is far below 0 ℃ , which is very unrealistic.

Reference

[1] International Energy Agency, Market Report Series: Energy Efficiency 2018. Analysis and outlooks to 2040, 19.10.2018. https://webstore.iea.org/market-report-series-energy-efficiency-2018

[2] Organization of the Petroleum Exporting Countries Secretariat, 2013 World Oil Outlook, 2013 https://www.opec.org/opec_web/static_files_project/media/downloads/publications/WOO_2013.pdf

[3] Organization of the Petroleum Exporting Countries Secretariat, 2018 World Oil Outlook, 2018

[4] https://www.opec.org/opec_web/en/press_room/5161.htm

[5] Mørch, C.S. & Bjerre, A. & Gøttrup, M.P. & Sorenson, S.C. & Schramm, Jesper. (2011). Ammonia/hydrogen mixtures in an SI-engine: Engine performance and analysis of a proposed fuel system. Fuel. 90. 854-864. 10.1016/j.fuel. 2010.09.042.

[6] Cheng, Song & Yang, Yi & Brear, Michael & Kang, Dongil & Bohac, Stanislav & Boehman, André. (2016). Autoignition of pentane isomers in a spark-ignition engine. Proceedings of the Combustion Institute. 36. 10.1016/j.proci.2016.08.042.

[7] KOLODZIEJ, C., WALLNER, T. Combustion characteristics of various fuels during research octane number testing on an instrumented CFR F1/F2 engine. Combustion Engines. 2017, 171(4), 164-169. DOI: 10.19206/CE-2017-427

[8] Szwaja, Stanislaw & Bhandary, K. & Naber, Jeffrey. (2007). Comparisons of hydrogen and gasoline combustion knock in a spark ignition engine. International Journal of Hydrogen Energy. 32. 5076-5087. 10.1016/j.ijhydene.2007.07.063.

[9] Juan P. Gomez Montoya, German J. Amador Diaz, Andres Adolfo Amell Arrieta, Effect of equivalence ratio on knocking tendency in spark ignition engines fueled with fuel blends of biogas, natural gas, propane and hydrogen, International Journal of Hydrogen Energy Volume 43, Issue 51, 20 December 2018, Pages 23041-23049

[10] Bika, Anil & Franklin, Luke & Kittelson, David. (2011). Engine knock and combustion characteristics of a spark ignition engine operating with varying

hydrogen and carbon monoxide proportions. Fuel and Energy Abstracts. 36. 5143-5152. 10.1016/j.ijhydene.2011.01.039.

[11] Zhongyuan, Chen & Yuan, Hao & Foong, Tien & Yang, Yi & Brear, Michael. (2019). The impact of nitric oxide on knock in the octane rating engine. Fuel. 235. 495-503. 10.1016/j.fuel.2018.08.039.

[12] Truedsson, Ida. “The HCCI Fuel Number - Measuring and Describing Autoignition for HCCI Combustion Engines.” (2014).

[13] Hoth, A., Kolodziej, C., Rockstroh, T., and Wallner, T., "Combustion Characteristics of PRF and TSF Ethanol Blends with RON 98 in an Instrumented CFR Engine," SAE Technical Paper 2018-01-1672, 2018, https://doi.org/10.4271/2018-01-1672.

[14] Morganti, Kai & Brear, Michael & da Silva, Gabriel & Yang, Yi & Dryer, Frederick. (2015). The autoignition of Liquefied Petroleum Gas (LPG) in spark-ignition engines. Proceedings of the Combustion Institute. 35. 2933–2940. 10.1016/j.proci.2014.06.070.

[15] Morganti, Kai & Foong, Tien & Brear, Michael & da Silva, Gabriel & Yang, Yi & Dryer, Frederick. (2014). Design and Analysis of a Modified CFR Engine for the Octane Rating of Liquefied Petroleum Gases (LPG). SAE International Journal of Fuels and Lubricants. 7. 10.4271/2014-01-1474.

[16] Choi, S., Kolodziej, C., Hoth, A., and Wallner, T., "Development and Validation of a Three Pressure Analysis (TPA) GT-Power Model of the CFR F1/F2 Engine for Estimating Cylinder Conditions," SAE Technical Paper 2018-01-0848, 2018, https://doi.org/10.4271/2018-01-0848.

[17] Salih, Saif & DelVescovo, Dan. (2018). Design and Validation of a GT Power Model of the CFR Engine towards the Development of a Boosted Octane Number. 10.4271/2018-01-0214.

[18] Pal, Pinaki & Kolodziej, Christopher & Choi, Seungmok & Som, Sibendu & Broatch, A. & Gomez-Soriano, Josep & Wu, Yunchao & Lu, Tianfeng & See,Yee. (2018). Development of a Virtual CFR Engine Model for Knocking

Combustion Analysis. SAE International Journal of Engines. 10.4271/2018-01-0187.

[19] Pal, P., Kolodziej, C., Choi, S., Som, S. et al., "Development of a Virtual CFR Engine Model for Knocking Combustion Analysis," SAE Int. J. Engines 11(6):1069-1082, 2018, https://doi.org/10.4271/2018-01-0187.

[20] Westbrook, C.K. & Sjöberg, M. & Cernansky, N.P.. (2018). A new chemical kinetic method of determining RON and MON values for single component and

[21] multicomponent mixtures of engine fuels. Combustion and Flame. 195. 10.1016/j.combustflame.2018.03.038.

[22] Morganti, K. J. (2013). A study of the knock limits of liquefied petroleum gas (LPG) in spark-ignition engines. PhD thesis, Department of Mechanical Engineering, The University of Melbourne.

[23] David O. Whitten, Bessie Emrick Whitten, Handbook of American Business History: Manufacturing

[24] George E. Totten, RJ Shah, SR Westbrook, Fuels and Lubricants Handbook: Technology, Properties, Performance, and Testing, ISBN 978-0-8031-4551-1

[25] (2007). Wiley Critical Content - Petroleum Technology, Volume 1-2 - 1.2 Chemical Properties. John Wiley & Sons.

[26] Shekhawat, Dushyant Spivey, J.J. Berry, David A.. (2011). Fuel Cells - Technologies for Fuel Processing - 3.2.1.1 Natural Gas. Elsevier.

[27] Rand, Salvatore J.. (2003). Significance of Tests for Petroleum Products (7th Edition): (MNL 1) - 3.4.5 Volatility and Performance. ASTM International.

[28] (2012). Dictionary of Metals - lay. ASM International.

[29] (2013). 2013 ASHRAE Handbook - Fundamentals (SI Edition). American Society of Heating, Refrigerating and Air-Conditioning Engineers, Inc. (ASHRAE).

[30] EU: FUELS: Diesel and gasoline, https://www.transportpolicy.net/standard/eu-fuels-diesel-and-gasoline/

[31] British Standards Institute Staff, Automotive fuels - Unleaded petrol - Requirements and test methods

[32] Basshuysen, Richard van Schäfer, Fred. (2016). Internal Combustion Engine Handbook - Basics, Components, System, and Perspectives (2nd Edition)

[33] Mang, Theo Dresel, Wilfried. (2017). Lubricants and Lubrication, 2 Volume Set (3rd Edition). John Wiley & Sons.

[34] Petchers, Neil. (2012). Combined Heating, Cooling & Power Handbook - Technologies & Applications (2nd Edition) - 9.1 Reciprocating Engine Types. Fairmont Press, Inc..

[35] John Heywood, Internal Combustion Engine Fundamentals 1st Edition

[36] The Internal combustion engine (Otto Cycle), http://web.mit.edu/16.unified/www/FALL/thermodynamics/notes/node26.html

[37] Zhi Wang, Hui Liu, Rolf D Reitz, Knocking combustion in spark-ignition engines, Progress in Energy and Combustion Science, Volume 61, 2017, Pages 78-112, ISSN 0360-1285

[38] Gunston, Bill. (2009). Cambridge Aerospace Dictionary (2nd Edition). Cambridge University Press.

[39] ASTM D2699 - 19, Standard Test Method for Research Octane Number of Spark-Ignition Engine Fuel. https://www.astm.org/Standards/D2699.htm

[40] ASTM D2700 -19, Standard Test Method for Motor Octane Number of Spark-Ignition Engine Fuel. https://www.astm.org/Standards/D2700.htm

[41] Waukesha CFR F1/F2 Octane Rating Engine With XCP Technology. http://www.compassinstruments.com/utilities/file_library/downloads/CFR/CFR_F1F2_brochure_(Compass_Instruments).pdf

[42] Zhen, Xudong & Wang, Yang & Liu, Daming. (2017). An overview of the chemical reaction mechanisms for gasoline surrogate fuels. Applied Thermal Engineering. 124. 10.1016/j.applthermaleng.2017.06.101.

[43] Sarathy, S.Mani & Farooq, Aamir & Kalghatgi, Gautam. (2017). Recent progress in gasoline surrogate fuels. Progress in Energy and Combustion Science. 65. 10.1016/j.pecs.2017.09.004.

[44] S.M. Aceves, J. Marthnez-Frias, D. Flowers, J.R. Smith, R. Dibble, J.Y. Chen, A Computer Generated Reduced Iso-octane Chemical Kinetic Mechanism Applied

[45] to Simulation of HCCI Combustion, SAE Technical Papers No. 2002-01-2870, 2002.

[46] Code of Federal Regulations, https://www.govinfo.gov/content/pkg/CFR-2014-title40-vol33/xml/CFR-2014-title40-vol33-sec1065-710.xml

[47] Eugene L. Keating, Applied Combustion 2nd Edition

[48] Pohanish, Richard P.. (2017). Sittig's Handbook of Toxic and Hazardous Chemicals and Carcinogens, 3 Volume Set (7th Edition) - Toluene. Elsevier.

[49] Speight, James G. 2017. Rules of thumb for petroleum engineers.

[50] Speight, James G.. (2015). Handbook of Petroleum Product Analysis (2nd Edition). John Wiley & Sons.

[51] (2007). Wiley Critical Content - Petroleum Technology, Volume 1-2. John Wiley & Sons.

[52] Liu, Yu Cheng & Savas, Anthony & Avedisian, C.. (2012). Comparison of the Burning Characteristics of Indolene and Commercial Grade Gasoline Droplets without Convection. Energy & Fuels. 26. 5740–5749. 10.1021/ef3007849.

[53] Gt-power built-in help documents

[54] Foong, T. M. (2013). On the Autoignition of Ethanol/Gasoline Blends in Spark-ignition Engines. Ph.D's thesis, Department of Mechanical Engineering, The University of Melbourne.

[55] Adam Erlandsson. Fast Running 1D Model of a Heavy-duty Diesel Engine. Master's thesis, Department of Mechanics and Maritime Sciences, Chalmers University of Technology.

Appendix I

Intake System Conditions under RON Conditions

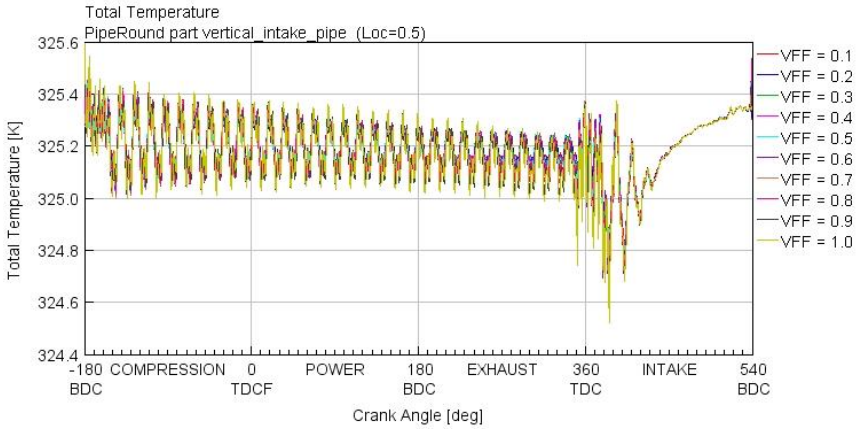

Figure 50 Temperature variation in the intake pipe under RON conditions

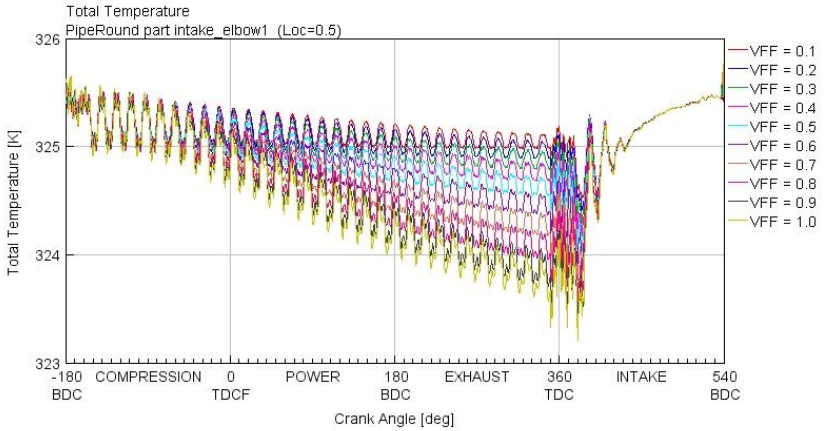

Figure 51 Temperature variation in the intake pipe elbow under RON conditions

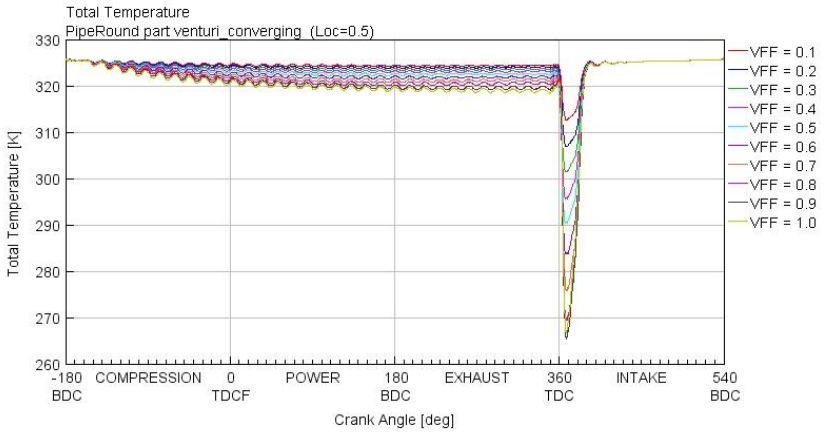

Figure 52 Temperature variation in the converging pipe of the carburettor under RON conditions

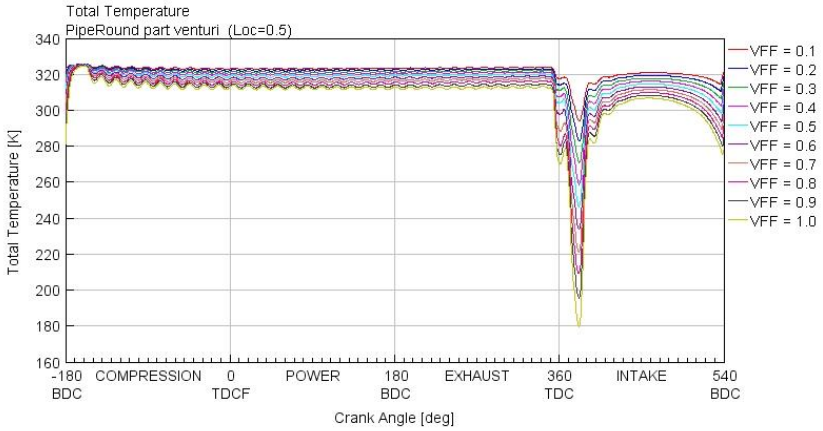

Figure 53 Temperature variation in the venturi pipe of the carburettor under RON conditions

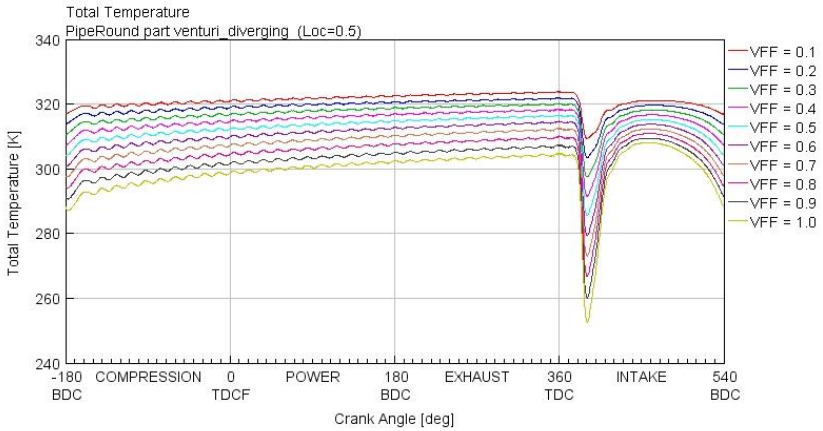

Figure 54 Temperature variation in the diverging pipe of the carburettor under RON conditions

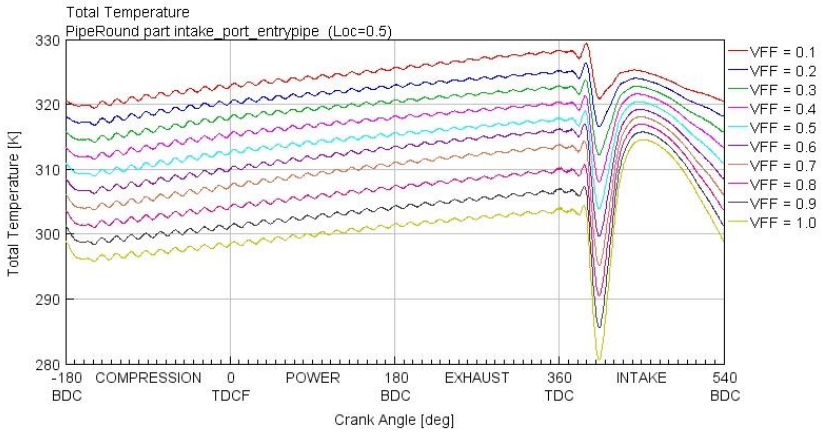

Figure 55 Temperature variation in the intake port pipe under RON conditions

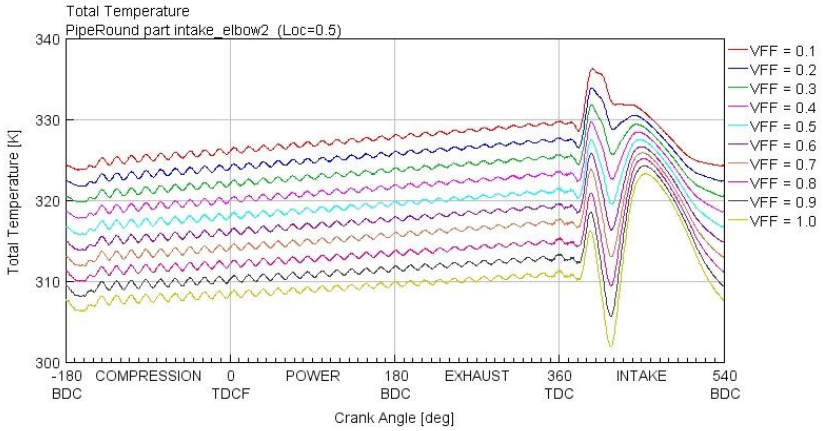

Figure 56 Temperature variation in the intake port elbow under RON conditions

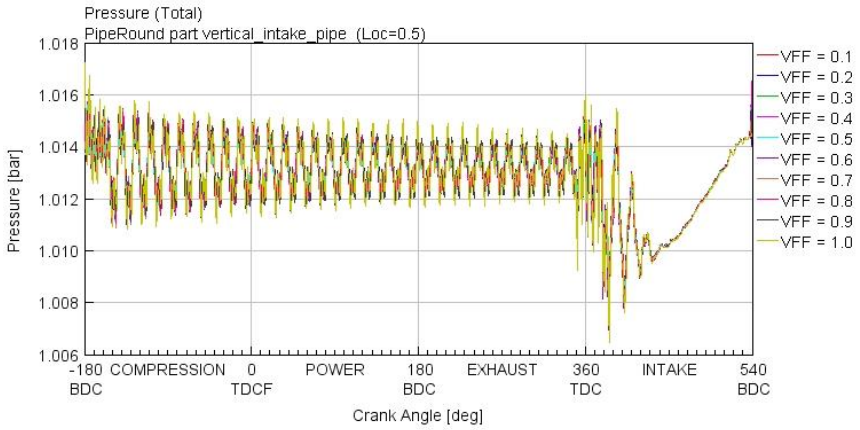

Figure 57 Pressure variation in the intake pipe under RON conditions

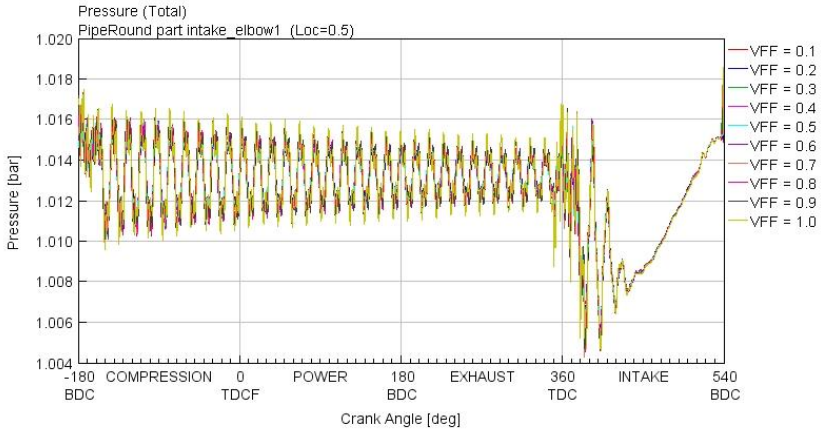

Figure 58 Pressure variation in the intake pipe elbow under RON conditions

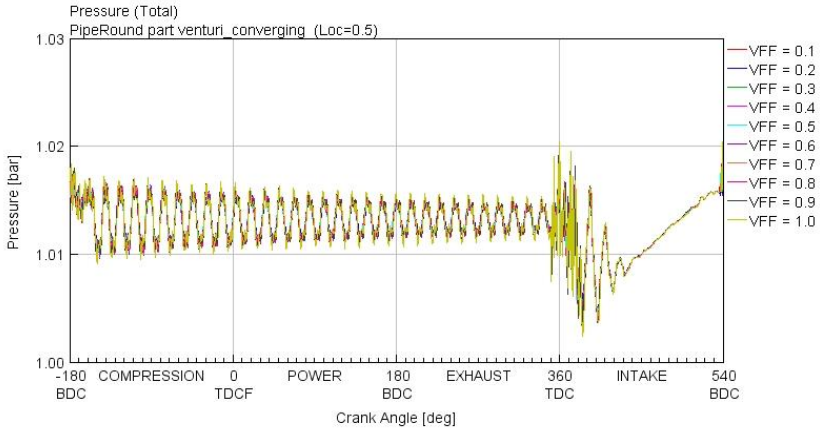

Figure 59 Pressure variation in the converging pipe in the carburettor under RON conditions

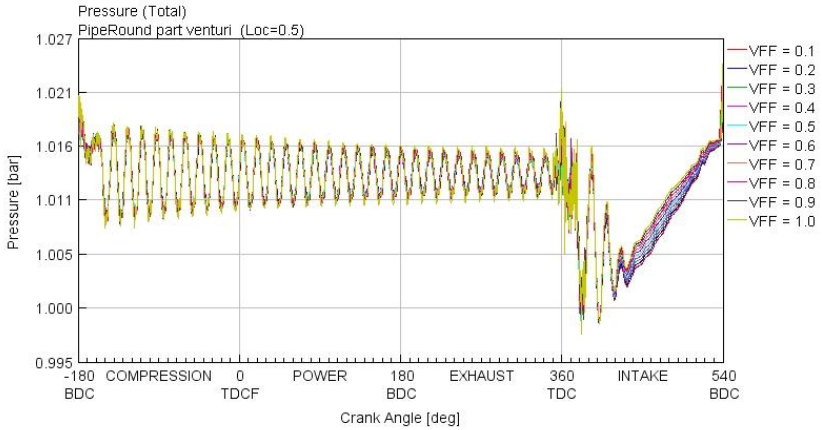

Figure 60 Pressure variation in the venturi pipe in the carburettor under RON conditions

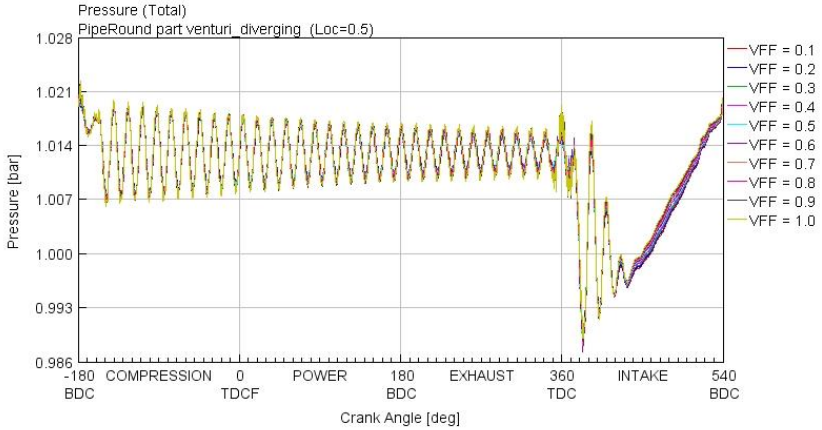

Figure 61 Pressure variation in the diverging pipe in the carburettor under RON conditions

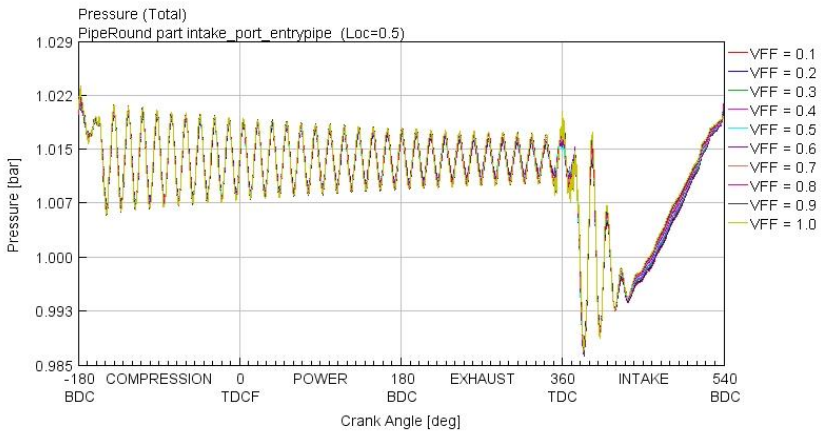

Figure 62 Pressure variation in the intake port pipe under RON conditions

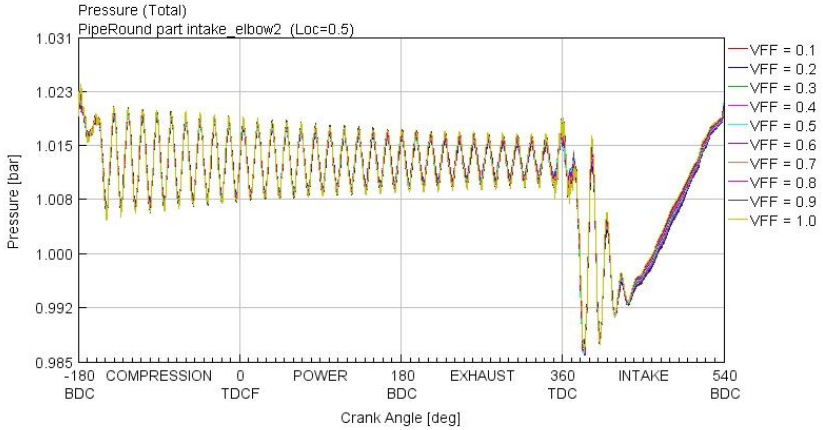

Figure 63 Pressure variation in the intake port elbow under RON conditions

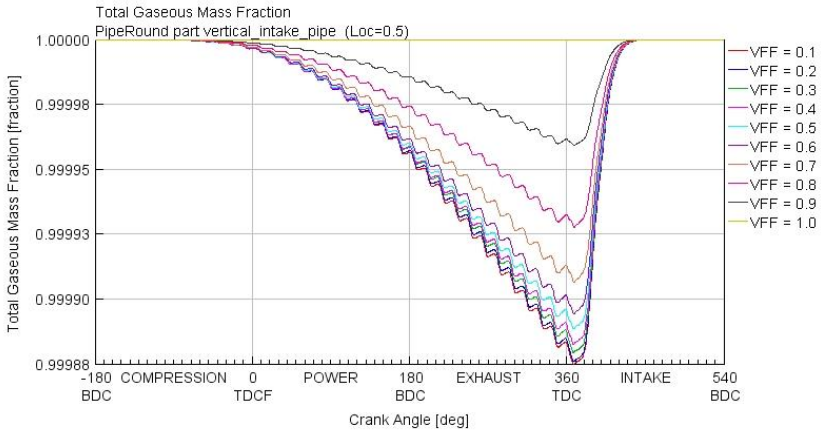

Figure 64 Gaseous mass fraction variation in the intake pipe under RON conditions

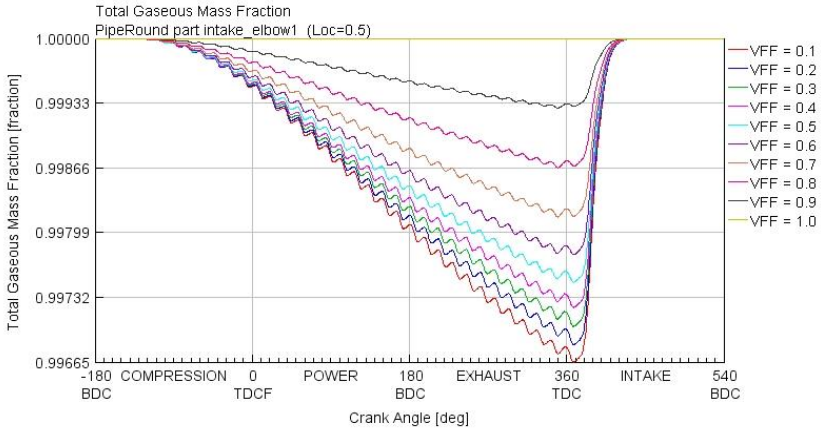

Figure 65 Gaseous mass fraction variation in the intake elbow under RON conditions

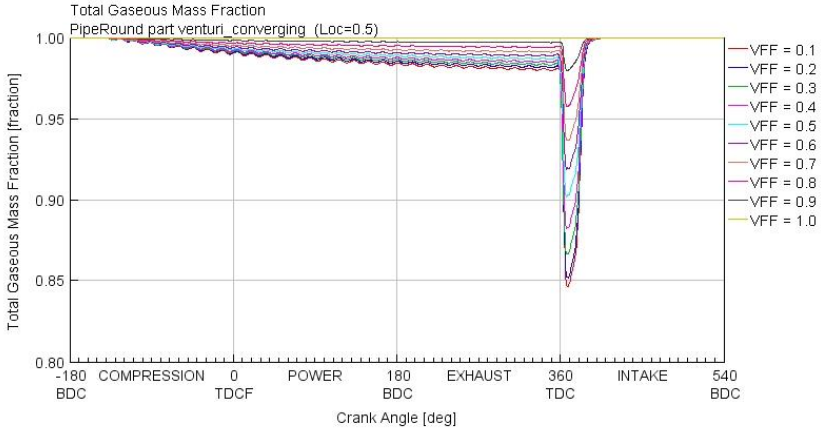

Figure 66 Gaseous mass fraction variation in the converging pipe of the carburettor under RON conditions

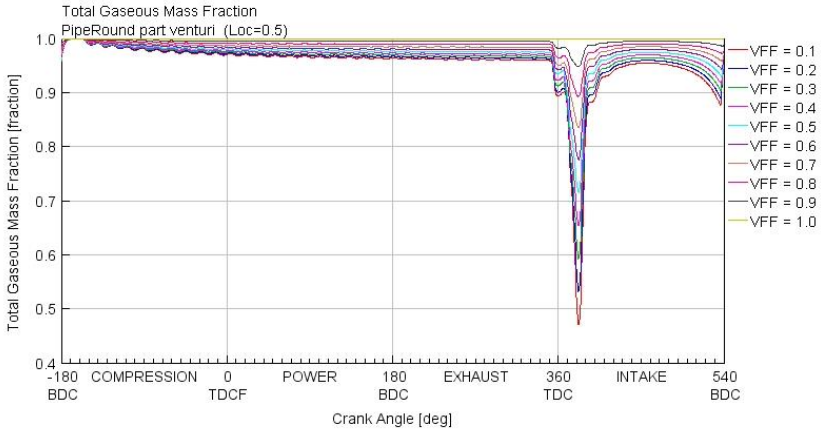

Figure 67 Gaseous mass fraction variation in the venturi pipe of the carburettor under RON conditions

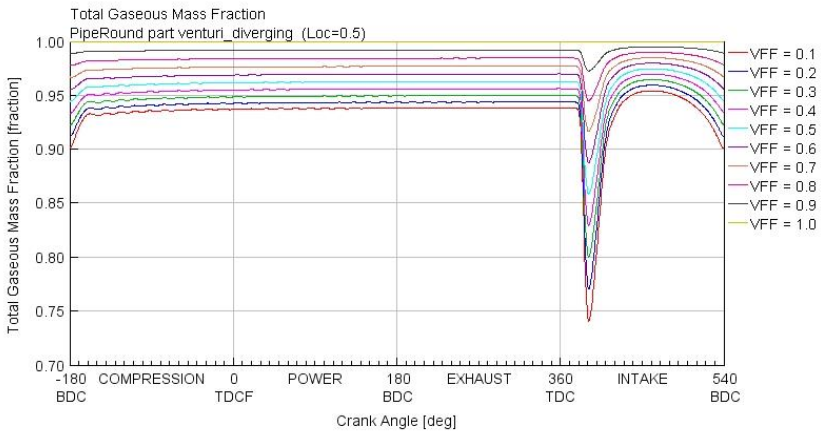

Figure 68 Gaseous mass fraction variation in the diverging pipe of the carburettor under RON conditions

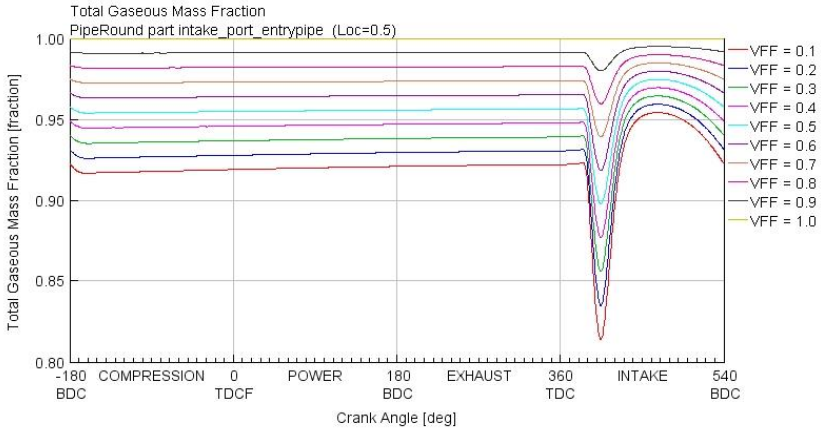

Figure 69 Gaseous mass fraction variation in the intake port pipe under RON conditions

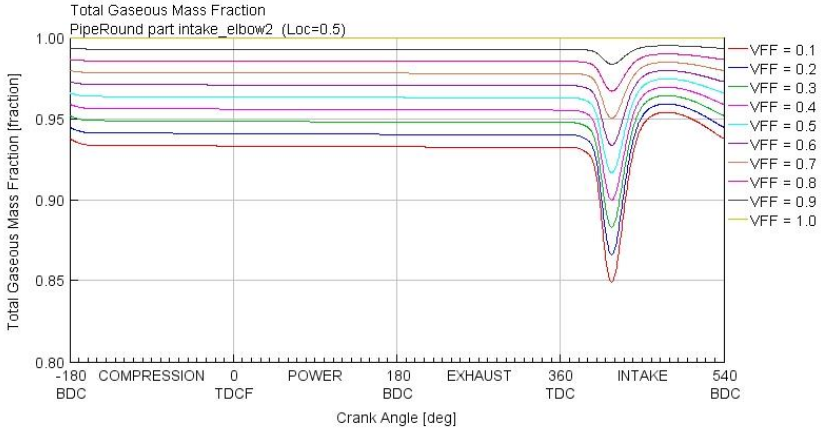

Figure 70 Gaseous mass fraction variation in the intake port elbow under RON conditions

Appendix II

Intake System Conditions under MON Conditions

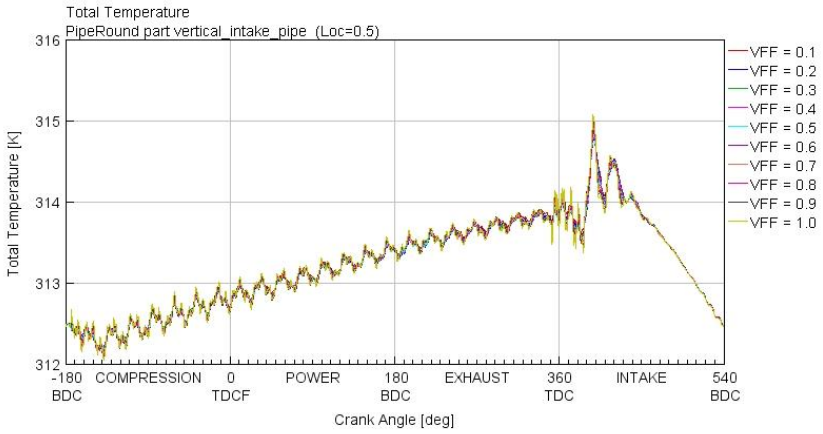

Figure 71 Temperature variation in the intake pipe under MON conditions

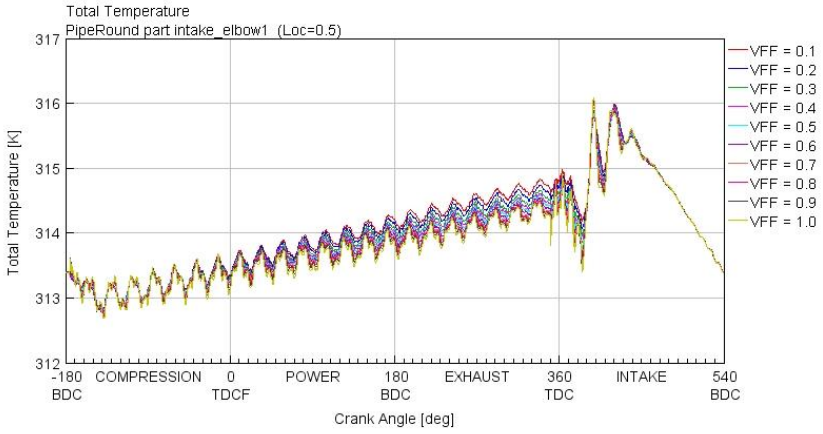

Figure 72 Temperature variation in the intake pipe elbow under MON conditions

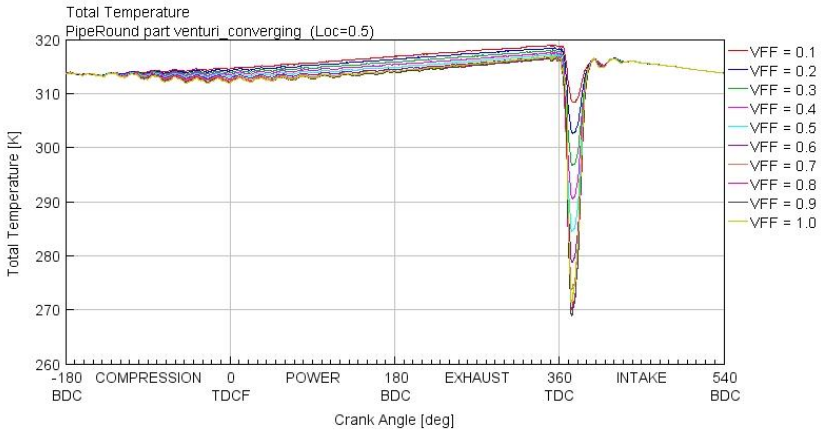

Figure 73 Temperature variation in the converging pipe of the carburettor under MON conditions

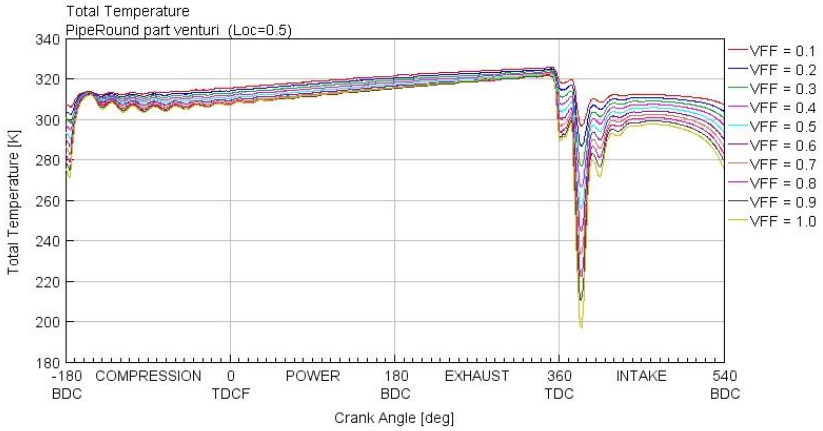

Figure 74 Temperature variation in the venturi pipe of the carburettor under MON conditions

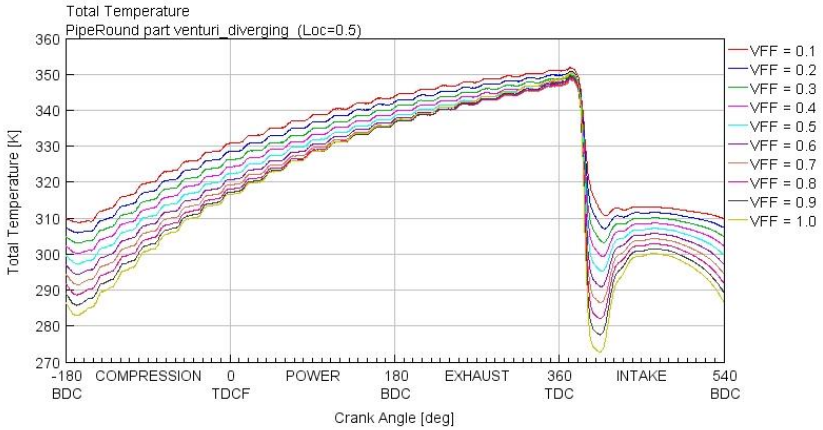

Figure 75 Temperature variation in the diverging pipe of the carburettor under MON conditions

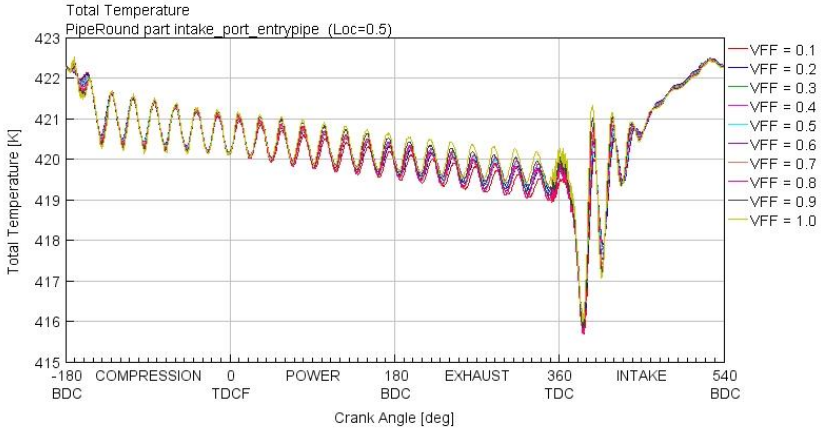

Figure 76 Temperature variation in the intake port pipe under MON conditions

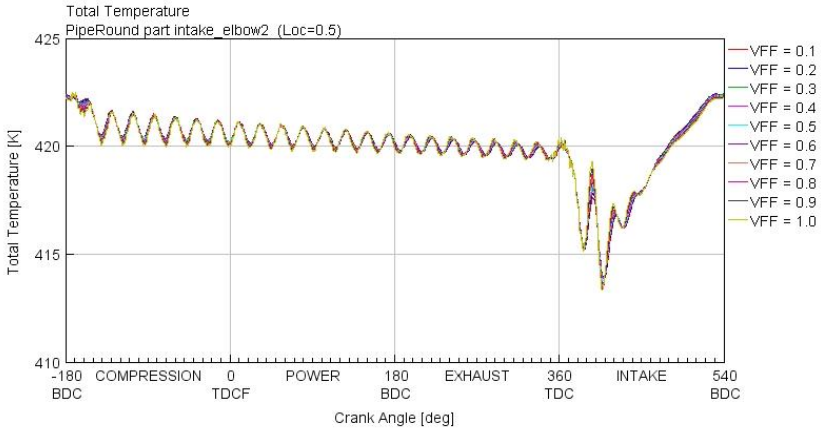

Figure 77 Temperature variation in the intake port elbow under MON conditions

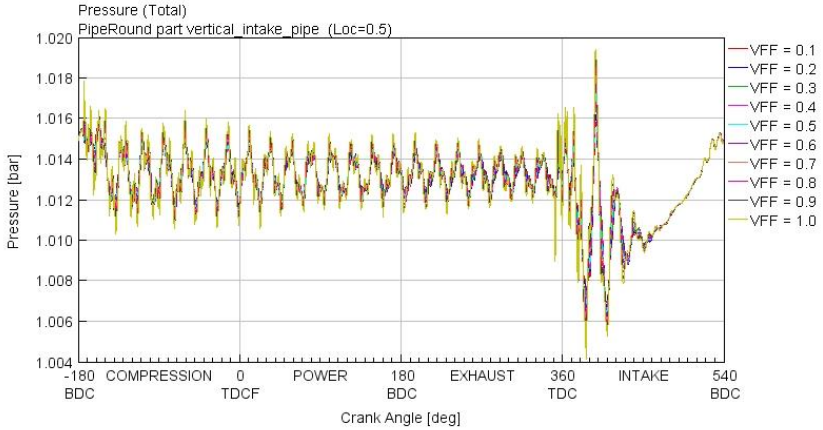

Figure 78 Pressure variation in the intake pipe under MON conditions

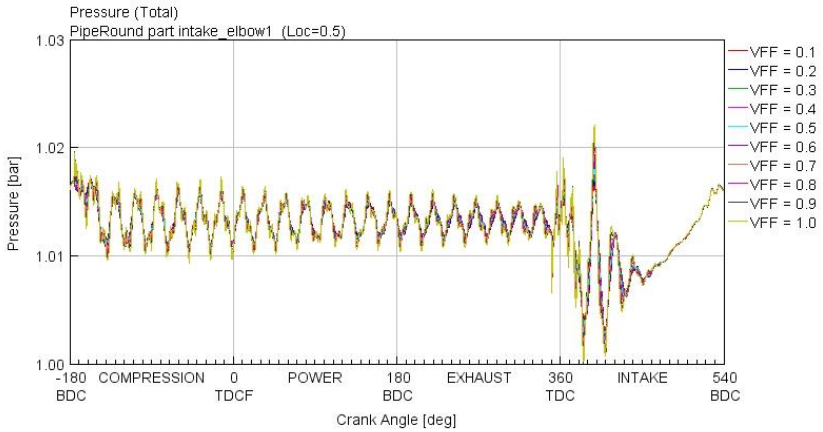

Figure 79 Pressure variation in the intake pipe elbow under MON conditions

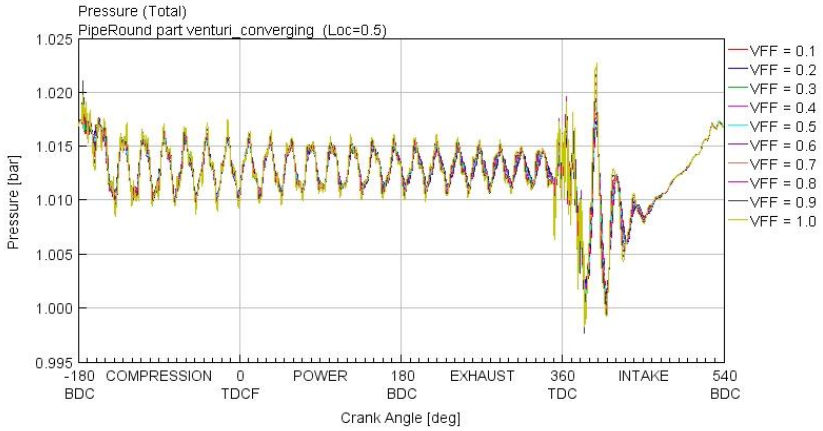

Figure 80 Pressure variation in the converging pipe of the carburettor under MON conditions

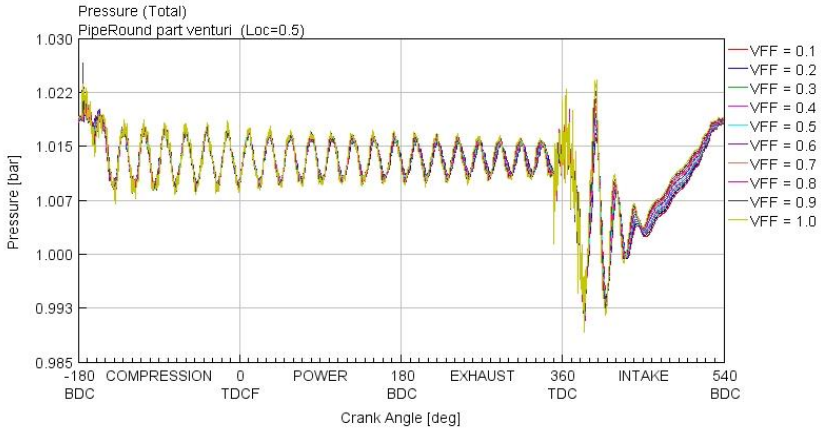

Figure 81 Pressure variation in the venturi pipe of the carburettor under MON conditions

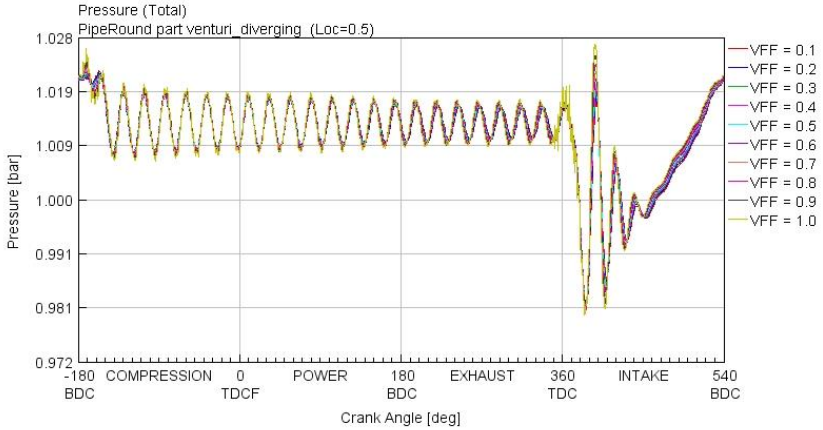

Figure 82 Pressure variation in the diverging pipe of the carburettor under MON conditions

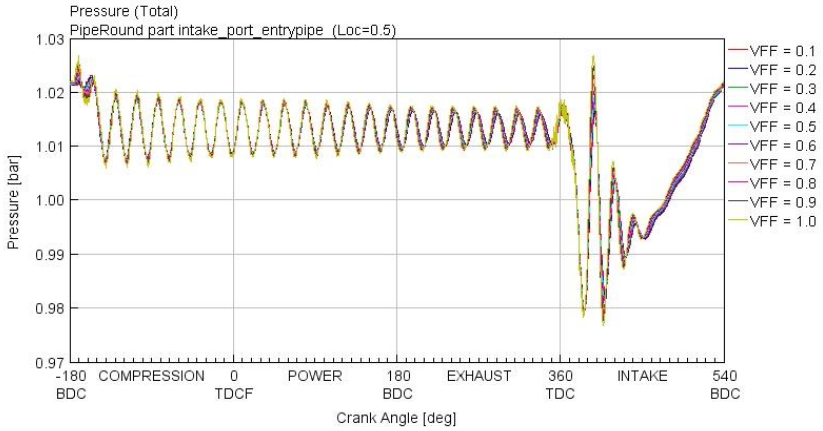

Figure 83 Pressure variation in the intake port pipe under MON conditions

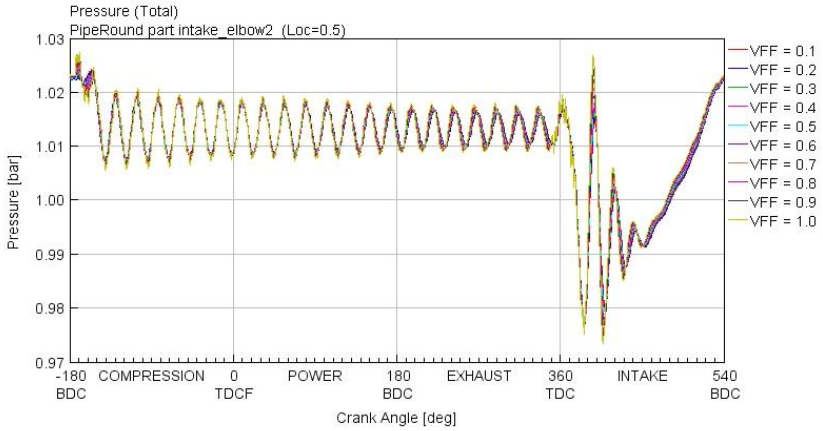

Figure 84 Pressure variation in the intake port elbow under MON conditions

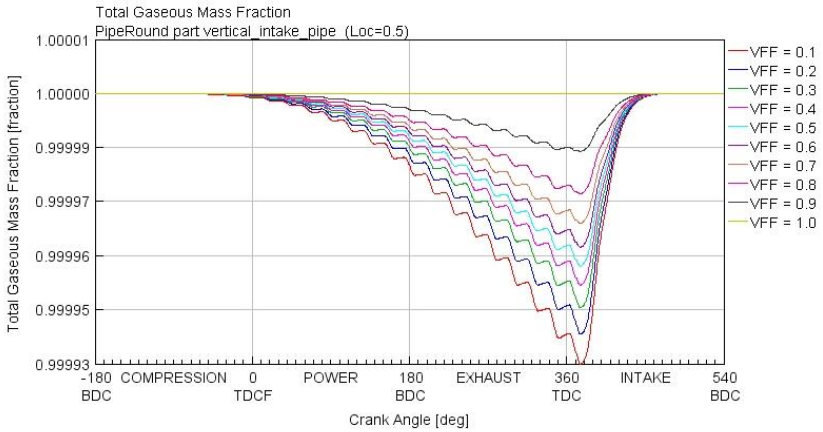

Figure 85 Gaseous mass fraction in the intake pipe under MON conditions

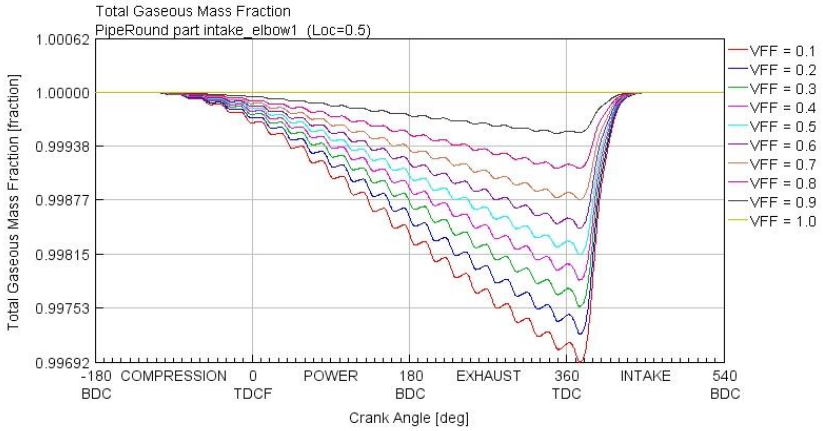

Figure 86 Gaseous mass fraction in the intake pipe elbow under MON conditions

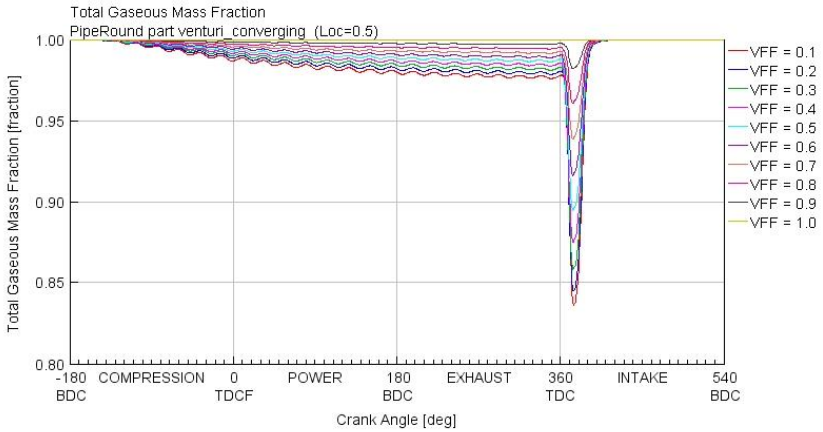

Figure 87 Gaseous mass fraction in the converging pipe of the carburettor under MON conditions

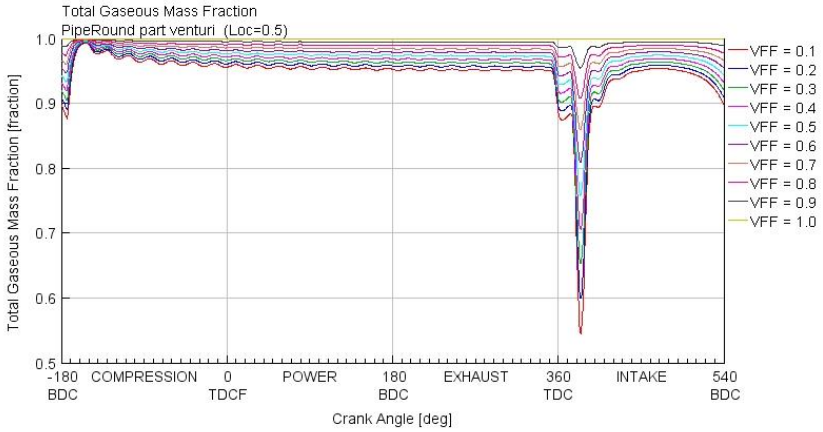

Figure 88 Gaseous mass fraction in the venturi pipe of the carburettor under MON conditions

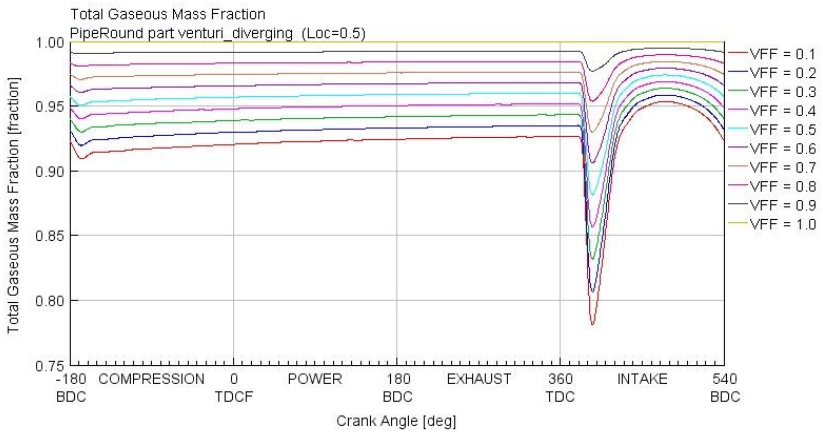

Figure 89 Gaseous mass fraction in the diverging pipe of the carburettor under MON conditions

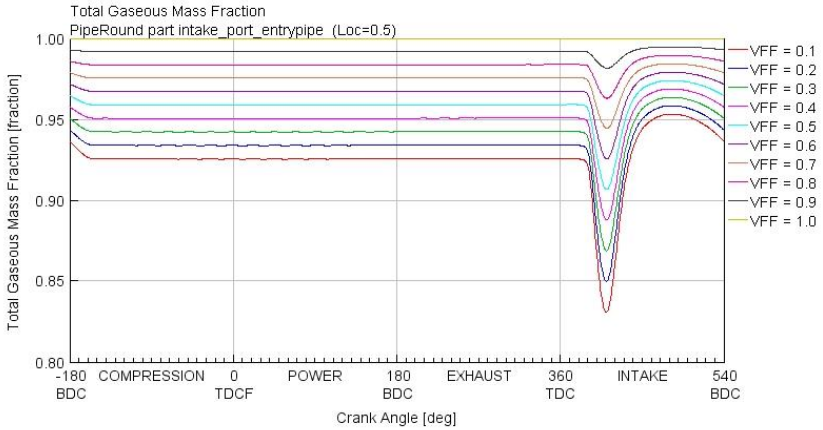

Figure 90 Gaseous mass fraction in the intake port pipe under MON conditions

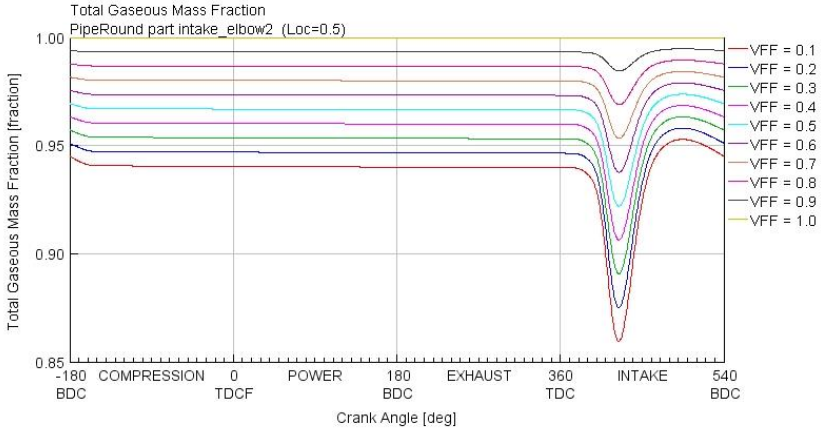

Figure 91 Gaseous mass fraction in the intake port elbow under MON conditions